Dominant Modes of Rainfall Variability over East Africa in Response to Multiscale Global Climate Analyses

by

Nana K.A. Appiah-Badu, BSc (Hons)

A Thesis Submitted to the Department of Physics Kwame Nkrumah University of Science and Technology in Partial Fulfillment of the Requirements for the Degree

of

MASTER OF PHILOSOPHY

IN

METEOROLOGY AND CLIMATE SCIENCE

College of Science

Department of Physics

October, 2016

DECLARATION

I hereby declare that this thesis is my own work towards the MPhil and that, to the best of my knowledge, it contains no material previously published by another person nor material which has been accepted for the award of any other degree of the University, except where due acknowledgement has been made in the text.

NANA KOFI AHOI APPIAH-BADU .... …………..

(PG8063312) Signature Date

Student Name & ID

Certified by:

Dr I.K. Tetteh ....

Name of Supervisor Signature Date

Certified by:

Prof. S.K. Danuor ....

Name of Head of Department Signature Date

ABSTRACT

The main interest was to carry out an analysis of time evolution of global climate during the climatologically prominent phase of El Niño Southern Oscillation (ENSO) from 1950-2008 and their relationship to the dominant modes of MarchMay (MAM) seasonal rainfall variability to provide useful climate information needed by end users for incorporation into sustainable climate change developmental goals. The study utilized monthly data consisting of horizontal global winds at 200 hPa from the National Centers for Environmental PredictionNational Center for Atmospheric Research (NCEP-NCAR) reanalysis data,

Climatic Research Unit (CRU) gridded terrestrial precipitation data and Extended Reconstructed Sea Surface Temperature (ERSST). The three major timescales of investigation in the annual cycle included monthly, bimonthly and seasonal. The study employed Empirical Orthogonal Function (EOF) analysis, lagged heterogeneous grid point correlation, composite analysis technique and multiple linear regression analysis. The EOF analysis was performed on the East African long rains (MAM) and the four leading modes were retained. Lagged heterogeneous grid point correlation between the time coefficients of the four leading modes and global SST were computed to evaluate, delineate and monitor the specific SST signals that were connected to the long rains. On the monthly timescale, the grid-point correlation showed that, EOF 1, 3 and 4 MAM precipitation modes responded differently to the Pacific ENSO, Atlantic and Indian Oceans. However, the second mode apparently was not well related to the global SST features. Meanwhile, EOF 3 showed an indirect relationship with the Pacific while an Atlantic Multidecadal Oscillation (AMO)-like feature captured in the North Atlantic was identified as

directly linked to the mode. The composite analysis revealed that divergent circulations and the centers of action at 200hPa level varied on the monthly, bimonthly and seasonal timescales. The distinction of the circulation patterns were based on their strengths, locations, and spatial extents. Similar observations were made on the combined timescale. The multiple linear regression model outputs between the rainfall modes and the climate indices, revealed the R^2 values ranging between 0.0-0.4, 0.01-0.3, 0.01-0.25 and
0.02-0.3 for monthly, bimonthly, seasonal and combined timescales respectively. On all the timescales, the highest R^2 values were recorded in January, December and May for EOF 1, EOF 3 and EOF 4 respectively. This is suggestive that the East African long rains variability is greatly modulated by global climate features on a monthly timescale. Overall, the findings provide useful prediction information required for improving capacity to adaptive climate change impacts.

ACKNOWLEDGMENTS

I give God Almighty all the Glory. My God has been faithful to me. It is indeed the Lord who gives wisdom and from His mouth cometh knowledge and understanding. I give God praise and honour for how far He has brought me.

I would like to express my profound gratitude to my supervisor Dr. I. K. Tetteh for his directions over the years. He has indeed been a great mentor. I am also grateful to Dr. L. K. Amekudzi and Prof K. Preko for their concern and encouragement. My sincere gratitude goes to my parents, Mr. K. Appiah-Badu and Mrs. Juliana Cobbina for their financial support and encouragement.

Finally, I appreciate the efforts from my family and friends in the successful completion of this work. May God increase all of you even as your days increase.

God bless you all.

TABLE OF CONTENTS

LIST OF TABLES

LIST OF FIGURES

CHAPTER ONE

INTRODUCTION

1.1 Background

Effective planning and execution of climate change adaptations is expected to bring new lease of hope to the affected societies confronted with the negative tendencies of climate change. Success of this activity to some extent is contingent on a good understanding of climate variability and change. On the global scale, eclectic adaptation strategies have evolved, or continue to evolve, in response to the specific menace created by climate variability and change, irrespective of the background driving force — natural or anthropogenic.

Interestingly, East Africa, one of the most vulnerable regions to global environmental change, has benefited from implementations of adaptation strategies derived directly or indirectly from a plethora of scholarly research efforts (e.g., Ropelewski and Halpert, 1987; Ogallo, 1988; Barnston and Ropelewski, 1992; Funk, 2012; Smith and Semazzi, 2014). Such efforts have been complemented by, for example, operationalization of seasonal forecasts of long (March-April-May: MAM) and short (October-November-December: OND) rains by the Greater Horn of Africa Climate Outlook Forum (GHACOF).GHACOF is organized by the IGAD (InterGovernmental Authority on Development) Climate Prediction and Application Centre (ICPAC), Nairobi, Kenya. It typically uses consensus forecasts, which derive inputs from empirical climate research outcomes. Empirical climate research on rainfall variability has documented the role of interannual variability of local and remote forcings of the East African seasonal climate, which are key precursors used in operational seasonal climate prediction scheme.

1.2 Problem Statement

Interannual variability has chiefly focused on climatic and dynamic features in the annual and seasonal cycles that govern the region's long and short rainfall variability. Three important ocean-atmosphere temporal scales, which may be identified in the interannual variability and have great influence on the region's seasonal rainfall patterns, are monthly, bimonthly, and seasonal timescales (e.g. Latif *et al.*, 1999; Saji *et al.*, 1999; Marchant *et al.*, 2006; Smith and Semazzi, 2014). As a general summary from these collections, the rainfall variability over the East African region points to the Pacific ENSO and Indian Ocean, and to a lesser extent the Atlantic Ocean, and their associated atmospheric dynamics. These, however, do not rule out orographic/land surface forcing and vegetation feedbacks or dynamics of the region's climate variability.

Generally, the sub-Saharan African countries are lagging far behind the advanced counterparts in efficient utilization of adaptation technologies commonly applied to ameliorate the detrimental effects of climate variability and change (Washington *et al.*, 2006; Akponikpe` *et al.*, 2010; Ford *et al.*, 2015). These are due to many constraints such as the lack of adaptive capacities and capital resources. These constraints are not the focus of this current study. However, a critical issue that warrants consideration is the need for adaptation strategy enhancement that would rely on new climate information for sustainable resilience to climate shocks. The climate information should unequivocally describe or contain features—behavior, characteristics and evolution at different timescales, as they interact with other complex climate systems or subsystems.

1.3 Justification

In spite of the numerous studies investigating the ocean-atmosphere features associated with the east African climate, empirical analysis of the region's climate variability in the global context, would further contribute to a better predictive understanding of the region's seasonal climate. This will also provide a validation framework for dynamical model outputs. However, few of such empirical studies have focused on the link of the global ocean surface and their associated atmospheric patterns, on monthly, bimonthly, seasonal and combined timescales to the dominant modes of long rains variability.

This study therefore seeks to provide an update on the region's seasonal climate variability. This would improve predictive understanding of the region's rains, on the premise that current numerical and statistical model predictive skills are far from perfect. Also, it would contribute to effective adaptation management, especially of sustainable agriculture, climate-induced health problems, flood and drought disasters, and other climate-sensitive socioeconomic problems.

1.4 Objectives

1.4.1 Main Objective

This study seeks to analysis global climate on multiscale and its implications for climate change adaptation over East Africa during the climatologically prominent ENSO phase.

1.4.2 Specific objectives

- To carry out an analysis of monthly evolution of global ocean-atmosphere features and their relationship to the dominant modes of MAM seasonal rainfall variability.
- To analyze bimonthly global ocean-atmosphere features and their relationship to the dominant modes of MAM seasonal rainfall variability.

- To carry out an analysis of seasonal evolution of global ocean-atmosphere features and their relationship to the dominant modes of MAM seasonal rainfall variability and
- To analyze the relationship between the global ocean-atmosphere features and the dominant modes of MAM seasonal rainfall variability on a combined timescale.

1.5 Structure of the Thesis

The chapter two consist of previous work done on the region. The chapter also contains an overview of the techniques used in this current study.

The chapter three was devoted to the data and methods that were used in the study, which include a brief description of the application of the techniques to be used and the analysis method.

The fourth chapter describes the results and discussion. This includes the oceanatmosphere features analysed on each of the timescale (i.e. monthly, bimonthly and seasonal) and It will also include the results of the combined impacts of the oceanatmosphere phenomena on the long rains. The implications for climate change adaptation are also contained in this chapter.

The final chapter presents the conclusions made from the study and recommendations for future studies.

CHAPTER TWO

2.0 Literature Review

The implementation of appropriate climate change adaptation strategies is contingent on a good understanding of climate variability. This chapter is focused on research carried on the climate of the study area. It presents various studies conducted into the phenomena responsible for the variability of the East African climate.

2.1 ENSO and East African Rainfall

The ENSO phenomenon which is as a result of the atmospheric and Oceanic interaction in the Pacific (Chiew *et al.*, 1998) has been established as the dominant mode contributing to east African rainfall variability (Ogallo, 1988; Hastenrath *et al.*, 1993).

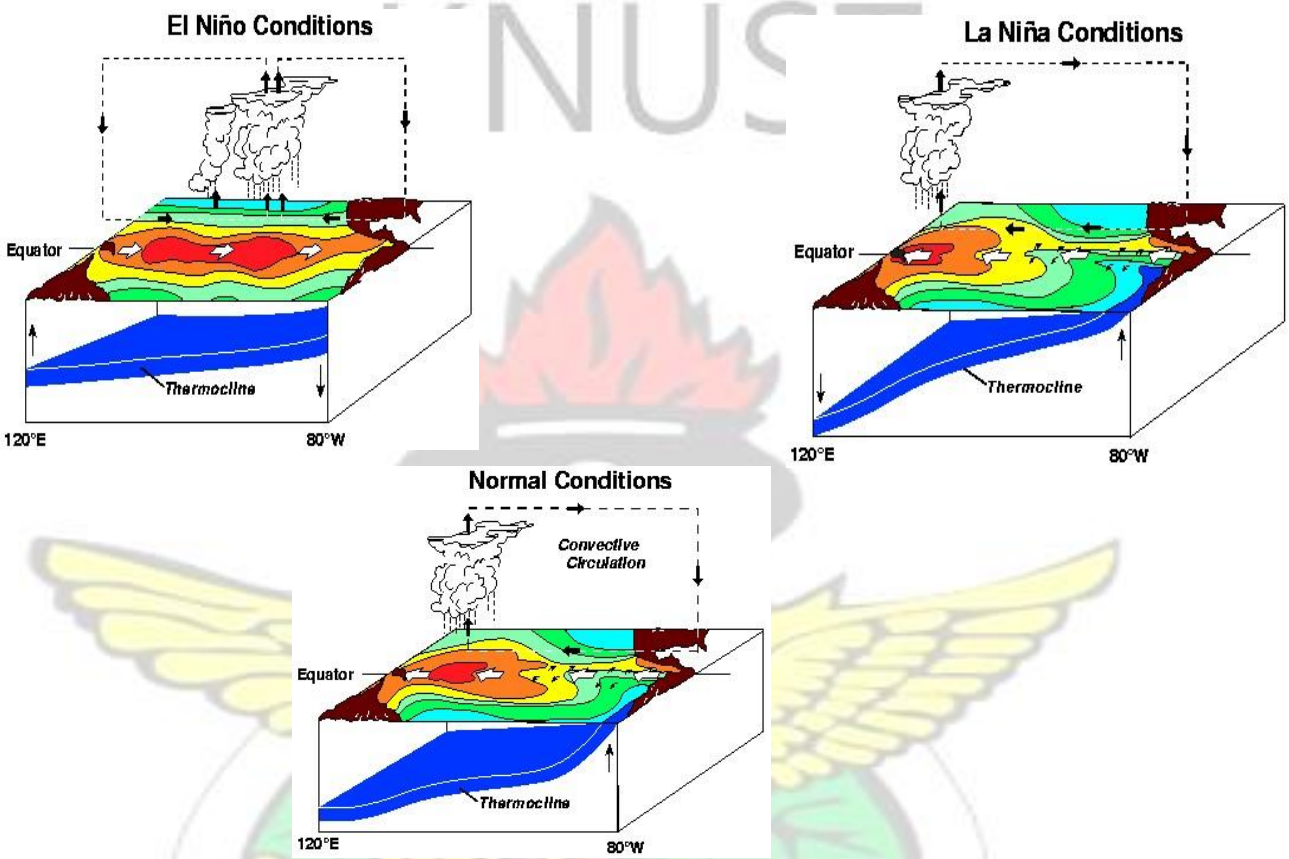

Figure 2.1 Schematic diagrams of El Niño, La Niña and normal conditions in the Pacific.

(Source: http://www.pmel.noaa.gov/tao/elnino/nino_normal.html#normal)

With respect to the normal conditions, high and low pressures are observed over the east and west Pacific respectively. During this condition, the prevailing trade winds and Ekman transport causes upwelling along the coast of western South America. The thermocline in the western Pacific as shown in Figure 2.1 deepens when the sea level increases. During El Niño conditions, warm surface water develops off the coast of Peru and Ecuador. This extends northward to Central America and Mexico. This phenomenon therefore causes atmospheric pressure to decrease in Eastern Pacific and weakens the trade winds in the east Pacific. The La Niña conditions are the reverse of the El Niño. During the period of this condition, strong trade winds are spotted in the Eastern Pacific. Generally, the El Nino phase enhances rainfall over East Africa whilst the La Nina suppresses the region's rainfall.

2.2 East African Climate Variability

The variability of the East African rainfall has been investigated by many researchers. In most of the studies conducted over the region, various phenomena were investigated on different timescales in relationship to the variability of the region's climate (e.g. Ogallo, 1988; Ropelewski and Halpert, 1987; Nicholson 1996; Barnston and Ropelewski, 1992; Saji *et al.,* 1999).

The Greater Horn of Africa which includes: Burundi, Djibouti, Eritrea, Ethiopia, Kenya, Rwanda, Somalia, Sudan, Tanzania and Uganda experiences rainfall patterns that are influenced by the fluctuations of the Inter-Tropical Convergence Zone (ITCZ). The ITCZ is a broad low-pressure area next to the equator where northeasterly and south-easterly trade winds converge. East African countries experiences different rainfall patterns due to the variability of the onset, duration and intensity of the rainfall. The variability of the East African rainfall on various timescales has been linked to various atmospheric and oceanic phenomena. One of such is the Madden-Julian Oscillation (MJO) which is as a result of coupled ocean-atmosphere phenomenon characterized by eastward progression of tropical convection located at the western part of the Pacific. This accounts for most of the weather variability's that occur in the tropics at intraseasonal time scales (10-90 days).

Berhane and Zaitchik (2013) investigated the impacts of the MJO on long rains on intraseasonal time scale. The study made use of Tropical Rainfall Measuring Mission

(TRMM) with a resolution of $0.25^0 \times 0.25^0$ and the atmospheric field was also sourced from NCEP. Comparing the associations of the MJO and daily precipitation records, a significant variation of the effect of the MJO on the long rains were established. The study considered the effect of the MJO on the separate months of the long rains (i.e. March, April and May). They found out that the influence of the MJO on the last month of the long rains (May) was shown to be greater as compared to the first month (March) of the season with the middle month (April) recording no effect of the MJO.

Pohl *et al.* (2005) also studied the Influence of the MJO on the rainfall variability of the East African region on intraseasonal time-scale (considering March–May). Daily rainfall-gauge data over 1971 to 1995 and data on atmospheric fields including; vertical velocity, relative humidity, temperature and the wind components were used in the study. They showed that the fluctuations of the MJO greatly affected the long rains season. One very important revelation the study made was that, on the synoptic to seasonal timescales, the variability of the rainfall showed distinct variation in the extratropics. Meanwhile, the rainfall variability exhibited similar patterns tropics.

Latif *et al.* (1999) studied the role played by the Indian Ocean Sea Surface temperature during the December–January 1997/98 rainfall anomalies observed in east Africa. According to their study, the two months (i.e. December and January) were chosen for the study because rainfall anomalies over the study area were severe during that period in 1997/98. The ECHAM3 atmospheric general circulation model was employed in the study. Using the model at a resolution of ($2.8^o \times 2.8^o$), they established a relationship between the rainfall over the eastern equatorial Africa and the Indian Ocean Sea Surface Temperature (SST) anomaly. An experiment conducted in the study on the response of rainfall to the Indian Ocean anomaly was positive. The conclusion they made was that the Indian Ocean sea surface temperatures played a major role in the floods experienced over eastern equatorial Africa during that period

(December-January 1997/98). Ogallo (1989) investigated the effects of ENSO on East African rainfall with a focus on the long rains (MAM). The study made use of monthly rainfall data from about 136 rainfall stations between the period1961-1990. Based on the North *et al.* (1982) sampling technique, the first three EOF modes were retained. It was shown that the first EOF associated with the MAM rainfall pointed at the movement of the ITCZ as a major factor that has an influence on the rainfall mode. Also, they revealed an interaction between the extra-tropical and tropical weather systems as playing major roles in the modulation of the East African long rains. The second EOF accounted for 10.8% of the total variance of the MAM rainfall season. During the ENSO onset years, above normal rains were shown over the coastal areas during the season but post-ENSO years were revealed to be associated with dry conditions especially, over parts of southern Tanzania. Moreover, Lyon and DeWitt (2012) identified the changes in SST in the tropical Pacific as a factor that influences the East African rainfall. They pointed out a decline in the MAM rainfall linked to the variations in the tropical pacific SST. EOF analysis technique was used in their study in establishing the dominant modes with the first EOF mode showing a 16.3% variance.

Smith and Semazzi (2014) in a recent study estimated the role of the dominant modes of precipitation variability in the modulation of the hydrology over Lake Victoria. An EOF analysis was performed over East Africa using CRU data for 1950-2012 during the long rains season. The first EOF mode accounted for 27.5% of the total variance and according to the study. The source of this mode was linked to the SSTs off the coast of Africa specifically between South Africa and Madagasca. A similar result was shown by Williams and Funk (2011). In their study of the trend of the dryness of the East

Africa long rains, they linked this condition to the warming of the Indian Ocean sea surface temperatures (SSTs) which was consistent with the findings of Latif *et al.* (1999). But a correlation between the second mode and global SSTs showed no clear signal. They further suggested the variability explained by the modes may be linked to the movement of the ITCZ and moisture convergence from the Indian Ocean. Furthermore, an investigation into the dynamics through which circulation and hydro climatic anomalies associated with South Pacific circulation anomalies and its effect on modulating east African rainfall has been carried by Mchugh (2004). The study employed NCEP/NCAR reanalysis data (Kalnay *et al.*, 1996) for the period 1948–2002, Global gridded sea level pressure (SLP) monthly precipitation datasets. A significant source of the decrease in long rains observed by the study was attributed to the northeasterly trade winds towards the Atlantic Ocean. The study identified established the effect of the north easterly trade winds to be responsible for the prevention of the unstable moist air masses form the western side that contribute to the rainfall over the East African region.

2.3 Overview of the Techniques

2.3.1 Empirical Orthogonal Functions (EOF)

The Empirical Orthogonal Functions (EOF) analysis is a tool used to reduce large amount of data into a small number of representative patterns that capture a large fraction of the variability with spatial patterns that resemble the observed data. This technique has been used by several researchers in establishing the temporal and spatial variability of different atmospheric variables over East Africa (e.g. Atwoki, 1975; Ogallo, 1980, 1983; Nyenzi, 1990; Smith and Semazzi, 2014, Mchugh, 2006). The first step is to form a matrix from the observation and the time mean of each time series is removed so that each column has zero mean and standard deviation equal to

1 (i.e. standardized).

Consider a space-time field $X(t,s)$.

$$X(t,s) = \sum_{K=1}^{M} C_K(t)\, u_k(s) \tag{1}$$

Where; t is the time position, s is the spatial position , M is the number of modes contained in the field and $U_k(s)$ represents the function of space and finally $C_k(t)$ is the function of time.

Suppose that a gridded data set composed of a space-time field $X(t, s)$ representing the value of a field X (e.g. SLP, SST etc) at time t and spatial position s. The value of the field at discrete time t_i grid point is denoted by;

$$x_{ij} \text{ where } i = 1.....n \text{ and } j = 1....p$$

The observed filled is represented by the data matrix as:

$$X = (x_1, x_2, \ldots\ldots, x_n)^T = \begin{pmatrix} x_{11} & x_{12} & \ldots\ldots & x_{1p} \\ x_{21} & x_{22} & \ldots\ldots & x_{2p} \\ x_{n1} & & \ldots\ldots & x_{np} \end{pmatrix} \tag{2}$$

Where $x_1 = (x_{t1}, x_{t2}, \ldots\ldots\ldots, x_{tp})^T, t = 1.....n$ representing the value of the field at time T.

Times average of the field $(\bar{x}_i)$ at the i[th] spatial grid point is given by:

$$\bar{x}_i = \frac{1}{n} \sum_{k=1}^{n} x_{ki} \tag{3}$$

The climatology of the field is defined by:

$$\bar{x} = \left(\bar{x}_{.1}, \ldots\ldots, \bar{x}_{.p}\right) = \frac{1}{n} 1_n^T X \qquad (4)$$

The anomaly field from the climatology is therefore defined in matrix form as:

$$X' = X - 1_n \bar{x}$$

Since $\bar{x} = \frac{1}{n} 1_n^T X$

Therefore

$$X' = X - 1_n \frac{1}{n} 1_n^T X$$

$$= \left(I_n - \frac{1}{n} 1_n 1_n^T\right) X \qquad (5)$$

I_n = the identity matrix.

The covariance matrix is defined as $S = \frac{1}{n} X'^T X'$ (6)

Using the decomposition in singular values of X so that

$$S = U \Lambda V^T V \Lambda U^T \qquad (7)$$

$$S = U \Lambda^2 U^T \qquad (8)$$

Dividing the total variance, which is the sum of the squared singular values by the trace, shows the percentage contribution U_i of each mode of σ_i^2

$$U_i = \frac{\sigma_i^2}{\sum_{i=1}^{n} \sigma_i^2}$$

The independent modes of variability in U, associated with nonzero singular values, via the singular value decomposition (SVD) of the data matrix are called Empirical Orthogonal Functions.

The variance is the measure of the sparsity among the data. A small variance indicate how close the data is to each other (i.e. expected value) whilst a high variance indicates how the data are spread out from each other. The fundamental aim of the EOF is to identify preferred patterns within many variables that also explain high variance. The EOFs (eigenvectors) are obtained by solving the eigenvalue problem. The eigenvectors (EOFs) are the eigenmodes of S and the eigenvalues λ_j expresses the amount of variance in each orthogonal eigenmode.

The total variance in the data as a result of the sum of the eigenvalues is expressed as:

$$\text{Variance} = \sum_{j=1}^{s} \lambda_j \tag{9}$$

Each EOF loading pattern (eigenvector) that is identified explains a certain percentage of the total variance of the grid points over time. The first EOF mode identified shows the most variance. The set of outcomes from the EOF analysis are firstly, it provides a set of EOF patterns (eigenvectors) and secondly a set of corresponding eigenvalues and amplitudes.

The North et al.'s (1982) rule thumb is applied to retain the most significant modes that contributed in the total explained variance.

The rule says that the sampling error $\delta\lambda$ given as;

$$\delta\lambda \approx \lambda\left(\frac{2}{N}\right)^{\frac{1}{2}} \tag{10}$$

The sample size N of a specific eigenvalue λ should be smaller than the spacing between the particular eigenvalue λ and its neighbouring eigenvalue. From the test of this rule, the first four EOF modes were retained.

CHAPTER THREE

3.0 Data and Methods

3.1 Study Area

The East African region which is also known as the Greater Horn of Africa (GHA) is the easternmost extension of the African continent separating the Gulf of Eden from the Indian Ocean (Figure 2). The GHA is bordered by the Red Sea, Gulf of Eden and the Indian Ocean. The countries constituting the GHA are Eritrea, Djibouti, Ethiopia, Somalia, Kenya, Tanzania, Burundi, Sudan, Rwanda and Uganda. GHA has an estimated population of about 300,596,772, whose agricultural activities are largely dependent on rainfall. The River Nile and other tributaries are major hydrological resources over the region for their socio-economic growth. The region is the home of Africa's largest natural lake: Lake Victoria, which is the source of water for most people in the region. One of the world's largest salt lakes, Lake Turkana is also located in the region.

The majority of the Greater Horn of Africa (GHA) region experiences a bimodal rainfall pattern which is linked to the progression of the intertropical convergence zone (ITCZ) across the region (Bowden and Semazzi, 2007). The two rainfall patterns are the March-May (long rains) and October-December (short rains). The long rains are the main rainy season which results in heavy rains over a longer period of time whilst the short rains are less intense over short period of time.

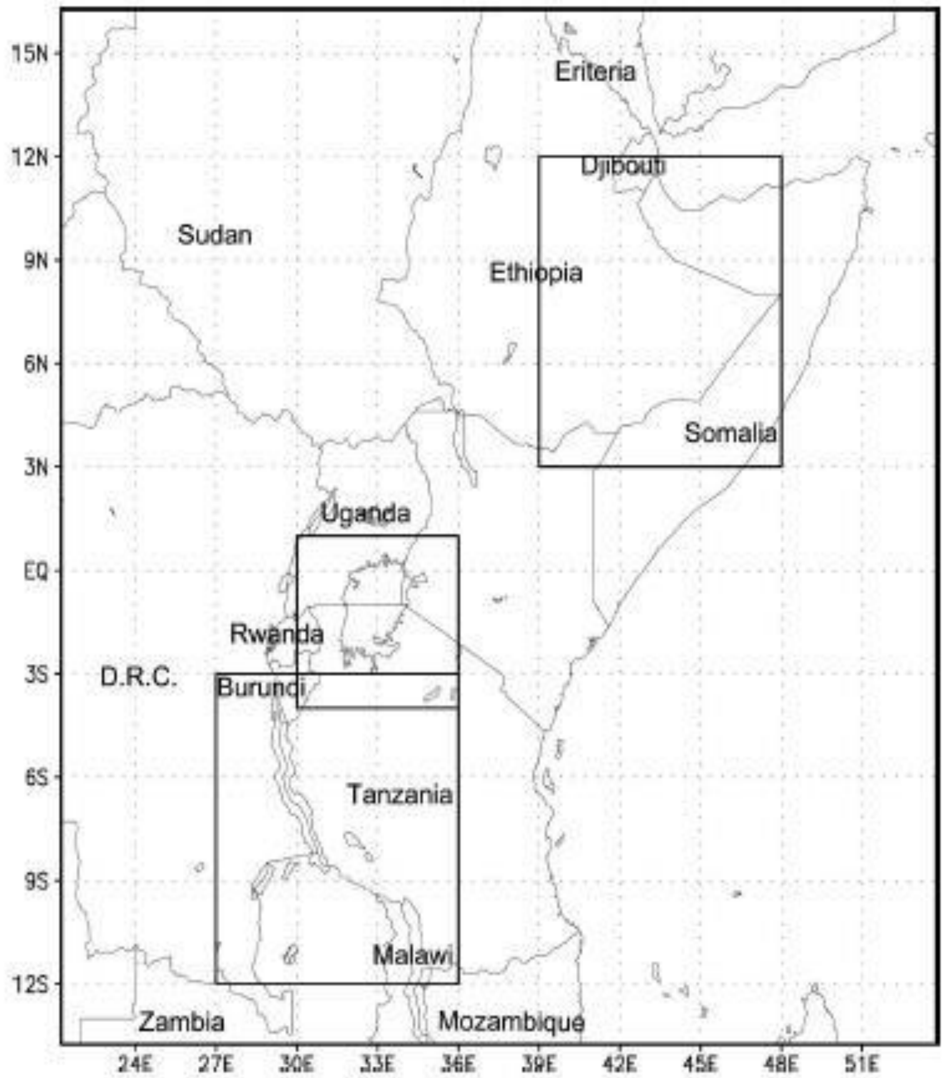

Figure 3.1 Map of Greater Horn of Africa. (Bowden and Semazzi, 2007)

3.2 Data Sources

3.2.1 NCEP-NCAR Reanalysis Data

The horizontal winds at 200 hPa level utilized in this study were sourced from the National Centers for Environmental Prediction-National Center for Atmospheric Research (NCEP-NCAR) reanalysis (Kalnay *et al.*, 1996). The data, covering periods from January 1948-March 2016 on a global grid of 2.5^o x 2.5^{o}spatial resolution, are continuously updated. On the monthly timescale, the specific data used covers:
December, January, February, March, April and May (D, J, F, M, A and M). The bimonthly timescale made use of data covering five consecutive two month period (December-January, January-February, February-March, March-April and April-May (DJ, JF, FM, MA and AM). On the seasonal timescale wind data covered, four consecutive three month period (December-February, January-March, February-April and March-May (DJF, JFM, FMA and MAM). On all the time-steps, data from 19502007 was used for December and data covering 1951-2008 for January through to May. This data can be accessed at http://www.cdc.noaa.gov/cdc/reanalysis/.

3.2.2 Precipitation Data

The precipitation dataset, with spatial resolution of 0.5^o×0.5^o resolution, was sourced from Climatic Research Unit (CRU). The data was recorded from about 4000 weather stations worldwide (land only) and covered the periods from January 1901 to December 2012 (Harris *et al.,* 2014). This dataset is periodically updated. This precipitation data is available at https://crudata.uea.ac.uk/cru/data/precip/.

3.2.3 Sea Surface Temperature Data

Extended Reconstructed SST (ERSST; Smith and Reynolds, 2004) data was used. The dataset extended from January 1854 to March 2016, and has a spatial resolution of 2.0^o x 2.0^{o}on a global grid. This dataset is also continuously updated.

3.2.4 Teleconnection Indices

The teleconnection indices used for this study are Nino 4, Nino 3.4, Nino 3, Nino 1+2, unsmoothed Atlantic Multidecadal Oscillation (AMO), Southern Oscillation Index (SOI), Pacific North American Index (PNA), Tropical South Atlantic (TSA) and Tropical North Atlantic (TNA).

3.3 Methods

3.3.1 Analysis Domain

The East African domain has been described in various dimensions under different studies (e.g. Camberlin and Philippon, 2001; Black, 2004; McHugh, 2006). McHugh (2006), referred to the east Africa domain covering 10^{o}N to 20^{o}S and 20^o to 40^{o}E. Camberlin and Philippon (2001) proposed a seasonal prediction model based on the atmospheric patterns associate the east African long rains. Their investigation into the long rains considered east Africa in the region 10^{o}N to 20^{o}S and 29^o to 50^{o}E. In this study, the east African region considered was confined to the domain used by Bowden and Semazzi (2007). The region covers 13.75^{o}S to 16.25^{o}N and 21.25^o to 53.75^{o}E. This region is the home of about thirteen countries including: Ethiopia, Mozambique, Eritrea, Djibouti, Somalia, Sudan, Uganda, Rwanda, Democratic Republic of Congo, Burundi, Tanzania, Malawi and Zambia.

3.3.2 Construction of Standardized Global SST and Upper Level Anomalies To put all data into the same proportion with one another, the precipitation, SST and the horizontal wind (200hPa) datasets were standardized to a mean of zero and a variance of one. The technique of normalization or standardization has been employed by many researchers. Janowiak (1988) normalized rainfall data by computing the average departure from the annual mean and expressed in percentage. In the study of the investigation of interannual rainfall variability in Africa (Janowiak, 1988), the normalization of the precipitation data was based on the equation:

$$100\% \times \frac{1}{N}\sum_{i=1}^{N}\left(\frac{\bar{X}_i - \bar{X}}{\bar{X}}\right) \qquad (3.1)$$

Where $\bar{X}i$, is the annual mean for any year at a location and $\bar{X}$ is the grand mean for all N years for that site.

Instead of the percentage average departure from the annual mean, this current study adopts the standardization technique. The two techniques (i.e. normalization and standardization) produce similar results. However, standardization is mostly preferred as it provides distinct information about each data point and the number of standard deviations from the average that the data lies in the normal distribution curve.

Following this, the standardization of the data was carried out by averaging the monthly fields before standardization by subtracting the averages from each grid point and dividing by the standard deviation of all the data points for six consecutive onemonth period (December, January, February, March, April and May (D, J, F, M, A and M). This rolled over from 1950-2007 for December to 1951-2008 (from January through to May). For the bimonthly it was first done by averaging the bimonthly fields before standardization for five consecutive two months period (DecemberJanuary, January-February, February-March, March-April and April-May (DJ, JF, FM, MA and AM). This rolled over from 1950-2007 for December to 1951-2008 (from January through to May). The seasonal timescale was carried out by averaging the seasonal fields before standardization by subtracting the averages from each grid point and dividing by the standard deviation of all the data points for four consecutive three months period (December-February, January-March, February-April and March-May (DJF, JFM, FMA and MAM). This rolled over from 1950-2007 for December to 1951-2008 (from January through to May). From the standardized data n the monthly, bimonthly and seasonal timescales, the combined SST and wind data used in the combined timescale analysis are the averages of the timesteps (i.e. monthly, bimonthly and seasonal) where SST features were captured. The new time steps (i.e. combined timescale) were December, December to January, December to February {D, DJ and DJF}, January, January to February, January to March {J, JF and JFM}, February, February to March, February to April {F, FM and FMA}, March, March to April, March to May {M, MA and MAM} and April, April to May {A and AM}.

The precipitation, winds and SST datasets were therefore standardized based on the following equation:

$$X_{i,1} = \frac{X_i - \bar{X}_s}{\sigma_{X,s}} \qquad (3.2)$$

Where

X_i = Each data point i

$\bar{X}_s$ = The average of all the sample data points

$\sigma_{X,s}$= The sample standard deviation of all sample data points

$X_{i,1\sigma}$= The data point i standardized to 1σ

The essence of standardizing the data was to remove outliers and to bring them into proportion with one another. This standardized data which is indicative of the number of standard deviations from the average shows how the data sets (SST, precipitation and wind) deviate from the normal distributions.

3.3.3 Construction of Standardized Indices

All the indices used in this study were standardized based on Equation 3.2.

3.3.3.1 Construction of Monthly Standardized Indices

For the monthly timescale, the mean and standard deviation of indices were constructed from 1951-2008 for January to May before standardizing based on the equation described in section 3.2. Except for December where the mean and standard deviations is constructed from 1950 to 2007.

3.3.3.2 Construction of Bimonthly Standardized Indices

First of all, the mean of both months was calculated for JF, FM, MA and MA from 1951 to 2008 before the new mean was constructed from the average of each year. The standard deviation was also constructed from the separate averages. Similar approach was used for DJ except for data covering 1950-2007 for December and 1951-2008 for January before it was standardized based on Equation 3.1.

3.3.3.3 Construction of Seasonal Standardized Indices

Similar approach used for bimonthly was used to construct the seasonal indices.

Except for DJF where data covering 1950-2007 for December and 1951-2008 for January and February, the rest of the time steps (i.e. JFM, FMA and MAM) made use of data spanning 1951-2008. In this case, the mean of each month in each year was constructed before the new mean was derived from it. The standard deviation was also constructed from the averages before it was standardized.

3.3.3.4 Construction of Combined Standardized Indices

Due to the standardized data on the monthly, bimonthly and seasonal timescales, the combined indices are the averages of the significant indices captured on all the timescales (i.e. monthly, bimonthly and seasonal).

3.3.4 Empirical Orthogonal Function (EOF) Analysis of MAM Rainfall

The primary mode of investigation applied in investigating the variability of the East African rainfall to identify the dominant modes is the standard EOF technique (Schreck and Semazzi, 2004; Wilks, 2006; Hannachi *et al.*, 2007), based on a correlation matrix. This technique has been adopted by many authors in investigation different climatic variables (e.g. Mistry and Conway, 2003; Schreck and Semazzi, 2004; McHugh, 2004; Funk *et al.*, 2014). In this study, the same technique has been employed to decompose the CRU precipitation data from 1951-2008 into spatially and temporally coherent patterns. The time frame considered was based on the framework developed by Tetteh (2012), for West African climate which has been extended to other sub-Saharan regional climates to investigate different hypotheses. The North *et al.* (1982) rule thumb was applied to retain the first four modes.

3.3.5 Lagged Heterogeneous Grid Point Correlations between the Rainfall Modes and Standardized Global SSTs and Velocity Potential (Divergence) Computations

To identify the specific global SST sectors linked to the long rains over the East African region lagged heterogeneous grid-point correlations were computed between the rainfall modes and global SST. This approach was similarly applied to the horizontal winds in computing the divergent circulations associated with the long rains. The divergence was computed based on the following equation (Krishnamurti *et al.*, 1971):

$$V = k \times \nabla\psi + \nabla \chi \tag{3.3}$$

Where, ψ, χ and ∇ represent the stream function, velocity potential and divergence operators respectively. It should be noted that the first part ($\nabla\psi$) is not nondivergent.

Grid point correlation between the EOFs and global SST and winds were computed using GrADS 2.0.2.

3.3.6 Multiple Linear Regression Model

To statistically evaluate the relationship between the dependent variable (i.e. rainfall) and the independent variables (climate indices displayed in Table 2-5 for the timescales).

On the monthly timescale, the independent variables (predictors) regressed unto the rainfall modes, were about eight climate indices. Similar number was used on the bimonthly, seasonal and combined timescales.

CHAPTER FOUR

4.0 Results and Discussion

4.1 East African MAM Rainfall Variability

Figure 4.2 depicts the spatio-temporal patterns of the rainfall modes, in which four leading modes retained were based on the *delta-test* (North *et al.*, 1982). The leading four modes in the function spectrum (Figure 4.1) that were statistically separated and retained contributed to 34.2% of the total explained variance. The value signified low interannual variance of the long rains, which was consistent with previous studies (Ropelewski and Halpert, 1987; Ogallo, 1989). The respective contributions of precipitation EOFs 1, 2, 3, and 4 were 10.1%, 9.1%, 8.2%, and 6.8%. Interestingly, all their EOF time series (Figures 4.2e-h) demonstrated interannual variability but with differences in their amplitude of fluctuations. The precipitation patterns displayed distinct variations.

The spatial pattern of EOF 1 showed a bipolar pattern with positive weights located over the much of the southern sector and negative weights covering the northeast. The time coefficients of EOF 1 (Figure4.2b) exhibited interannual-like oscillations. The principal components of EOF 1 showed below normal rains in the years including 1957, 1962, 1963, 1977, 1981 and 1986. Meanwhile very intense drought conditions were recorded in 1951, 1967 and 1968. During 1973, 1984 and 2000, intense precipitation was recorded with above normal rains recorded in 1955, 1959, 1965 and 1994. A similar pattern was shown in a study that investigated the east African droughts (Funk *et al.*, 2014). In that study, the spatial pattern of the EOF 1 exhibited the same structure as seen in this current study. Intense droughts that were recorded in 1984 and 2000 were consistent to this study. Meanwhile other years that recorded droughts in their study were 2004, 2008, 2009 and 2011. The difference in the years of intense drought in their study and this current study may have been as a result of the year range considered in both studies. While we analysed the precipitation pattern from 1951-2008, their study focused on 1981-2013. Another contributing factor to the differences in the temporal patterns could be the domain for the study. The east African region defined in their study covered 13^oS to 20^oN and 25^o to 55^oE.

A dipole structure was also noticed in the EOF 2 (Figure 4.2c). The spatial pattern was nearly opposite to the EOF 1 with positive loadings located over the northern portion and negative loadings shown within 3^0S to 15^0S. The time coefficient associated with the second EOF (Figure 4.2d) depicted interannual oscillation. It also showed intense drought in 1961 and 1986 with high rains recorded in 1963. The EOF 3 spatial loadings (Figure 4.2e) was characterised with positive weights over the western and southern boundaries covering the countries including Tanzania, Burundi and parts of Malawi with remaining parts dominated by negative weights. The time coefficients of this mode also showed interannual oscillations. Generally, the EOF 4 loadings was characterised with negative weights almost over the entire region with localised positive weights located over Ethiopia, Somalia and Djibouti. The time coefficients exhibited interannual oscillation.

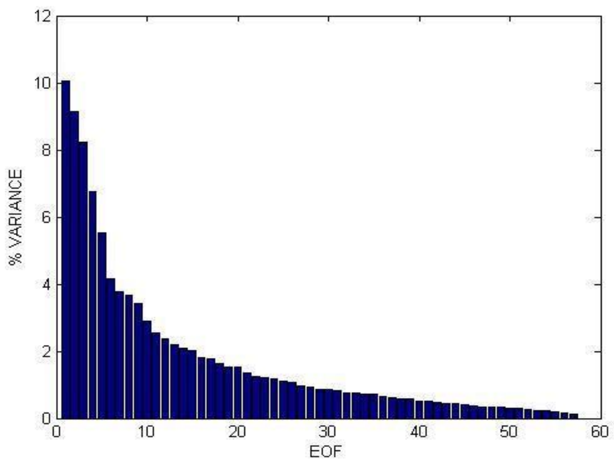

Figure 4.1-Eigenvalue histogram for the eastern Africa EOF rainfall analysis

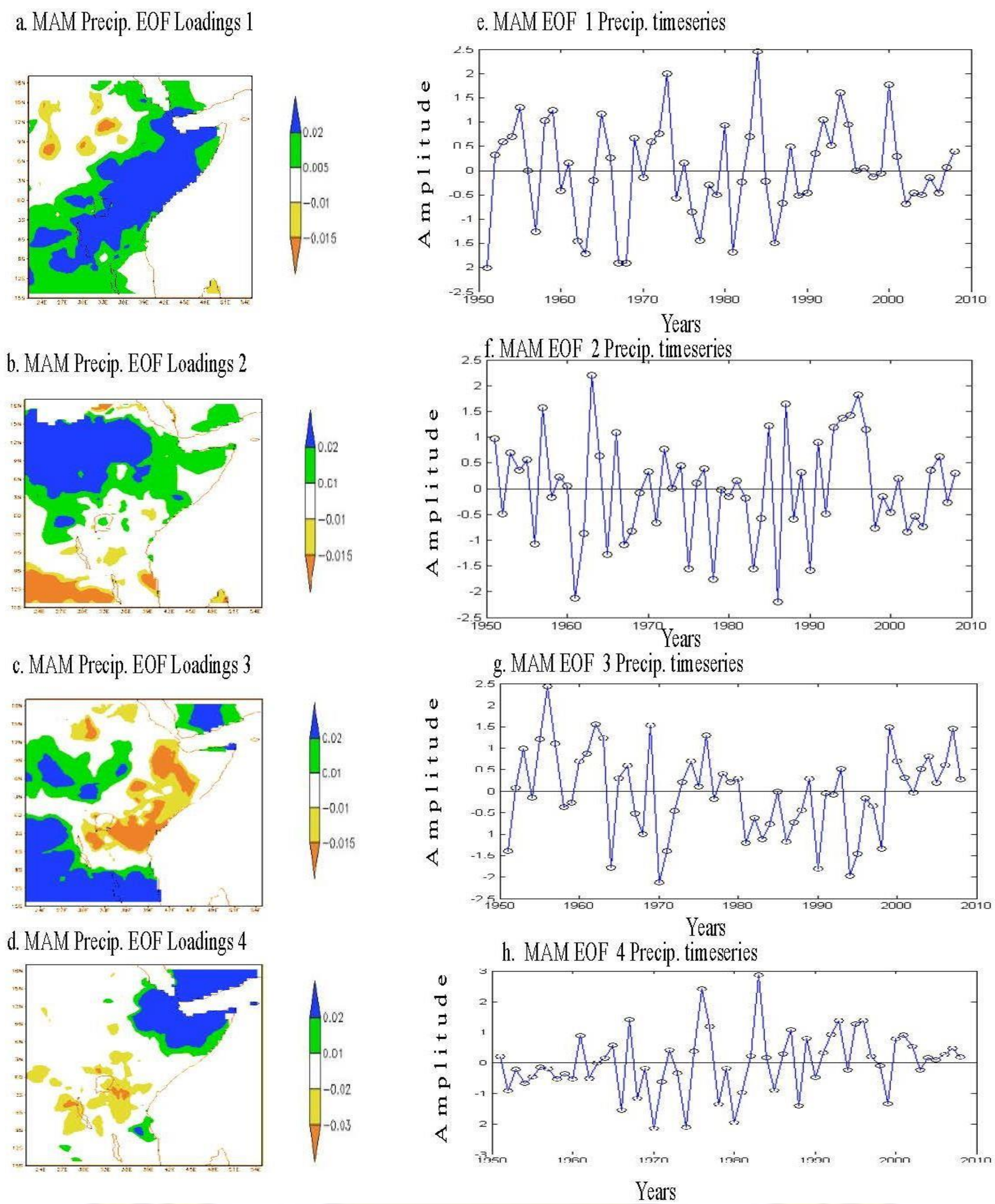

Figure 4.2-Dominant modes of long rains(MAM) variability over East Africa. Panels a-d are the spatial patterns of the rainfall with corresponding legends. Blue and green shades depict areas of above-normal rainfall while all other shades correspond to below-normal rainfall. Panels e-h are the corresponding timeseries of the rainfall patterns.

4.2 Global SST and MAM Precipitation Covariability

This section presents the results of grid point correlation between the rainfall modes and global SST. Lagged heterogeneous grid point correlations were computed between each of the leading rainfall modes and monthly, bimonthly and seasonal global SSTs. The computations were done on time lags from Dec (1950-2007) and Jan to May (1951-2008), centered on MAM rainfall season. The combined timescale consists of the averages of the three timescales where SST signals were detected.

The boundary conditions of the ocean surface among other factors drive atmospheric circulations, including rainfall patterns, beyond weather timescale. In this study as shown above, four dominant MAM seasonal rainfall modes were identified. The spatio-temporal features were distinct but similar to earlier studies (e.g. Smith and Semazzi, 2014). Several factors are known to contribute to MAM rainfall variability.
Indeje *et al.*(2000) reported that local factors over the region played an important role. In a spatially remote sense, ENSO has been found to be the prime driver of the interannual variability of the region's rainfall (Nicholson and Entekhapi, 1986; Ogallo, 1989).In this section, it is revealed that even though the precipitation temporal patterns displayed low interannual variance (Ogallo, 1989), their relationships
(displayed in the tables 4.1) with global SST distributions were distinct.

EOF 1 vs. Prominent Global SST Features

MONTHLY/SST FEATURES	BIMONTHLY/SST FEATURES	SEASONAL/SST FEATURES	COMBINED FEATURES
D- Pacific ENSO- Niño 3 (5N-5S, 150W-90W), Niño 3.4(5N-5S, 170-120W) , Niño 4(5N-5S, 160E-150W), Niño 1+2 (0-10S, 90W-80W), PNA	**DJ-** Pacific ENSO- Niño 3 (5N-5S, 150W-90W), Niño 3.4(5N-5S, 170-120W), Niño 4(5N-5S, 160E-150W), Niño 1+2 (0-10S, 90W80W), PNA, SOI	**DJF-** Pacific ENSO- Niño 3 (5N-5S, 150W-90W), Niño 3.4(5N5S, 170-120W), Niño 4(5N-5S, 160E-150W) , PNA, TSA, SOI	**D, DJ, DJF**
J- Pacific ENSO- Niño 3 (5N-5S, 150W-90W), Niño 3.4(5N-5S, 170-120W), Niño 4(5N-5S, 160E-150W) , TSA, PNA, SOI	**JF-** Pacific ENSO- Niño 3 (5N-5S,150W-90W), Niño 3.4(5N-5S, 170-120W), Niño 4(5N-5S, 160E-150W), PNA, SOI	**JFM-** Pacific ENSO- Niño 3 (5N-5S, 150W-90W), Niño 3.4(5N5S, 170-120W), Niño 4(5N-5S, 160E150W), SOI, PNA, TSA	**J, JF, JFM**
F- Pacific ENSO- Niño 3 (5N-5S,150W-90W), Niño 3.4(5N-5S, 170-120W), Niño 4(5N5S, 160E-150W) , TSA, SOI, TNA (5.5N to 23.5N and 15W to 57.5W)	**FM-** Pacific ENSO- Niño 3 (5N-5S,150W-90W), Niño 3.4(5N-5S, 170-120W), Niño 4(5N-5S, 160E-150W), SOI, PNA, TNA (5.5N to 23.5N and 15W to 57.5W), TSA	**FMA-** Pacific ENSO- Pacific ENSO- Niño 3 (5N-5S, 150W-90W), Niño 3.4(5N-5S, 170120W), Niño 4(5N-5S, 160E-150W), SOI, TSA, PNA	**F, FM, FMA**
M- Pacific ENSO- Niño 3 (5N-5S,150W-90W), Niño 3.4(5N-5S, 170-120W), Niño 4(5N-5S, 160E-150W), PNA, TNA, SOI	**MA-** Pacific ENSO- Niño 3, Niño 4 and Niño 3.4, TSA, T Niño 3 (5N-5S,150W90W), Niño 3.4(5N-5S, 170-120W), Niño 4(5N-5S, 160E-150W), SOI, PNA, TNA, TSA	**MAM-** Niño 3 (5N5S,150W-90W), Niño 3.4(5N-5S, 170-120W), Niño 4(5N-5S, 160E-150W), PNA, TNA (5.5N to 23.5N and 15W to 57.5W)	**M , MA, MAM**
A- Pacific ENSO- Niño 3.4(5N-5S, 170-120W), Niño 4(5N-5S, 160E-150W),TNA (5.5N to 23.5N and 15W to 57.5W), TSA	**AM-** Niño 3 (5N-5S,150W90W), Niño 3.4(5N-5S, 170-120W), Niño 4(5N-5S, 160E-150W), PNA, TSA	________________	**A, AM**
M- TNA (5.5N to 23.5N and 15W to 57.5W)	____________________	____________________	**M**

Table 4.1. Global scale SST features related to East African MAM seasonal rainfall EOF 1 mode

EOF 2 vs. Prominent Global SST Features

MONTHLY/SST FEATURES	BIMONTHLY/SST FEATURES	SEASONAL/SST FEATURES	COMBINED FEATURES
D- NIL	**DJ**- NIL	**DJF**- NIL	**NIL**
J-NIL	**JF-** NIL	**JFM**- NIL	**NIL**
F- NIL	**FM-** NIL		**NIL**
M-NIL	**MA-** NIL	**MAM-** NIL	**NIL**
A- NIL	**AM**-NIL	_______________	**NIL**
M- NIL	_________________	_________________	**NIL**

Table 4.2. Global scale SST features related to East African MAM seasonal rainfall EOF 2 mode

EOF 3 vs. Prominent Global SST Features

MONTHLY/SST FEATURES	BIMONTHLY/SST FEATURES	SEASONAL/SST FEATURES	COMBINED FEATURES
D- Pacific ENSO— Niño 1+2 (010S, 90W-80W), Niño 3 (5N5S,150W-90W), Niño 3.4(5N-5S, 170-120W), Niño 4(5N-5S, 160E-150W) , AMO (45-60N, 6015W)and PNA (45-60N, 60-15W)	**DJ-** Pacific ENSO- Niño 3 (5N-5S, 150W-90W), Niño 3.4(5N-5S, 170-120W), Niño 4(5N-5S, 160E-150W), AMO (45-60N, 60-15W), PNA (45-60N, 60-15W)	**DJF-** Pacific ENSO- Niño 3 (5N-5S, 150W-90W), Niño 3.4(5N-5S, 170-120W), Niño 4(5N-5S, 160E-150W), AMO (45-60N, 60-15W), PNA (45-60N, 6015W)	**D, DJ, DJF**
J-Pacific ENSO- Niño 3 (5N5S,150W-90W), Niño 3.4(5N-5S, 170-120W), Niño 4(5N-5S, 160E-150W), AMO (45-60N, 60-15W)	**JF-** AMO (45-60N, 6015W)	**JFM-** Pacific ENSO- Niño 3 (5N-5S, 150W-90W), Niño 3.4(5N-5S, 170120W), Niño 4(5N-5S, 160E-150W), AMO (45-60N, 60-15W), PNA (4560N, 60-15W)	**J, JF, JFM**

F- AMO (45-60N, 60-15W)	**FM-** AMO (45-60N, 60-15W), PNA (45-60N, 6015W)	**FMA-** Pacific ENSO- Niño 3 (5N-5S, 150W-90W), Niño 3.4(5N-5S, 170120W), Niño 4(5N-5S, 160E-150W), AMO (45-60N, 60-15W), PNA (45-60N, 60-15W)	**F, FM, FMA**
M- AMO (45-60N, 60-15W), PNA (45-60N, 60-15W), Niño 4(5N-5S, 160E-150W)	**MA-** Pacific ENSO- Niño 3 (5N-5S, 150W-90W), Niño 3.4(5N-5S, 170-120W), Niño 4(5N-5S, 160E-150W), AMO (45-60N, 60-15W), PNA (45-60N, 60-15W)	**MAM-** Pacific ENSO- Niño 3 (5N-5S, 150W-90W), Niño 3.4(5N-5S, 170120W), Niño 4(5N-5S, 160E-150W), AMO (45-60N, 60-15W), PNA (4560N, 60-15W), SOI	**M , MA, MAM**
A- AMO (45-60N, 60-15W), PNA (45-60N, 60-15W)	**AM-** Pacific ENSO- Niño 3 (5N-5S, 150W-90W), Niño 3.4(5N-5S, 170-120W), Niño 4(5N-5S, 160E-150W), AMO (45-60N, 60-15W), PNA (45-60N, 60-15W), SOI	____________	**A, AM**
M- Niño 3 (5N-5S,150W-90W), Niño 3.4(5N-5S, 170-120W), Niño 4(5N-5S, 160E-150W), AMO (45-60N, 60-15W), SOI		______________	**M**

Table 4.3. Global scale SST features related to East African MAM seasonal rainfall EOF 3 mode

EOF 4 vs. Prominent Global SST Features

MONTHLY/SST FEATURES	BIMONTHLY/SST FEATURES	SEASONAL/SST FEATURES	COMBINED FEATURES
D- TSA (Eq-20S and 10E-30W)	**DJ-** Niño 1+2 (0-10S, 90W80W)	**DJF-** Niño 1+2 (0-10S, 90W-80W)	**DJ, DJF**
J- Niño 1+2 (0-10S, 90W-80W)	**JF-** Pacific ENSO- Niño 1+2 (0-10S, 90W-80W), Niño 3 (5N-5S, 150W-90W), Niño 3.4(5N-5S, 170-120W),	**JFM-** Pacific ENSO- Niño 1+2 (0-10S, 90W-80W), Niño 3 (5N-5S, 150W90W), Niño 3.4(5N-5S, 170-120W),	**J, JF, JFM**

F- Pacific ENSO- Niño 1+2 (010S, 90W-80W), Niño 3 (5N-5S, 150W-90W), Niño 3.4(5N-5S, 170-120W), SOI, TSA (Eq-20S and 10E-30W)	**FM-** Pacific ENSO- Niño 1+2 (0-10S, 90W-80W), Niño 3 (5N-5S, 150W-90W), Niño 3.4(5N-5S, 170120W), TSA (Eq-20S and 10E-30W)	**FMA-** Pacific ENSO- Niño 1+2 (0-10S, 90W-80W), Niño 3 (5N-5S, 150W90W), Niño 3.4(5N-5S, 170-120W), AMO (45-60N, 60-15W)	**F, FM , FMA**
M- Pacific ENSO- Niño 1+2 (010S, 90W-80W), Niño 3 (5N-5S, 150W-90W), Niño 3.4(5N-5S, 170-120W), localised in the Indian Ocean (15-30S, 60-90E).	**MA-** Pacific ENSO-- Niño 1+2 (0-10S, 90W-80W), Niño 3 (5N-5S, 150W-90W), Niño 3.4(5N-5S, 170-120W), AMO (45-60N, 60-15W)	**MAM**- Pacific ENSO- Niño 1+2 (0-10S, 90W-80W), Niño 3 (5N-5S, 150W90W), Niño 3.4(5N-5S, 170-120W), AMO (45-60N, 60-15W)	**M, MA, MAM**
A- Pacific ENSO- Niño 1+2 (010S, 90W-80W), Niño 3 (5N-5S, 150W-90W), Niño 3.4(5N-5S, 170-120W), AMO (45-60N, 60-15W)	**AM**- Pacific ENSO-- Niño 1+2 (0-10S, 90W-80W), Niño 3 (5N-5S, 150W-90W), Niño 3.4(5N-5S, 170-120W), AMO (45-60N, 6015W)and the Indian Ocean (15-30S, 45-75E)	____________	**A, AM**
M- Pacific ENSO- Niño 1+2 (010S, 90W-80W), Niño 3 (5N-5S, 150W-90W), Niño 3.4(5N-5S, 170-120W), AMO (45-60N, 60-15W), and the Indian Ocean(15-30S, 45-60E / 0-30S, 75-120E)	______________	_____________	**M**

Table 4.4Global scale SST features related to East African MAM seasonal rainfall EOF 4 mode

4.2.1 Monthly Timescale

The relationships between the dominant modes of MAM precipitation and global SSTs at different time lags: D, J, F, M, A and M rolled over from 1950-2007 for December to 1951-2008 (from January through to May) are presented in this section. The global scale circulation anomalies associated with the MAM rainfall modes are also presented here.

4.2.1.1 MAM East African Rainfall and Global SST Relationships

The grid point correlations between the four rainfall modes and the standardized global SST anomalies at different time lags are displayed in Figures 4.3-4.6. In general, the four modes responded differently to the Pacific ENSO, Indian and Atlantic Ocean at different time lags. The dominant contribution of global SST distributions were located in the tropical Pacific; Niño3 (5ºN-5ºS, 150ºW-90ºW), Niño3.4 (5ºN-5ºS, 170º-120ºW) and Niño 4 (5ºN-5ºS, 160ºE-150ºW).

Specifically, the EOF 1 mode was associated with the El Niño and La Niña conditions which are associated with the warming and cooling of the Pacific SSTs. These phenomena tend to enhance or suppress precipitation over the East African region. The relationship of the Pacific SST and the MAM rainfall mode 1 was strongest in December with a weak relationship identified in May. The other features identified were SST conditions in the tropical and south Atlantic which were prominent in February (Figure 4.3c) and March (Figure 4.3d). These signals were lost in December but localised conditions were noted in January and April.

Despite the major contribution of the Pacific, the Indian and Atlantic Oceans also played separate roles to the variability of the rainfall over the region. Comparatively, the Indian Ocean was seen to be more prominent than the Atlantic Ocean. The contribution of the Indian Ocean in modulating the East African rains has been reported (e.g. Saji *et al.*, 1999; Funk, 2012). This is consistent with the findings of Latif *et al*. (1999). Moreover, this study showed both the Pacific and Indian Oceans contributed to the variability of the rainfall mode more than the Atlantic Ocean. This is in contrast with part of the findings of Latif *et al.* (1999). Their study showed no relationship between the rainfall variability and the Pacific during the period of their study. Meanwhile the EOF 2 showed poor signal relationship with global SST distributions. This observation has been recently made by Smith and Semazzi (2014). It is important this mode (EOF 2) is further investigated either by using other datasets or possibly by climate modeling to ascertain the mechanism driving it.

With respect to EOF 3, it was observed that the mode had direct (indirect) relationship with the AMO-like (ENSO) phenomena. Interestingly on all the time steps from December to May, the rainfall mode showed a direct relationship with the AMO. The relationship was shown to be progressing from December with the peak observed in March. However, the intensity slightly reduces from April to May. The warm (cool) phase of the AMO is associated with the wet (dry) conditions of the East African region. This association of the AMO and the Eat African long rains have been investigated in a recent project over East Africa. One of the conclusions made from the study was that, the AMO had a high correlation with the rainfall over the Greater Horn of Africa during the month of May. Meanwhile, the Pacific showed an indirect relationship to EOF 3. This contrast was evident from December through to May with the strongest in December and the weakest signal observed in February.

Generally, the EOF 4 was dominated by the Pacific SST. A direct relationship between the EOF 4 and ENSO was prominent in May. The SST signal related to the rainfall mode was shown peaking from January to April. In December there was no clear signal between the EOF 4 and global SST but in May, an Indian Ocean signal was detected.

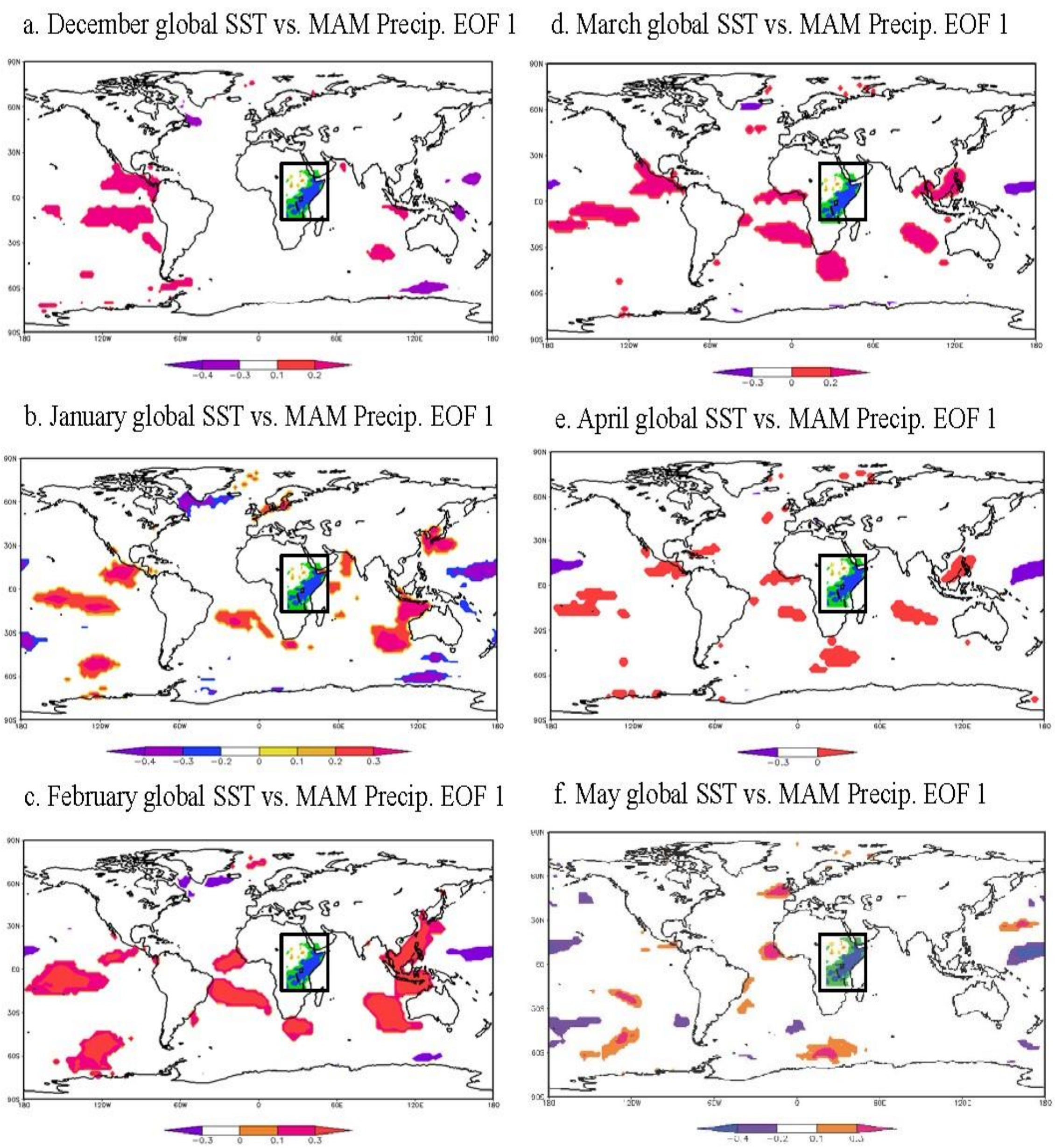

Figure 4.3- Relationship between standardized monthly global SST anomalies and East African MAM precipitation EOF 1-time series at different lags. Legend is for the range of correlation coefficient. Significant areas at 95% confidence level, using ttest, are shaded. The precipitation spatial patterns over the region are enclosed in boxes

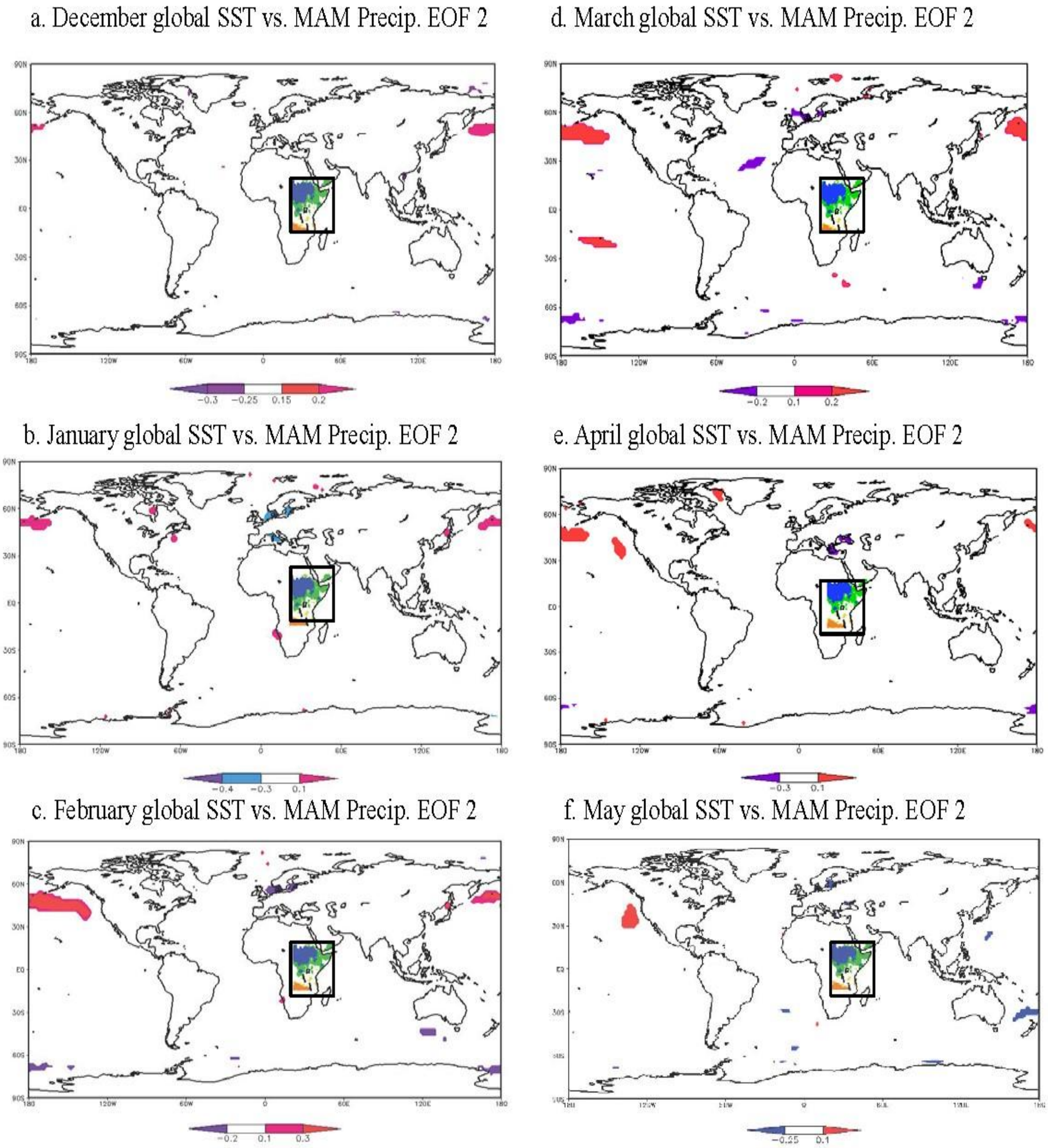

Figure 4.4- Relationship between standardized monthly global SST anomalies and East African MAM precipitation EOF 2-time series at different lags. Legend is for the range of correlation coefficient. Significant areas at 95% confidence level, using t- test, are shaded. The precipitation spatial patterns over the region are enclosed in boxes

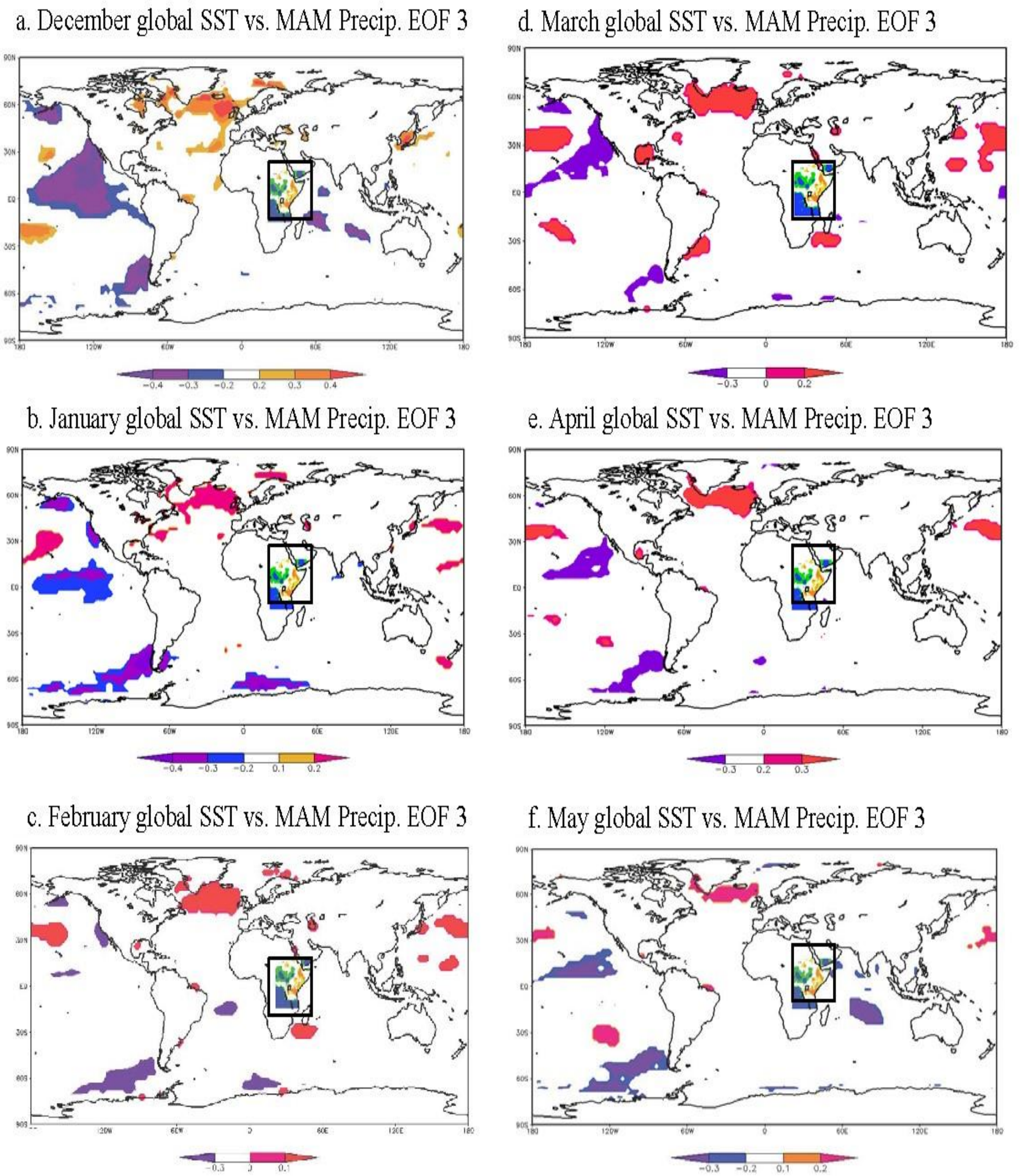

Figure 4.5- Relationship between standardized monthly global SST anomalies and East African MAM precipitation EOF 3-time series at different lags. Legend is for the range of correlation coefficient. Significant areas at 95% confidence level, using ttest, are shaded. The precipitation spatial patterns over the region are enclosed inboxes

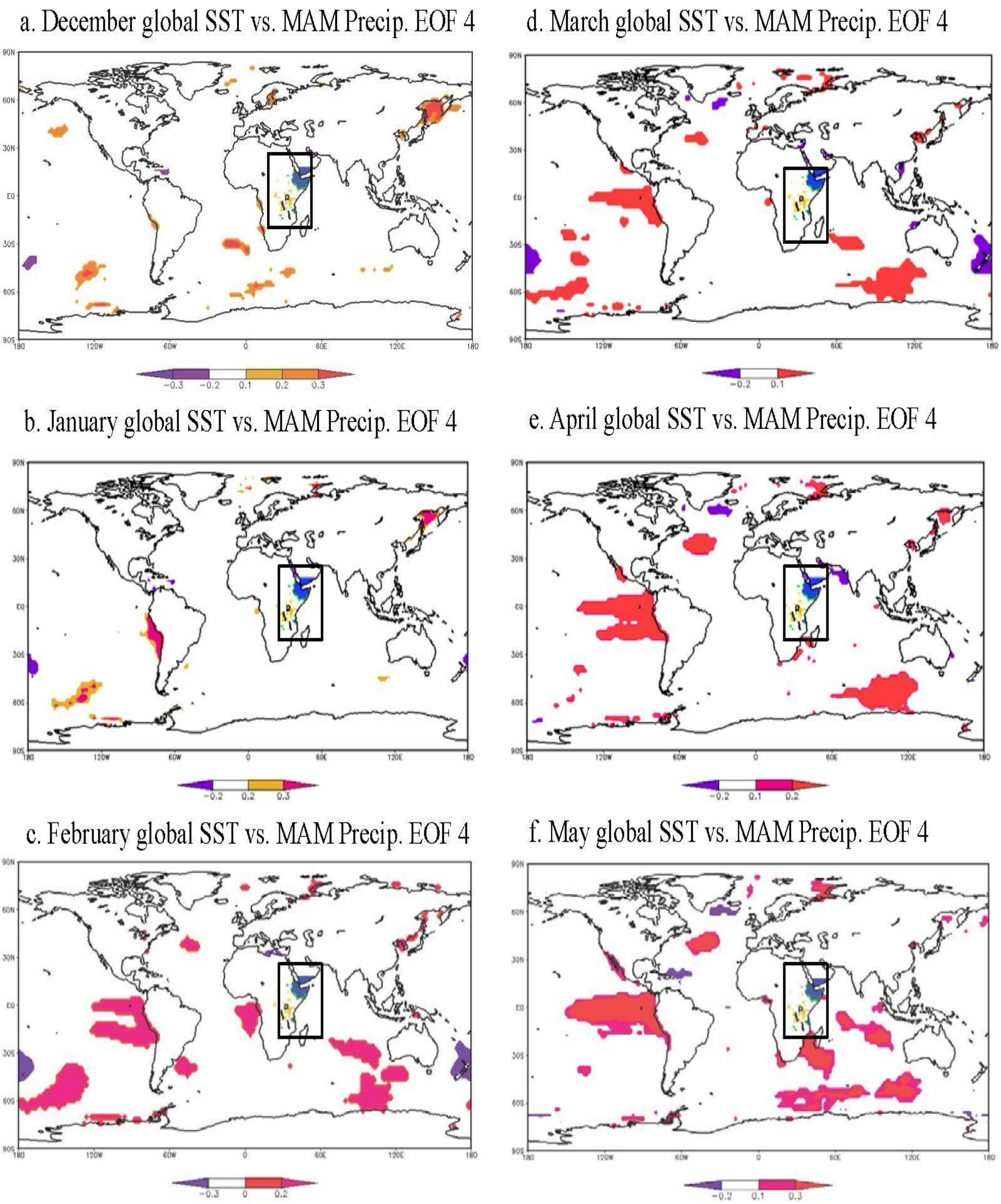

.

Figure 4.6- Relationship between standardized bimonthly global SST anomalies and MAM East African precipitation EOF 4-time series at different lags. Legend is for the range of correlation coefficient. Significant areas at 95% confidence level, using ttest, are shaded. The precipitation spatial patterns over the region are enclosed in boxes.

4.2.1.2 Composites of Standardized Global-Scale Divergent Circulation

Anomalies and East African MAM Precipitation Modes

This section constitutes upper-level (200hPa) velocity potential and anomalous divergent winds and its association with the MAM EOF modes 1, 3 and 4 with the exception of EOF 2 which is not related to global SST. Generally, regions of low (high) velocity potentials were associated with divergence (convergence).

With respect to EOF 1, mode upper level divergence was located over the western Pacific from December-February. This feature was weakened from March to May. In December, the EOF 1 was associated with a large scale divergence located over Asia. This feature was seen stretching into the coastal region of the horn of Africa which may suggest enhancement of moisture into the region. Upper level convergence was spotted in the Indian Ocean which is suggestive of subsidence in the ocean. Meanwhile in January the divergence over the Pacific region was weakened. Similar divergence over Asia and the convergence observed in the Indian Ocean during

December was seen in January. The upper-level divergence was shifted to the coast of Asia and East Africa in February. Another significant feature observed in February was strong convergence over the northern part of Africa stretching down to the Gulf of Guinea (Figure 4.7c).

Moreover, in March (Figure 4.7d) the northern part of Africa was characterised with divergence which is suggestive of Tropical Easterly Jet (TEJ). This was associated with the convergence located over the entire horn of Africa. In April, the divergence over North Africa was absent but seen in the Indian Ocean (Figure 4.7e). With respect to EOF 3, the rainfall mode was associated with divergence in the Indian Ocean during December. Furthermore, upper-level convergence linked to the rainfall mode was located over the coast of North America and the coast of Indonesia. An upperlevel divergence which is suggestive of the TEJ was located over the northern part of Africa during February and March. Also the upper level convergence located at the shores of the East African region is indicative of convective enhancement that could result in rainfall enhancement over the Ocean. A strong upper level convergence stretching from the Asian region into the Horn of Africa was observed in March. This is indicative of rainfall deficit over the Horn of Africa. In April and May, upper level convergence was shifted from the Asian region into the Indian Ocean. This could be responsible for the transport of moisture from the coast of the East African region into the Indian Ocean.

With respect to EOF 4, upper level divergence was located over the east African region. This mode was associated with the convergence observed in the Indian Ocean during the same period. In January, the EOF 4 was associated with upper level convergence centered over Australia. The horn of Africa was characterised by weak divergence. In February, an upper level divergence over the Pacific was associated to the rainfall mode. In the Indian Ocean, a large scale divergence was also observed. This divergence was seen stretching into the coastal area of East Africa. Upper level divergence in the Pacific during March and April could also be associated with rainfall enhancement in East Africa. A corresponding upper level divergence was also located in the Indian Ocean during the same period. These significant observations associated with EOF 4 were also made: strong upper level convergence over the northern part of Africa during February and March but disappears in April. In May, upper level convergence was located in the Asian region with divergence spotted over the East African region which is indicative of rainfall enhancement. In the proximity of East Africa, upper level divergence would lead to cloud formation and consequently precipitation, depending on other factors. Upper level convergence would be associated with transport of dry air mass from the upper atmosphere to the surface, which would indicate drought conditions.

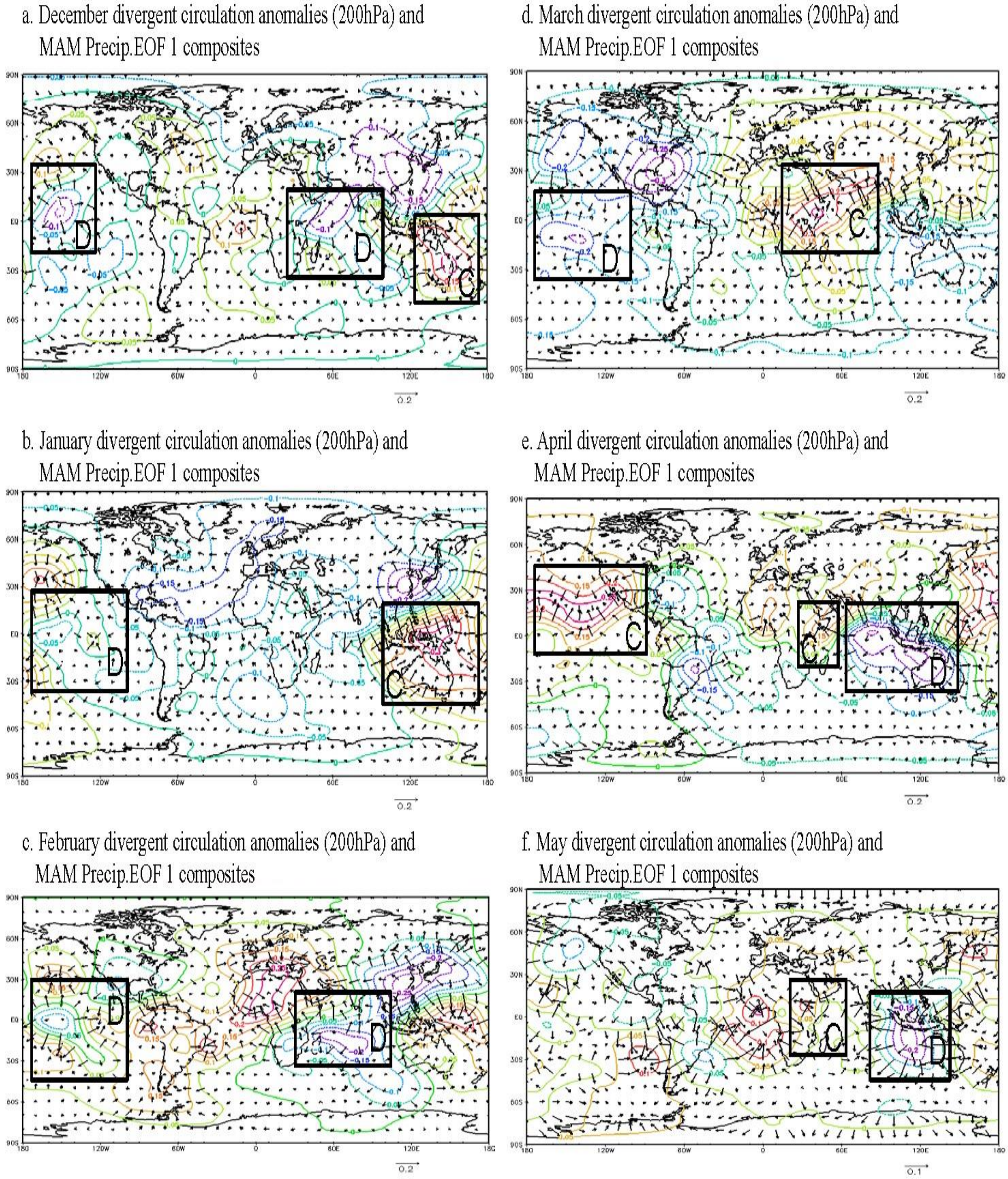

Figure 4.7- Standardized monthly global divergent circulation anomalies and MAM precipitation EOF 1 mode composites at different lags. The boxes indicate centres of action: D= Divergence (which implies rainfall enhancement) and C= Convergence (which implies rainfall suppression)

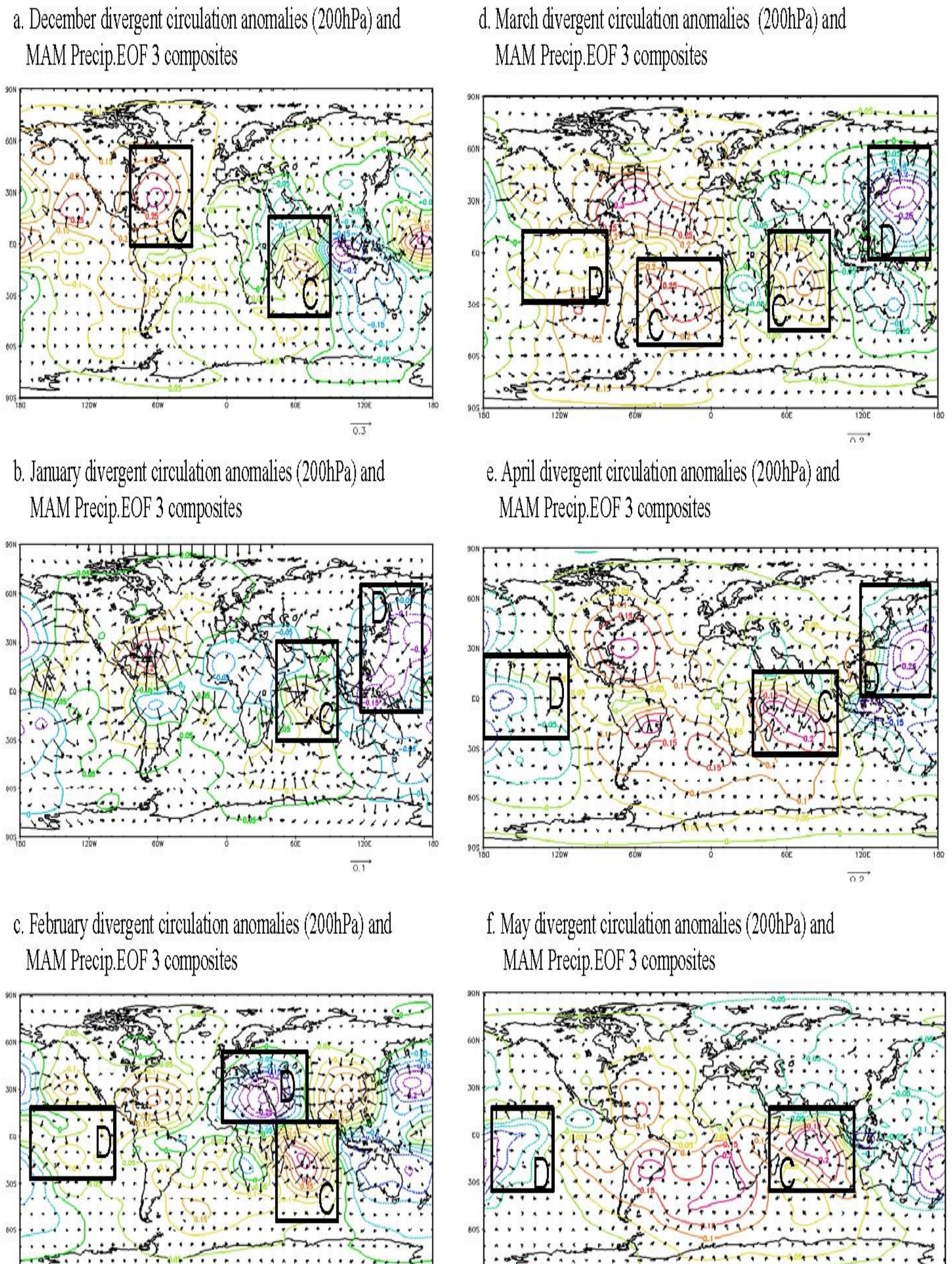

Figure 4.8 Standardized monthly global divergent circulation anomalies and MAM precipitation EOF 3 mode composites at different lags. The boxes indicate centres of action: D= Divergence (which implies rainfall enhancement) and C= Convergence (which implies rainfall suppression)

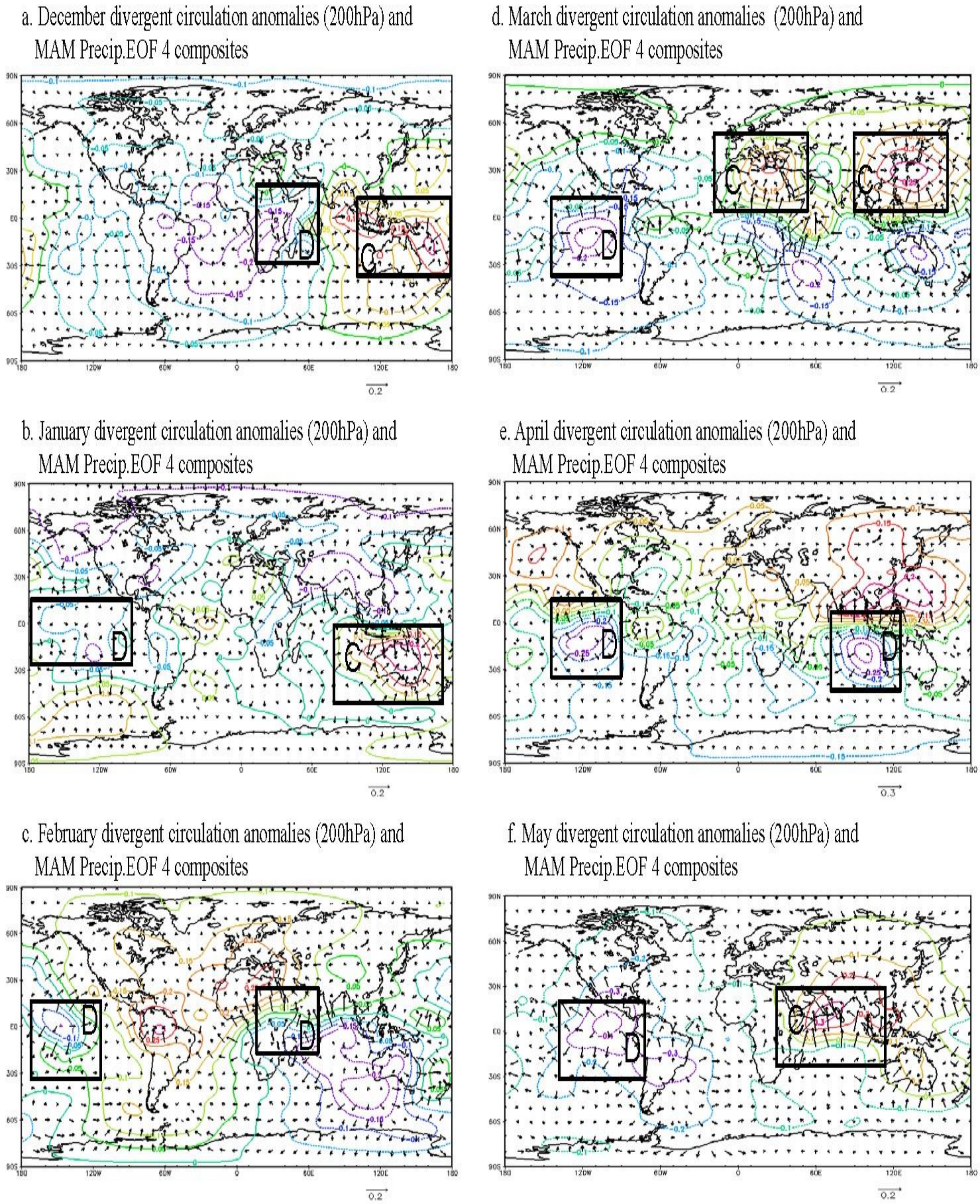

Figure 4.9- Standardized bimonthly global divergent circulation anomalies and MAM precipitation EOF 4 mode composites at different lags. The boxes indicate centres of action: D= Divergence (which implies rainfall enhancement) and C= Convergence (which implies rainfall suppression)

4.2.2 Bimonthly Timescale

This section also presents the relationship between the dominant modes of MAM precipitation and global SSTs at different time lags (bimonthly timescale): DJ, JF, FM, MA and AM. As done on the monthly timescale, this was also rolled over from 1950-2007 for December to 1951-2008 (from January through to May). Global scale circulation anomalies associated with the MAM rainfall modes are also shown.

4.2.2.1 MAM East African Rainfall Modes and Global SST Relationships In this section, grid-point correlations between the four rainfall modes and the standardized global SST anomalies are presented at various time lags (Figures 4.10- 4.13). Generally, as exhibited during the monthly timescale, the four modes on this timescale again responded differently to the Pacific ENSO, Atlantic and the Indian Oceans. Close observation showed that most of the Pacific Niños were greatly represented. Specifically, these were Niño3 (5^oN-5^oS, 150^oW-90^oW), Niño3.4 (5^oN5^oS, 170^o-120^oW) and Niño 4 (5^oN-5^oS, 160^oE-150^oW) regions. The analysis captured specific ones that had linkages to specific rainfall modes and these interactions were time-dependent.

It was noticed from Figure 4.10 that the influence of global SST distributions in the tropical Pacific was strongest in DJ, but had the weakest association in AM. The DJ signal captured the climatologically active phase of ENSO, which is consistent with literature (e.g. Latif *et al.*, 1999). Warm (cold) oceanic conditions in the Pacific enhanced (suppressed) convective activities associated with MAM precipitation EOF 1 mode. Other features identified were the localized SST conditions in the Indian Ocean off the western seaboard of India and a more prominent one on the western-tonorthern seaboard of Australia. The latter persisted up to MA, where it shifted to the vicinity of the Indian Ocean Dipole (IOD) domain (Saji *et al.*, 1999; Marchant *et al.*, 2006).

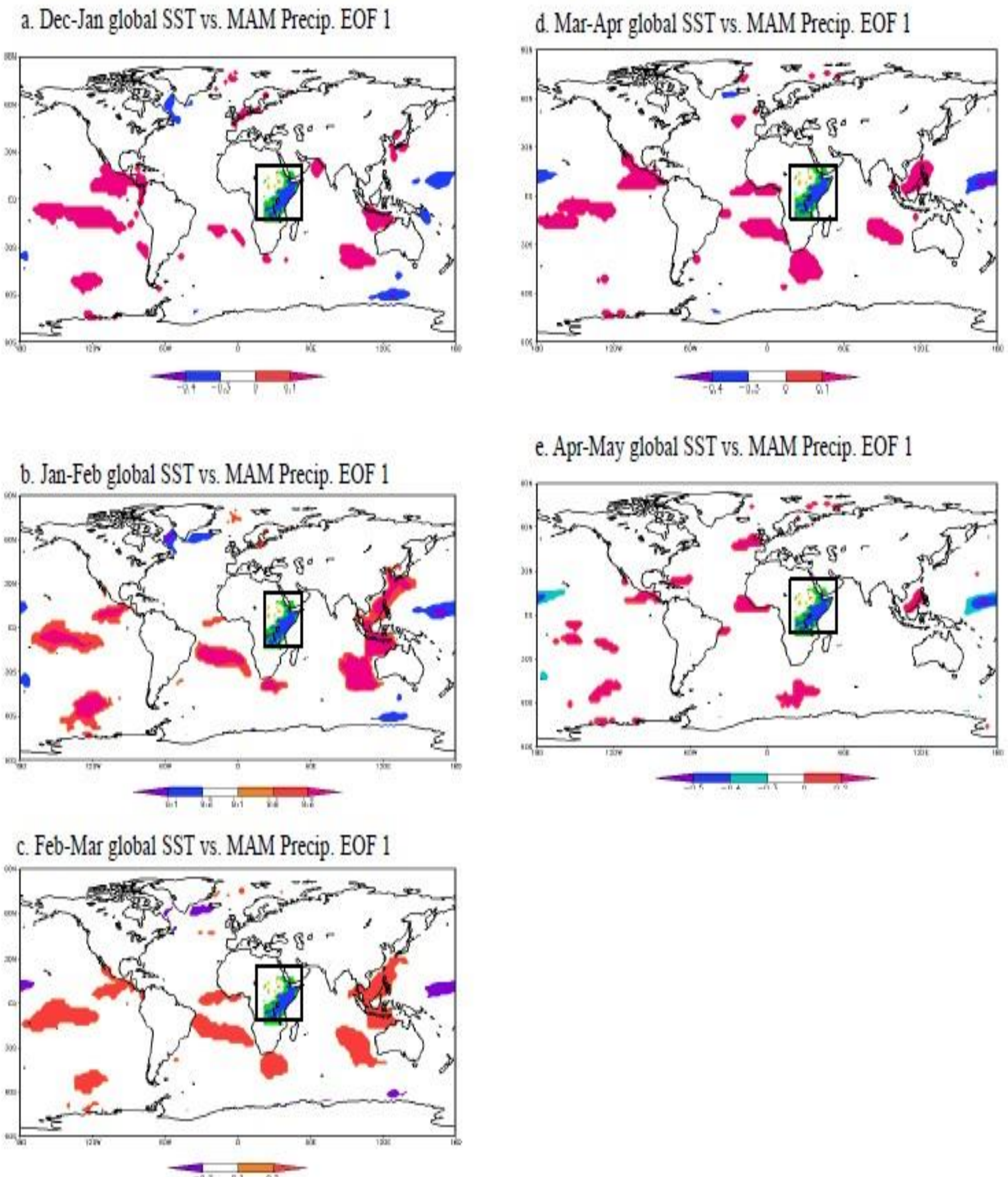

Figure 4.10- Relationship between standardized bimonthly global SST anomalies and East African MAM precipitation EOF 1-time series at different lags. Legend is for the range of correlation coefficient. Significant areas at 95% confidence level, using ttest, are shaded. The precipitation spatial patterns over the region are enclosed in boxes.

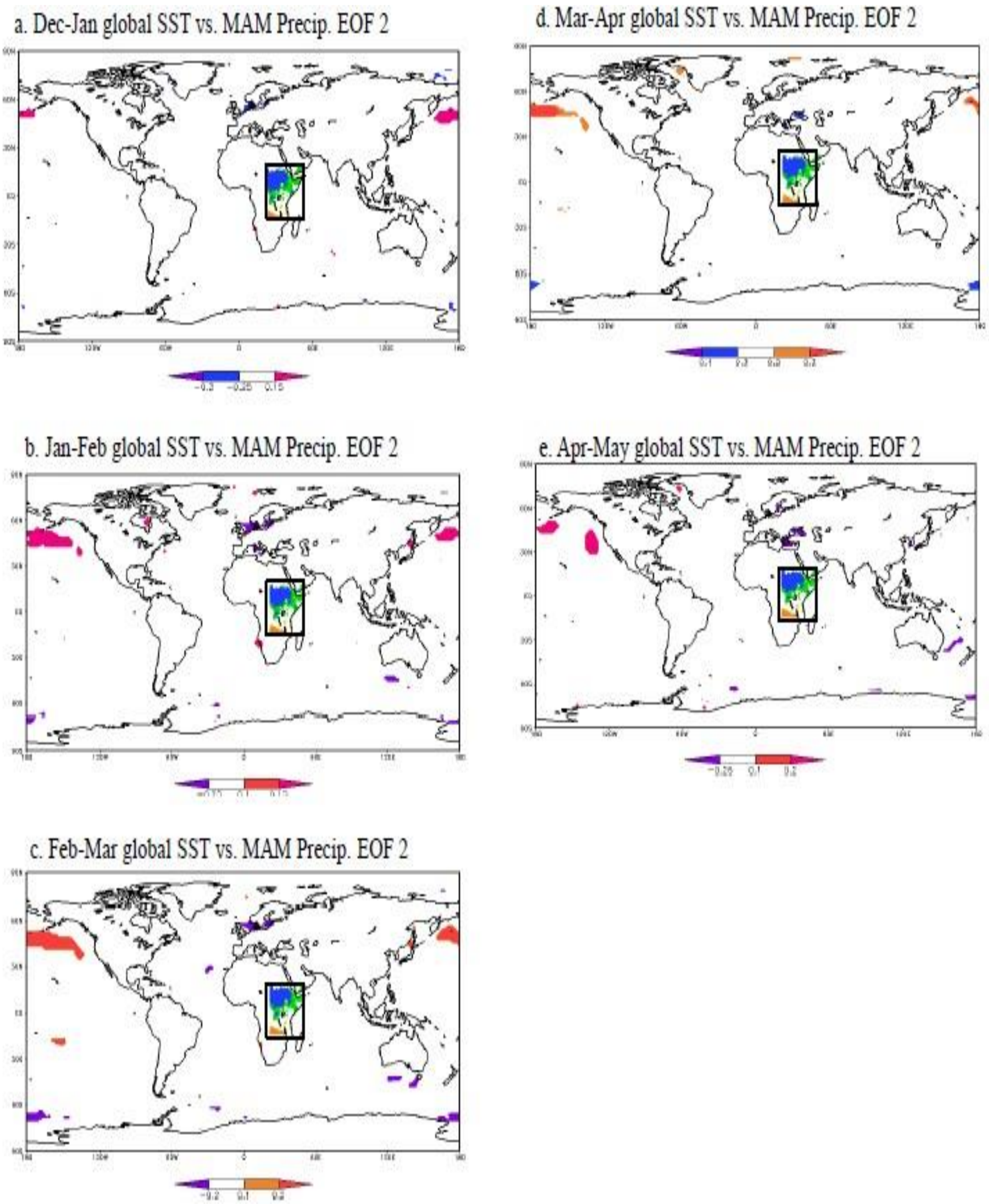

Figure 4.11- Relationship between standardized bimonthly global SST anomalies and East African MAM precipitation EOF 2 time series at different lags. Legend is for the range of correlation coefficient. Significant areas at 95% confidence level, using ttest, are shaded. The precipitation spatial patterns over the region are enclosed in boxes.

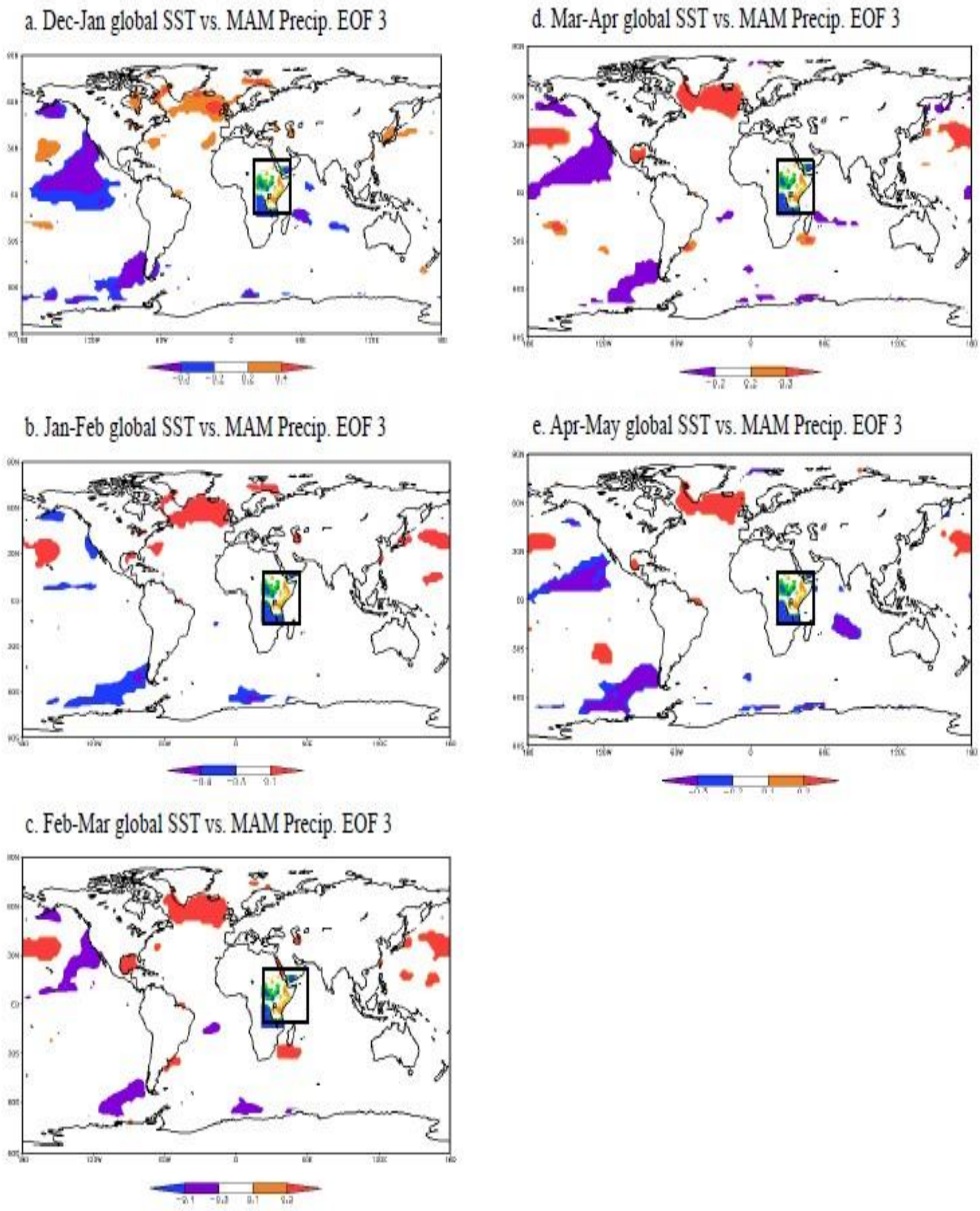

Figure 4.12- Relationship between standardized bimonthly global SST anomalies and East African MAM precipitation EOF 3 time series at different lags. Legend is for the range of correlation coefficient. Significant areas at 95% confidence level, using ttest, are shaded. The precipitation spatial patterns over the region are enclosed in boxes.

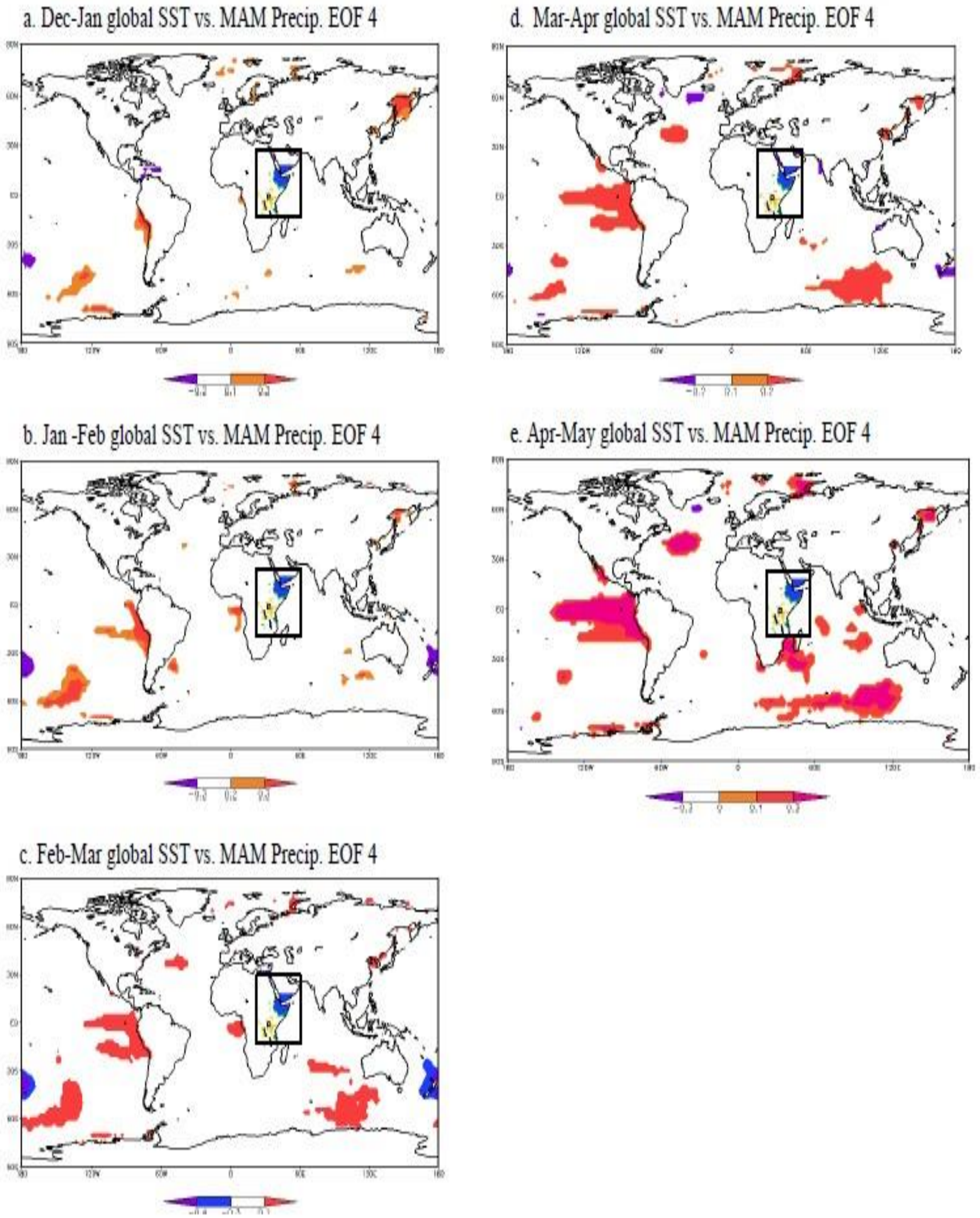

Figure 4.13- Relationship between standardized bimonthly global SST anomalies and East African MAM precipitation EOF 4 time series at different lags. Legend is for the range of correlation coefficient. Significant areas at 95% confidence level, using ttest, are shaded. The precipitation spatial patterns over the region are enclosed in boxes.

The Indian Ocean features were in phase with the tropical Pacific conditions from DF to MA, but experienced a complete annihilation in AM. The tropical South Atlantic warming became discernible from JF up to MA and also had a good link to the precipitation mode. However, it started to weaken in AM, which indicated the onset of the cooling phase of the tropical South Atlantic Ocean — a vital driver of the West African climate.

Interestingly, precipitation EOF 2 mode in reality had no substantial relationship with the basin wide SST distributions over the study period (Figure 4.11). The precipitation EOF 3 mode tended to display direct relationship with persistent mid-latitude North Atlantic conditions (Figure 4.12), which could be reminiscent of the Atlantic Multidecadal Oscillation (AMO). In contrast, the Pacific generally displayed an indirect relationship with the strongest (weakest) events captured in DJ (JF). No feature of climatological significance was observed over the Indian Ocean except a small-scale signal in AM, which resided in one of the arms of the IOD domain. Direct relationship between precipitation EOF 4 and the global SST was found to be impressively dominated by the Pacific (Figure 4.13), peaking from MA to AM. The evolution of the Gulf of Guinea SST showed a progressive but abysmal development from DJ to MA, and thereafter decayed till the end of the rainy season. In tandem with this event was the detection of a North Atlantic SST pattern, also reminiscent of a small-scale AMO which persisted on all the timesteps on this timescale. The Indian Ocean's link to the precipitation mode was discernible from FM to AM.

The relationship of global SST and the rainfall modes on the bimonthly timescale has revealed that over the Pacific key bimonthly warm (cold) oceanic features that drove or were in association with, the rainfall EOF 1 mode, representing El Niño (La Niña) tended to enhance (suppress) rainfall in GHA. The mechanism, however, was indirect and involved tropical Walker and Hadley circulations. The role of the tropical

Atlantic, as with the Pacific, was also critical. It was observed that a warming (cooling) of the tropical Atlantic enhanced (suppressed) convective development over the region. This was pronounced when the Atlantic started warming up in the Northern Hemisphere (NH) spring. The Indian Ocean also played a role to some extent which had similar effects or associations as with the other two oceans.

The poor relatedness between rainfall EOF 2 and global SST distributions again showed up on this timescale. The results from Figure 4.12 indicated a persistent and a direct AMO-like relationship with precipitation EOF 3. This oceanic mode is an essential part of the Atlantic Meridional Overturning Circulation, which has a great influence on the region's climate. Positive (negative) AMO phase was linked to anomalous wetness (dryness) of GHA, which was consistent with literature. However, the spatial extent of the effects of or associations with, the AMO was not expected to be homogeneous. In contrast, the Pacific as a whole indicated an inverse relationship with the rainfall mode, but the strongest (weakest) events detected in DJ (JF) emphasized the climatological significance of ENSO in NH winter. The competition between AMO-like feature and ENSO was important in further understanding of the region's climate variability. A localized climatic signal detected in AM over southwestern Indian Ocean was indicative of the association of the region's climate with Indian Ocean Dipole (IOD) (Saji *et al.*, 1999; Marchant *et al.*, 2006). While ENSO is known to be prominent in NH winter, the direct relationship between precipitation EOF 4 and the Pacific SST (Figure 5) rather peaked from MA to AM. This suggested that the Niño regions have their specific decay times. The AMO-like feature captured in the North Atlantic had similar role as the one detected for EOF 3.

4.2.2.2 Composites of Standardized Global-Scale Divergent Circulation

Anomalies and MAM East African Rainfall Modes

The standardized divergent circulation anomalies associated with the time-evolving global SST distributions and with respect to the three rainfall modes (i.e. EOF 1, 3 and 4) have been investigated with the exception of EOF 2 which again did not relate well to global SST on the bimonthly timescale. The importance of global divergent circulations in monsoon dynamics has been reported (Trenberth*et al.*, 2000). On this timescale, composite analysis revealed that divergence (convergence) and the centers of action at 200 hPa level provided useful information on how the bimonthly atmospheric flows could be applied to explain the precipitation patterns. The distinction of the circulation patterns (Figures 4.14-4.16) were based on their strengths, locations, and spatial extents. Diabatic heating is known to provide energy for driving such circulation patterns in the global tropics (Trenberth*et al.*, 2000)

Figures 4.14- 4.16 show the standardized global-scale velocity potential and divergent circulation anomalies at the upper (200 hPa) in relationship to the MAM rainfall modes. With respect to MAM precipitation EOF 1, it was observed that upper level divergence was centered over the equatorial western Pacific from DJ to AM, but became weaker from MA to AM. Correspondingly, upper level divergence was located over Asia spreading to the Indian Ocean in DJ. In JF, there was a shift of the field more eastward over Asia, where it became more intensified. In tandem with this development was the formation of a smaller divergence center specifically located over the Indian Ocean. This signified convective development leading to rainfall over the ocean. However, a weak upper level convergence was found over GHA which suggested transport of weak subsidence anomalies of dry air mass from the upper atmosphere to the surface. This was indicative of a small rainfall deficit. In FM, the divergence center over Asia weakened, but the systems over the Indian Ocean and

GHA persisted. In MA, an upper level divergence center, suggestive of Tropical East Jet (TEJ), was found over northern Africa. This co-occurred with a strong divergence center over the Indian Ocean. It appeared that the two centers were associated with a shift of the upper level convergence to the horn area, leading to rainfall deficit. In AM, similar conditions persisted, but with disappearance of the TEJ-like feature. In DJ and with respect to precipitation EOF 3, upper level divergence was located over equatorial western Pacific and over the GHA. There was a corresponding upper level convergence over the Indian Ocean (Figure 4.20). Convective development leading to rainfall would occur over the region, in contrast to rainfall deficit over the Indian Ocean. Similar systems persisted from JF to MA, but the divergence center over the Pacific weakened. In AM, re-emergence of the divergent circulation was observed over the equatorial Pacific. While the upper level convergence over the Indian Ocean was maintained, the GHA divergence center disappeared. This was indicative of rainfall surplus (deficit) over the Pacific Ocean (GHA and Indian Ocean).

In DJ, the center of action of upper level convergence was located over equatorial western Pacific and Indian Oceans in relationship to precipitation EOF 4. No upper level divergence was detected over GHA, which was indicative of rainfall deficit. In JF, upper level divergence replaced convergence in the Pacific. This was accompanied by weak (strong) convergence over Indian Ocean (northern Africa), which persisted to FM. In MA, divergence developed over the equatorial central Pacific and the Indian Ocean, but a strong northern African convergence was observed. Finally, in AM the following observations were made: divergence over the central Pacific, convergent-divergent dipole system over the Indian Ocean, and disappearance of the northern African convergence

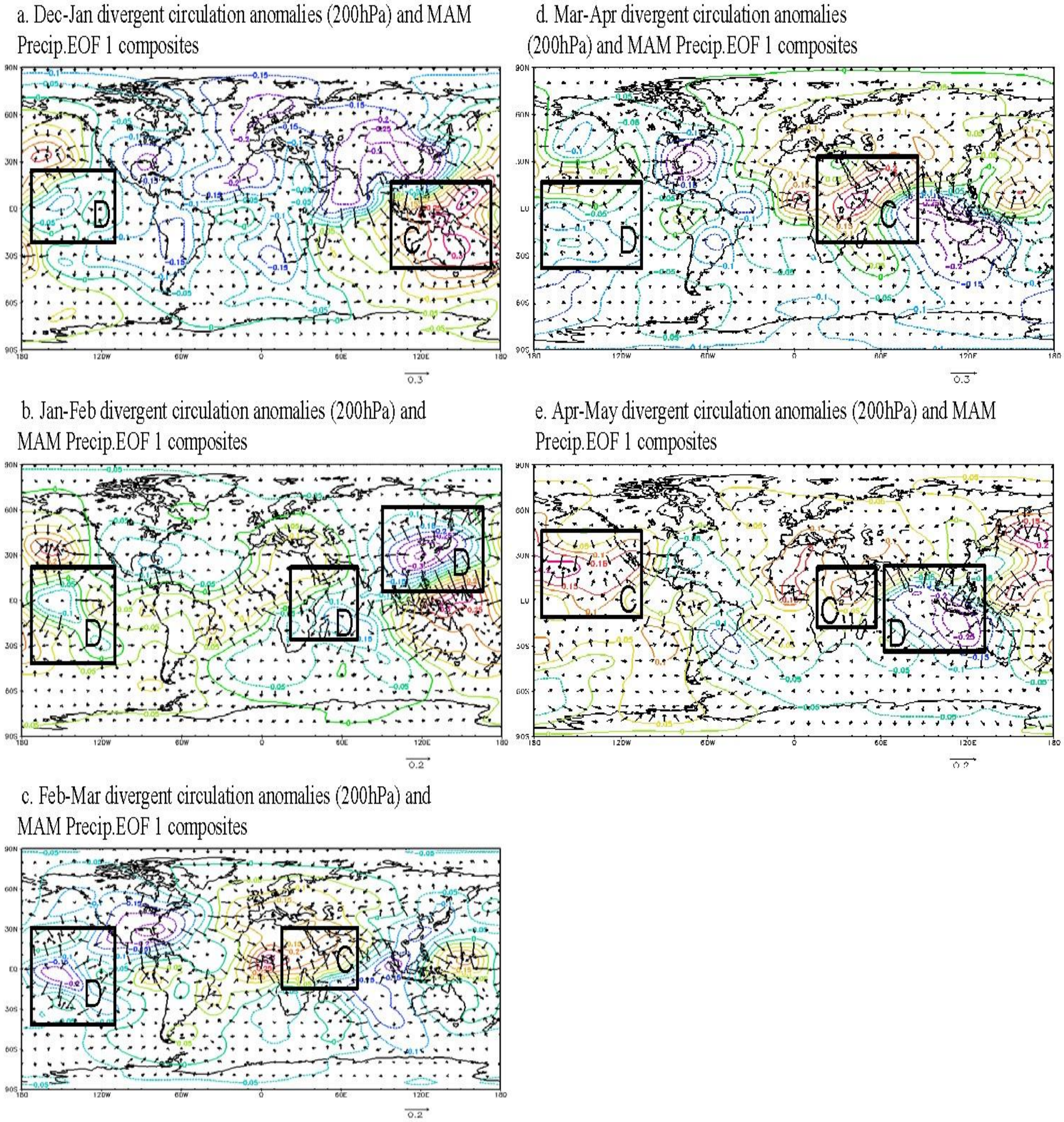

Figure 4.14- Standardized bimonthly global divergent circulation anomalies and MAM precipitation EOF 1 Figure 4.14- Standardized bimonthly global divergent circulation anomalies and MAM precipitation EOF 1 mode composites at different lags. The boxes indicate centres of action: D= Divergence (which implies rainfall enhancement) and C= Convergence (which implies rainfall suppression

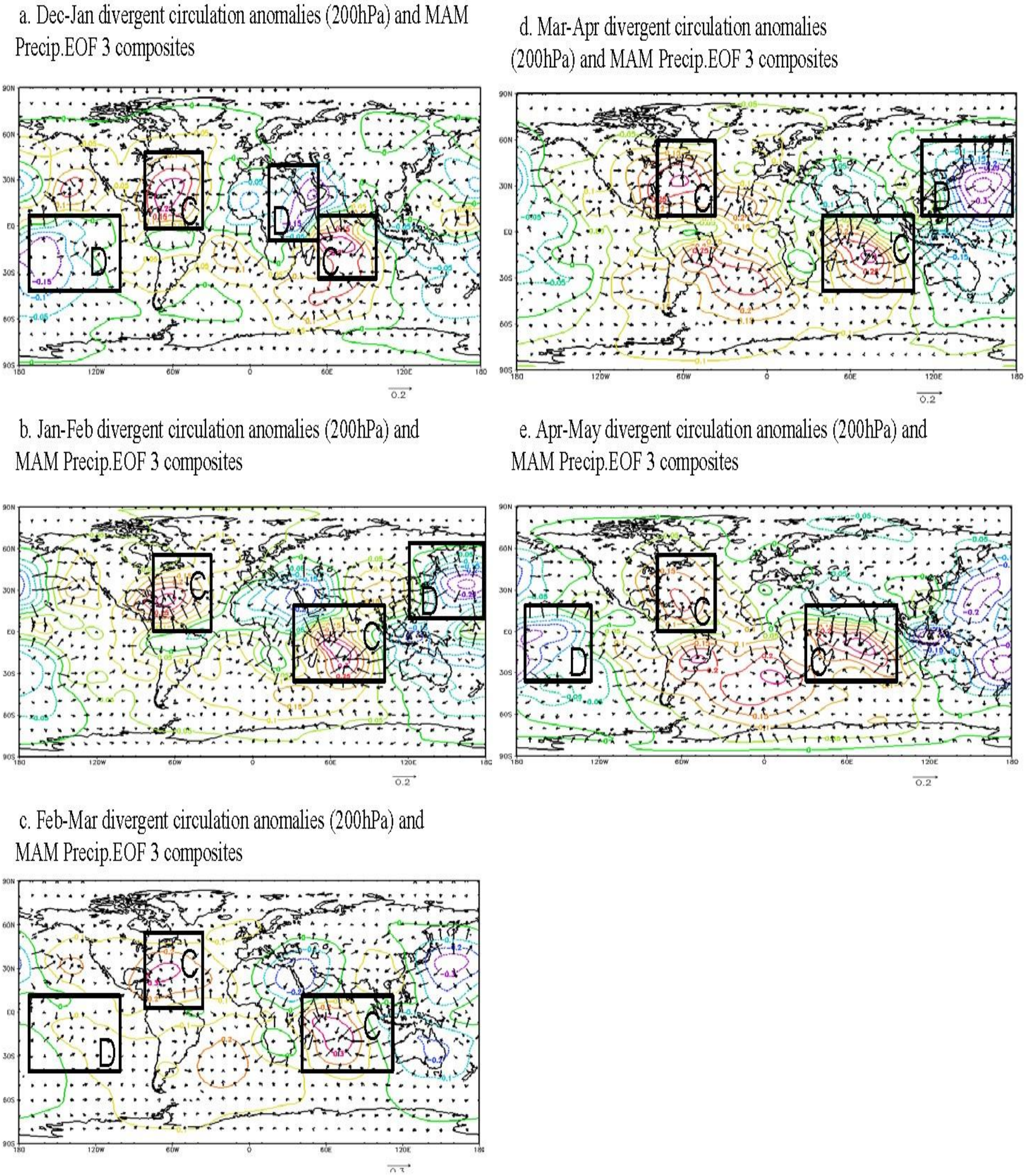

Figure 4.15- Standardized bimonthly global divergent circulation anomalies and MAM precipitation EOF 3 mode composites at different lags. The boxes indicate centres of action: D= Divergence (which implies rainfall enhancement) and C= Convergence (which implies rainfall suppression)

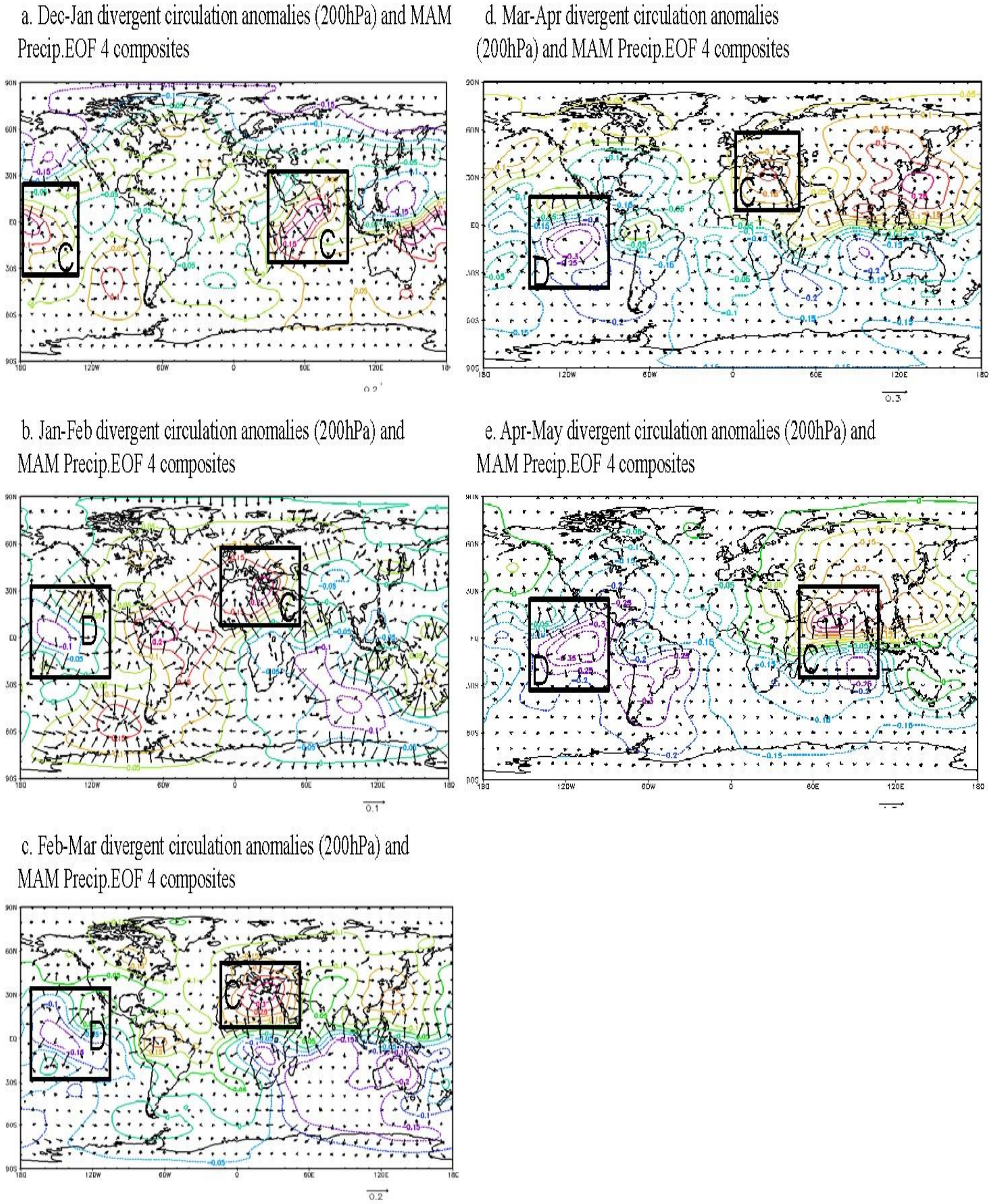

Figure 4.16- Standardized bimonthly global divergent circulation anomalies and MAM precipitation EOF 4 mode composites at different lags. The boxes indicate centres of action: D= Divergence (which implies rainfall enhancement) and C= Convergence (which implies rainfall suppression)

4.2.3 Seasonal Timescale

This section also deals with the relationship between the dominant modes of MAM precipitation and global SSTs on a seasonal timescale: (December-February, JanuaryMarch, February-April and March-May (DJF, JFM, FMA and MAM). This was also rolled over from 1950-2007 for December to 1951-2008 (from January through to May). The section also presents the global scale circulation anomalies associated with the MAM rainfall modes.

4.2.3.1 MAM East African Rainfall Modes and Global SST Relationships Global SST anomalies and tropical rainfall variability especially the East African region on seasonal timescale has been investigated by many authors (e.g. Nicholson, 1996; Saji *et al.*, 1999; Webster *et al.*, 1995).

With respect to EOF 1 precipitation mode, the contribution of the Pacific, Atlantic and the Indian Oceans were strong during December through to February (Figure 4.17a). In January to March (Figure 4.17b), the influence of these SST sectors were stronger on the rainfall mode. The warm SST features in the Pacific were associated with enhanced rainfall activities over the East African region. Meanwhile cold SST suppresses convective activities associated with the rainfall over the region. The influences of these three SST sectors were weakened during February to April. This mode is also shown to have an indirect relationship with the north Atlantic during this period. As shown in Figure 4.17d, the period of March-May had the weakest association of the SST sectors to the rainfall mode.

The association between the Pacific and the east Africa variability has been documented (e.g. Ogallo, 1988; Hastenrath *et al.*, 1993; Camberlin, 1995; Mutai *et al.*, 2000). The cold of phase of ENSO, La Nina has been linked to the drought conditions observed over the region (Indeje *et al.*, 2000; Williams and Funk, 2011) with the warm phase El Nino associated with enhanced rainfall. However, the second rainfall mode as shown in Figures 4.18a- 4.18d shows no clear relationship with any SST feature, which is consistent with recent literature (Smith and Semazzi, 2014).

Generally, the EOF 3 precipitation mode is indirectly associated with SSTs over

Pacific ENSO- Pacific ENSO- Nino3 (5^oN-5^oS, 150^o-90^oW), Nino 3.4(5^oN-5^oS, 170^o120^oW), Nino 4(5^oN-5^oS, 160^o-150^oW) but a direct relationship is located north Atlantic (45^o-60^oN, 60^o-15^oW).The localised Indian Ocean shown to be contributing to the variability of the rainfall of the East African is consistent with findings of Saji *et al.*, 1999. In both studies to a large extent linked the Indian Ocean dipole to the rainfall of the region.

The contribution of the north Atlantic conditions was strongest from January-March (Figure 4.19b) to March-May (Figure 4.19d). In December to February, this feature was shown weakened. A direct relationship between this rainfall mode and the Indian Ocean was captured during February-April (Figure 4.19c) and during March-May (Figure 4.19d), an indirect relationship was observed. The circulation pattern juxtaposed with the SST anomalies located in the Pacific and the Indian Oceans is indicative of subsidence in the Indian Ocean, therefore reducing influx of moisture into the East African region which may cause rainfall deficit (Ogallo, 1988; Nicholson and Kim, 1997). This rainfall deficit condition affected by the La Nina event has been linked to the influence of the western Pacific gradient (Hoell and Funk, 2013). A visual inspection of Figure 4.20 clearly shows that the EOF 4 precipitation mode was strongly associated with the Pacific region and parts of the Indian Ocean during February-April and March-May (Figures 4.20c and 4.20d). The direct relationship between the precipitation EOF 4 mode and the Pacific was progressively shown strengthening from December to May. The mode was strongly influenced by all the Nino regions during March-May (Figure 4.20d) with the weakest association recorded during December to February.

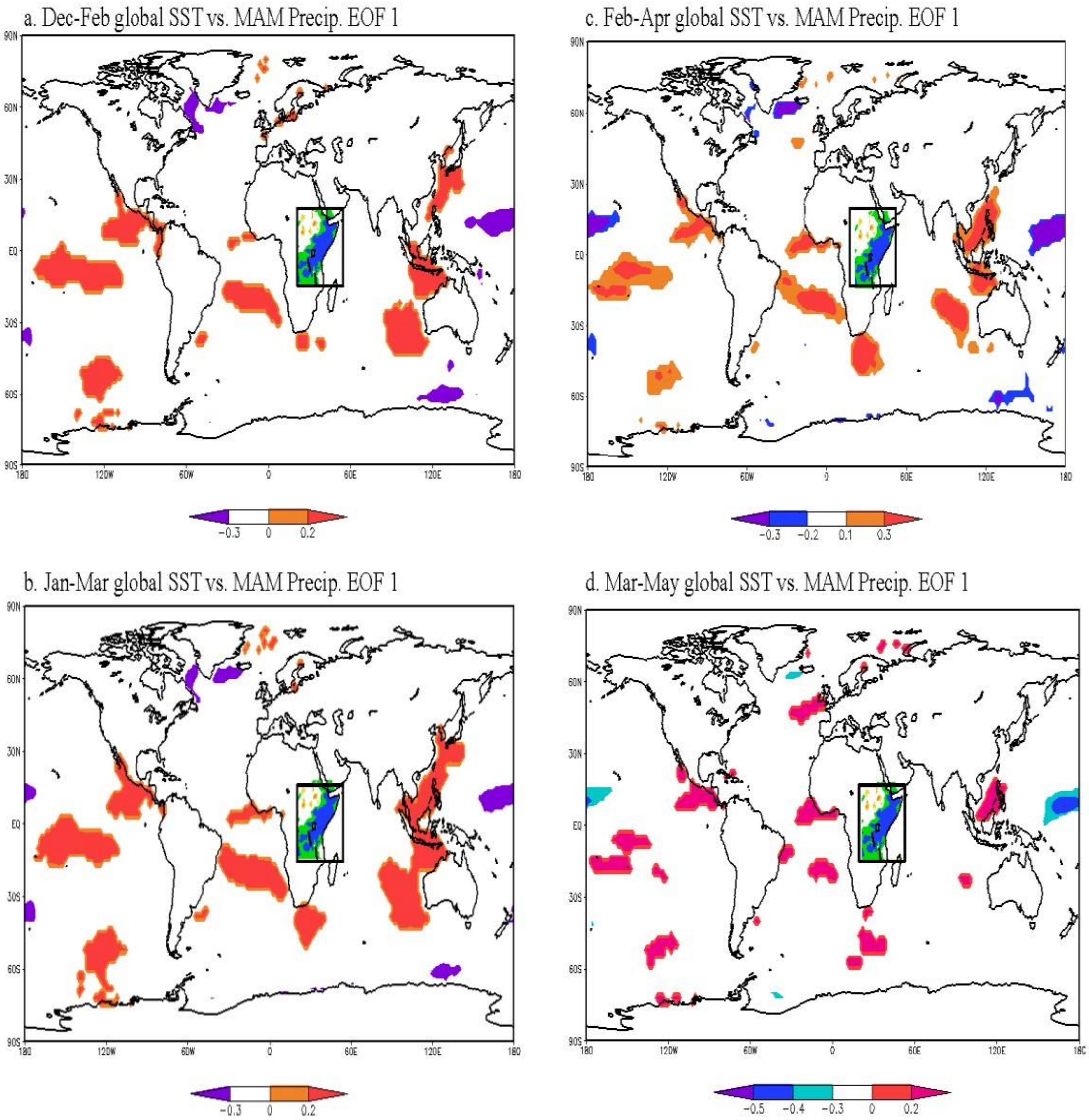

Figure 4.17- Relationship between standardized seasonal global SST anomalies and East African MAM precipitation EOF 1 time series at different lags. Legend is for the range of correlation coefficient. Significant areas at 95% confidence level, using ttest, are shaded. The precipitation spatial patterns over the region are enclosed in boxes.

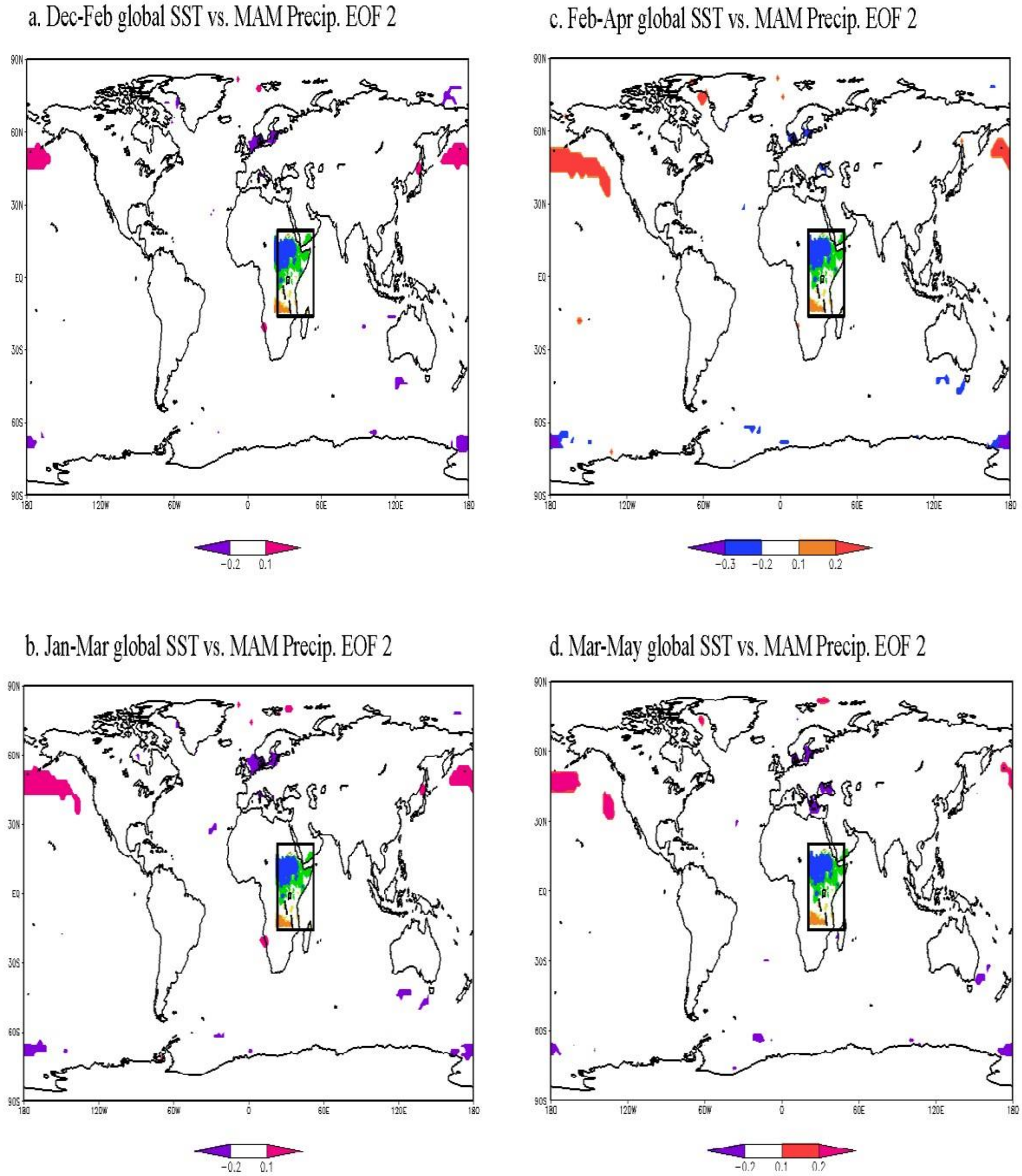

Figure 4.18- Relationship between standardized seasonal global SST anomalies and East African MAM precipitation EOF 2 time series at different lags. Legend is for the range of correlation coefficient. Significant areas at 95% confidence level, using ttest, are shaded. The precipitation spatial patterns over the region are enclosed in boxes.

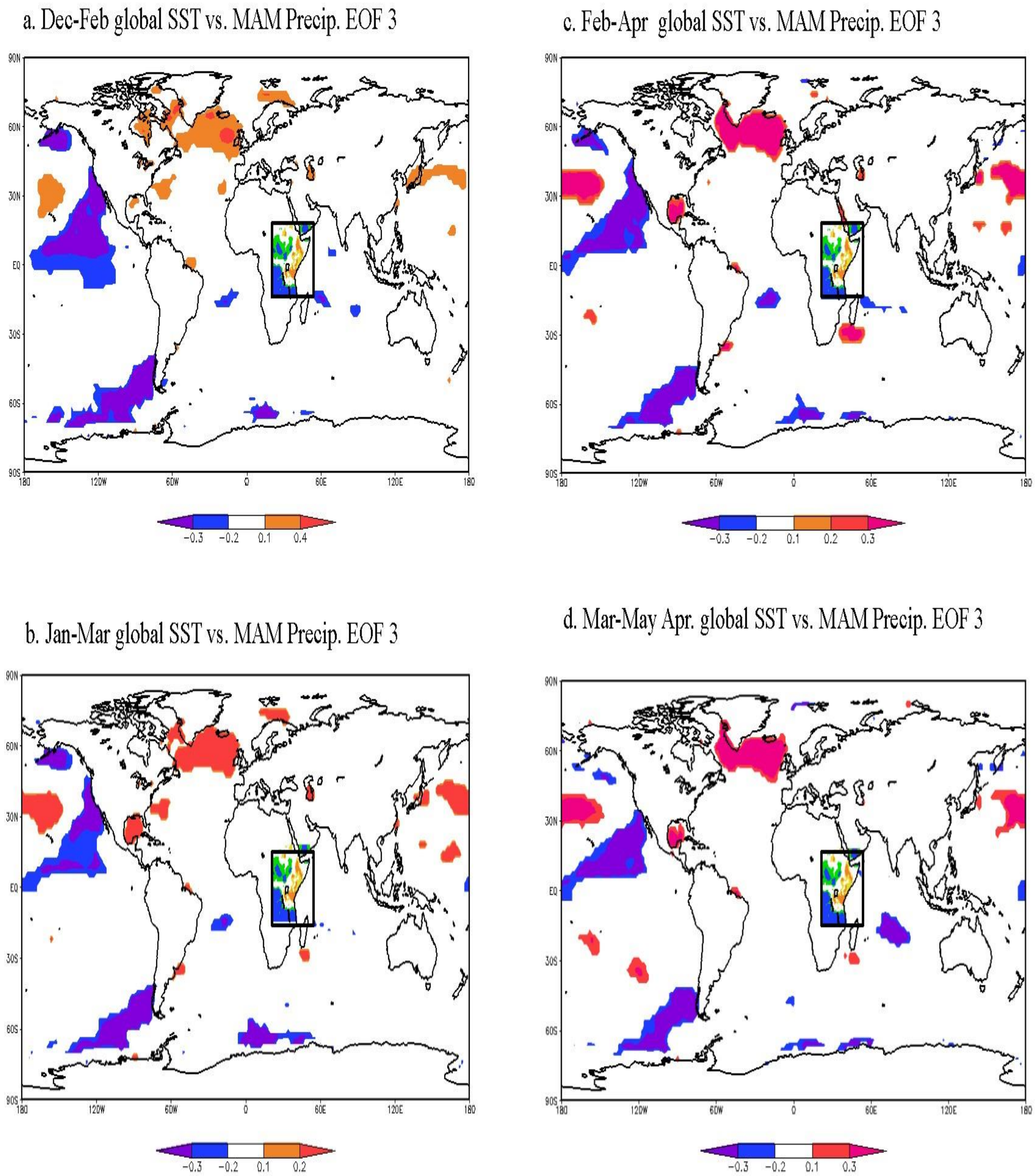

Figure 4.19- Relationship between standardized seasonal global SST anomalies and East African MAM precipitation EOF 3 time series at different lags. Legend is for the range of correlation coefficient. Significant areas at 95% confidence level, using ttest, are shaded. The precipitation spatial patterns over the region are enclosed in boxes.

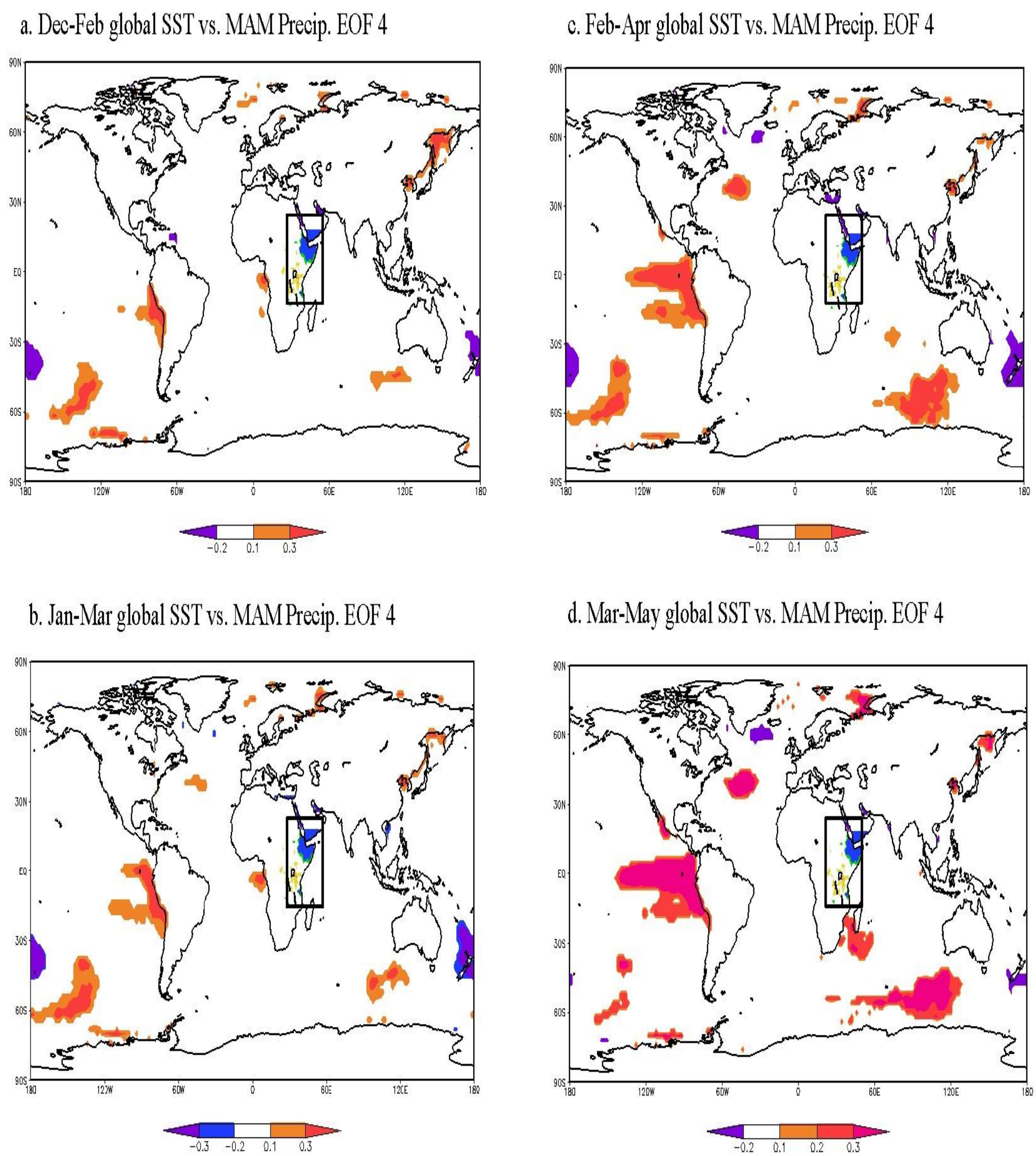

Figure 4.20- Relationship between standardized bimonthly global SST anomalies and MAM East African precipitation EOF 4 time series at different lags. Legend is for the range of correlation coefficient. Significant areas at 95% confidence level, using ttest, are shaded. The precipitation spatial patterns over the region are enclosed in boxes.

4.2.3.2 Composites of Standardized Global-Scale Divergent Circulation

Anomalies and East African MAM Precipitation Modes

The standardized global-scale velocity potential and divergent circulation anomalies

(200 hPa) and their relationship to the precipitation modes are displayed in Figures 4.21-4.23. The atmospheric circulations associated with rainfall modes showed varying centres of action. Especially the strong upper level divergence centered over the Indian Ocean in most cases is suggestive of the contribution of the Indian Ocean to rainfall pattern of the study area (Latif *et al.*,1999; Funk *et al.*, 2014). The circulation pattern shown (Figure 4.21c) is indicative of the transport of moisture from the Indian Ocean into the region which exhibits the Walker circulation. This circulation (Figure 4.21c) juxtaposed with the standardized SST anomaly during the same period further confirms the convective activity supporting the rainfall.

During December to February (Figure 4.21a), upper level divergence was located over the eastern Pacific. Over the western Pacific, convergence was located at the Indonesian region. A similar convergence was also over the north Pacific between latitude 20^o-40^{o}N. Meanwhile over east Africa, weak upper level convergence was observed. This was indicative of weak subsidence of air (dry) to the surface thus low drought conditions expected over the region. During January-March, upper level convergence was located over the tropical Atlantic and the western Pacific. Similar conditions were observed at the coast of Asia during the same period. The most significant feature was the upper level convergence stretching from West Africa through the central part of Africa and its seen covering most parts of east Africa. This strong upper level convergence may be suggestive of high rainfall deficit which may be due to high amount of dry air mass to the surface. Similar features were observed during February to April and March to May.

In December to February and with respect to EOF 3, upper level divergence was located over the Pacific and the east African region. This was indicative of rainfall enhancement over both areas. Meanwhile in January-March, upper level convergence was spotted in the Indian Ocean close to the east African coast. This feature may lead to rainfall deficit over the Indian Ocean. This similar feature was shown persisting during February to April (Figure 4.22c) and March to May (Figure 4.22d). The center of action associated with the precipitation EOF 4 mode was the upper level convergence located over the northern part of Africa during January to March and February to April. In March-May, upper level convergence associated to this rainfall mode was located at the coast of Asia stretching into the East African region.

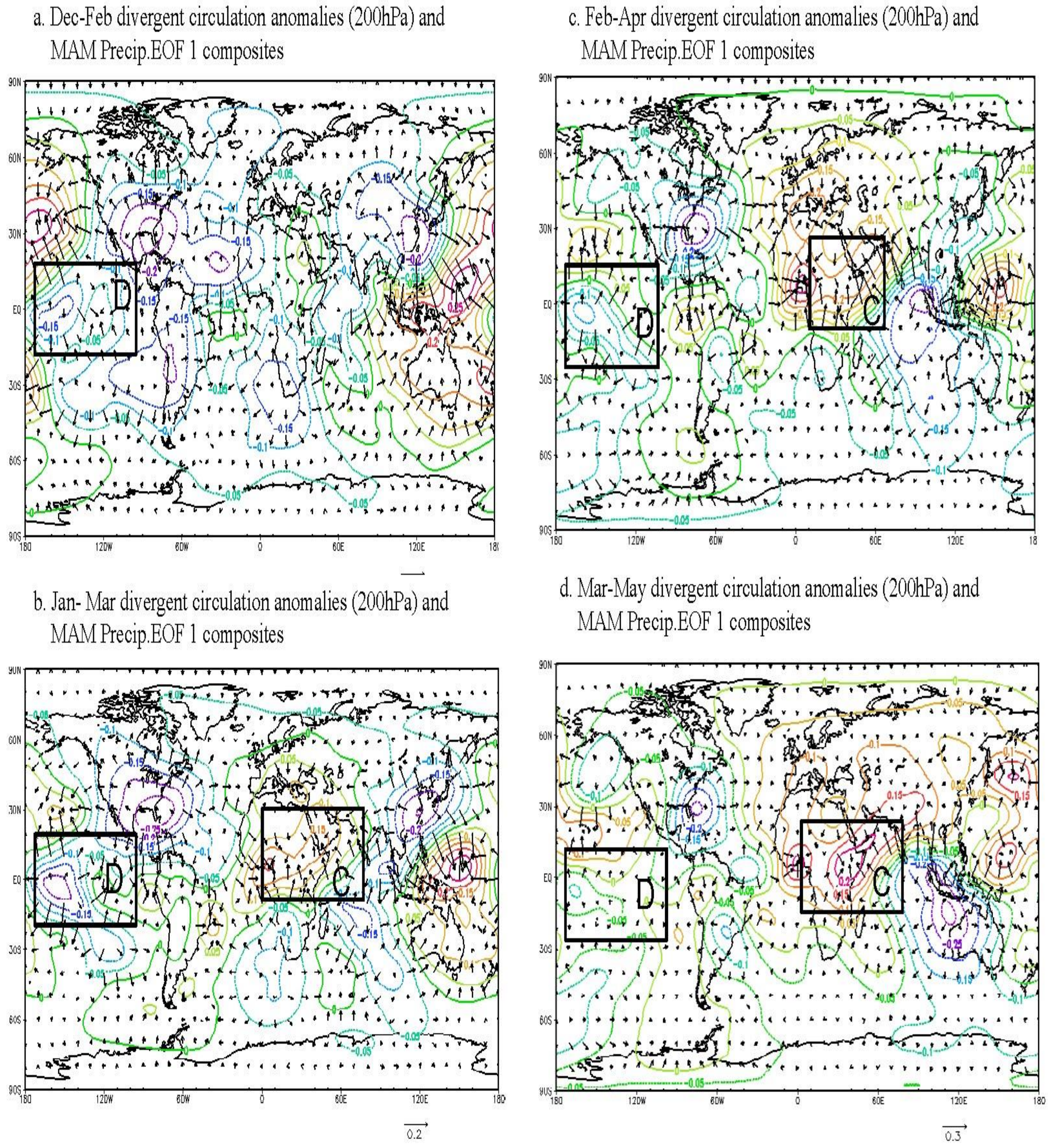

Figure 4.21- Standardized seasonal global divergent circulation anomalies and MAM precipitation EOF 1 mode composites at different lags. The boxes indicate centres of action: D= Divergence (which implies rainfall enhancement) and C= Convergence (which implies rainfall suppression)

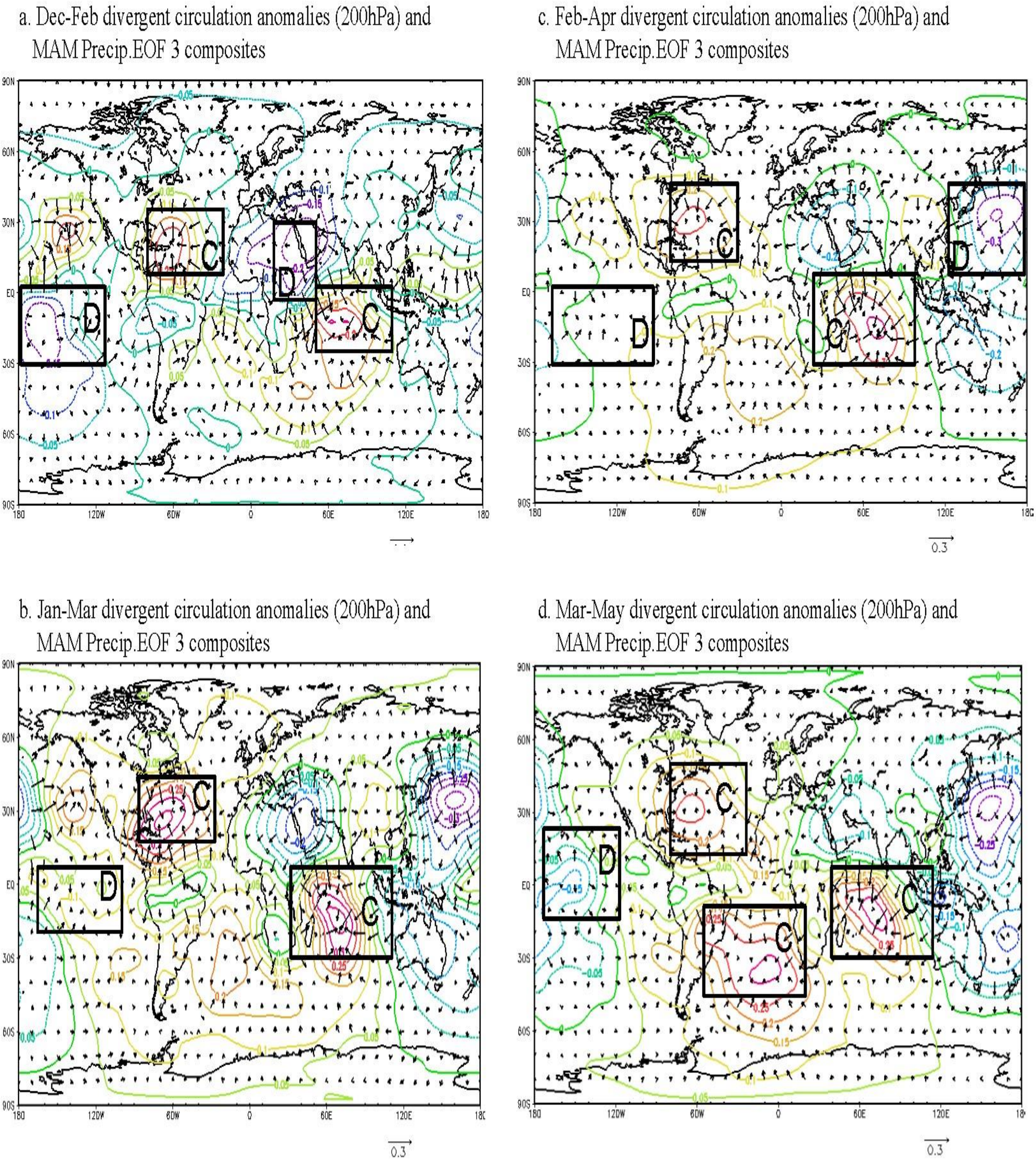

Figure 4.22- Standardized seasonal global divergent circulation anomalies and MAM precipitation EOF 3 mode composites at different lags. The boxes indicate centres of action: D= Divergence (which implies rainfall enhancement) and C= Convergence (which implies rainfall suppression)

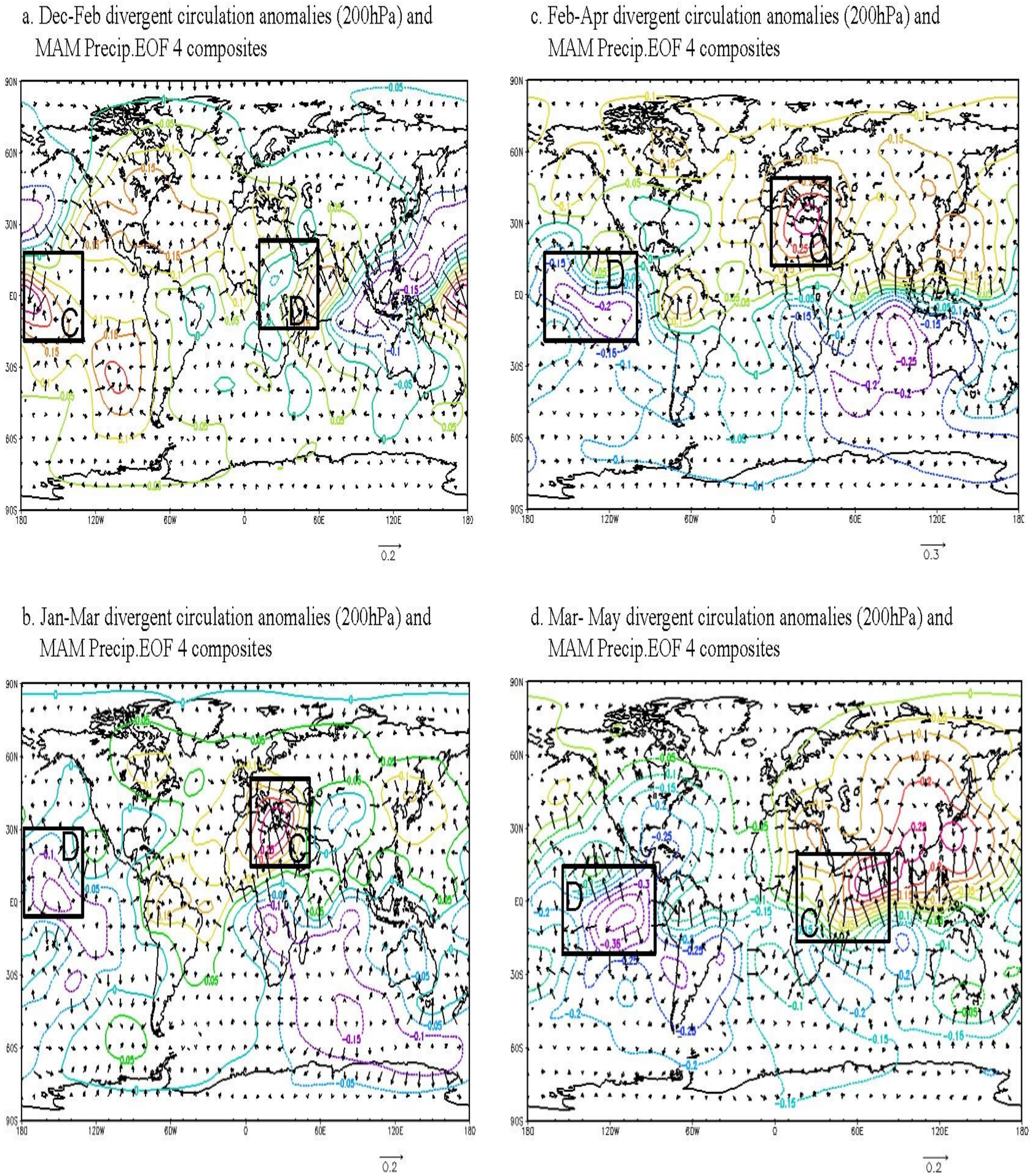

Figure 4.23- Standardized seasonal global divergent circulation anomalies and MAM precipitation EOF 4 mode composites at different lags. The boxes indicate centres of action: D= Divergence (which implies rainfall enhancement) and C= Convergence (which implies rainfall suppression)

4.2.4 Combined Timescale

This section presents the results of the combined scale consisting of the dominant features located on monthly, bimonthly and seasonal timescales in relationship to the modes of MAM precipitation.

4.2.4.1MAM East African rainfall modes and global SST relationships

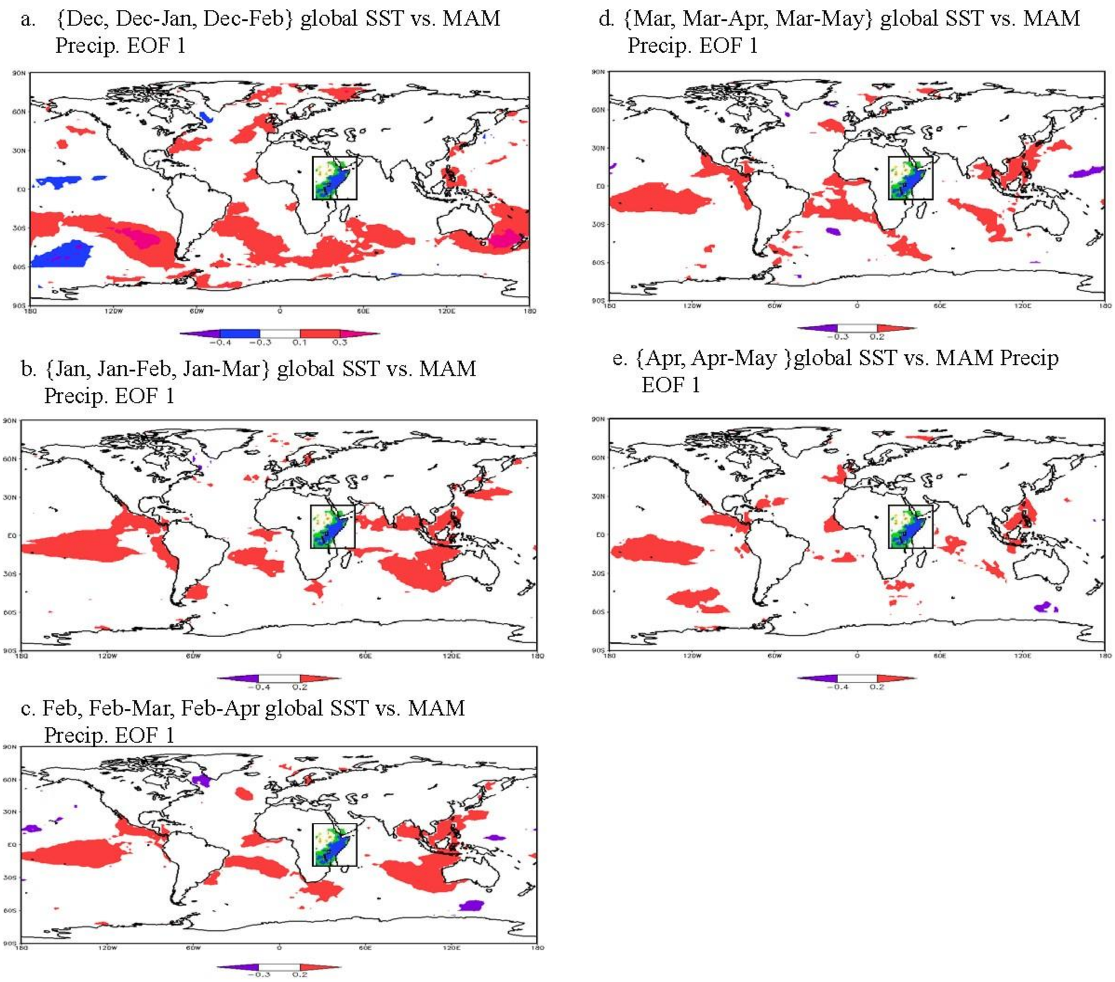

Figure 4.24- Relationship between standardized combined global SST anomalies and East African MAM precipitation EOF 1 time series at different lags. Legend is for the range of correlation coefficient. Significant areas at 95% confidence level, using ttest, are shaded. The precipitation spatial patterns over the region are enclosed in boxes.

a. {Dec, Dec-Jan, Dec-Feb} global SST vs. MAM Precip. EOF 3

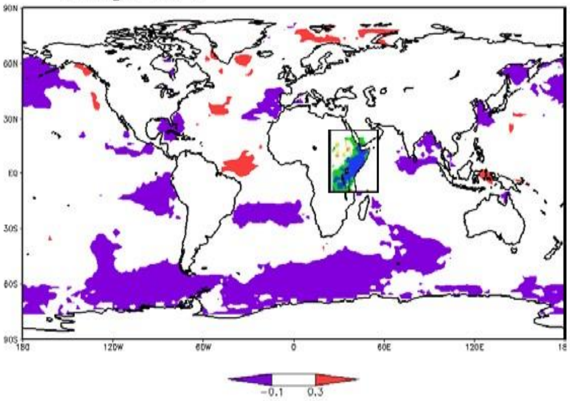

d. {Mar, Mar-Apr, Mar-May} global SST vs. MAM Precip. EOF 3

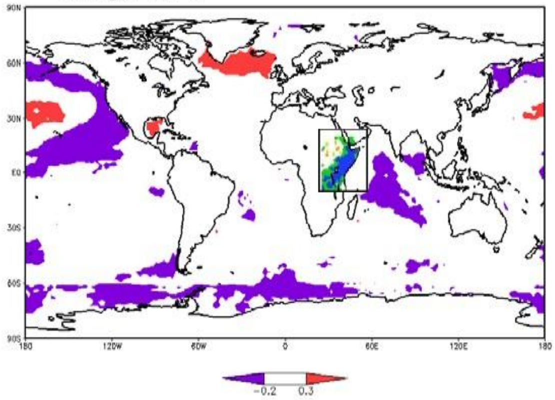

b. {Jan, Jan-Feb, Jan-Mar }global SST vs. MAM Precip. EOF 3

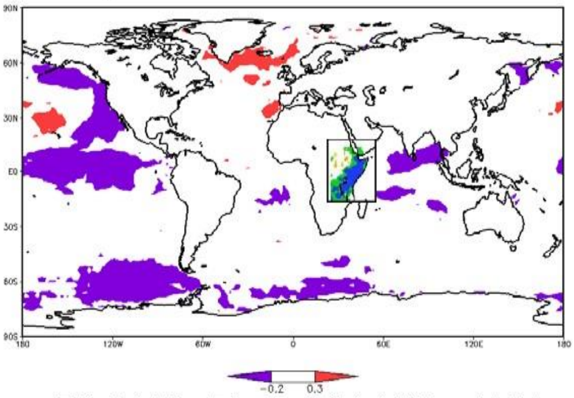

e. {Apr, Apr-May} global SST vs. MAM Precip. EOF 3

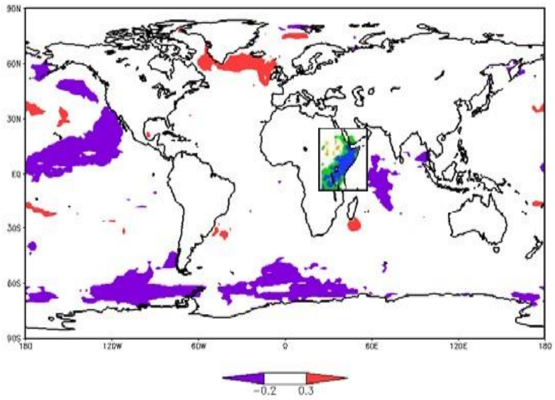

c. {Feb, Feb-Mar, Feb-Apr } global SST vs. MAM Precip. EOF 3

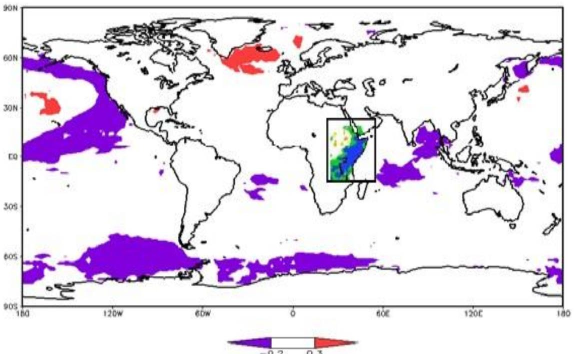

Figure 4.25- Relationship between standardized combined global SST anomalies and East African MAM precipitation EOF 3-time series at different lags. Legend is for the range of correlation coefficient. Significant areas at 95% confidence level, using ttest, are shaded. The precipitation spatial patterns over the region are enclosed in boxes.

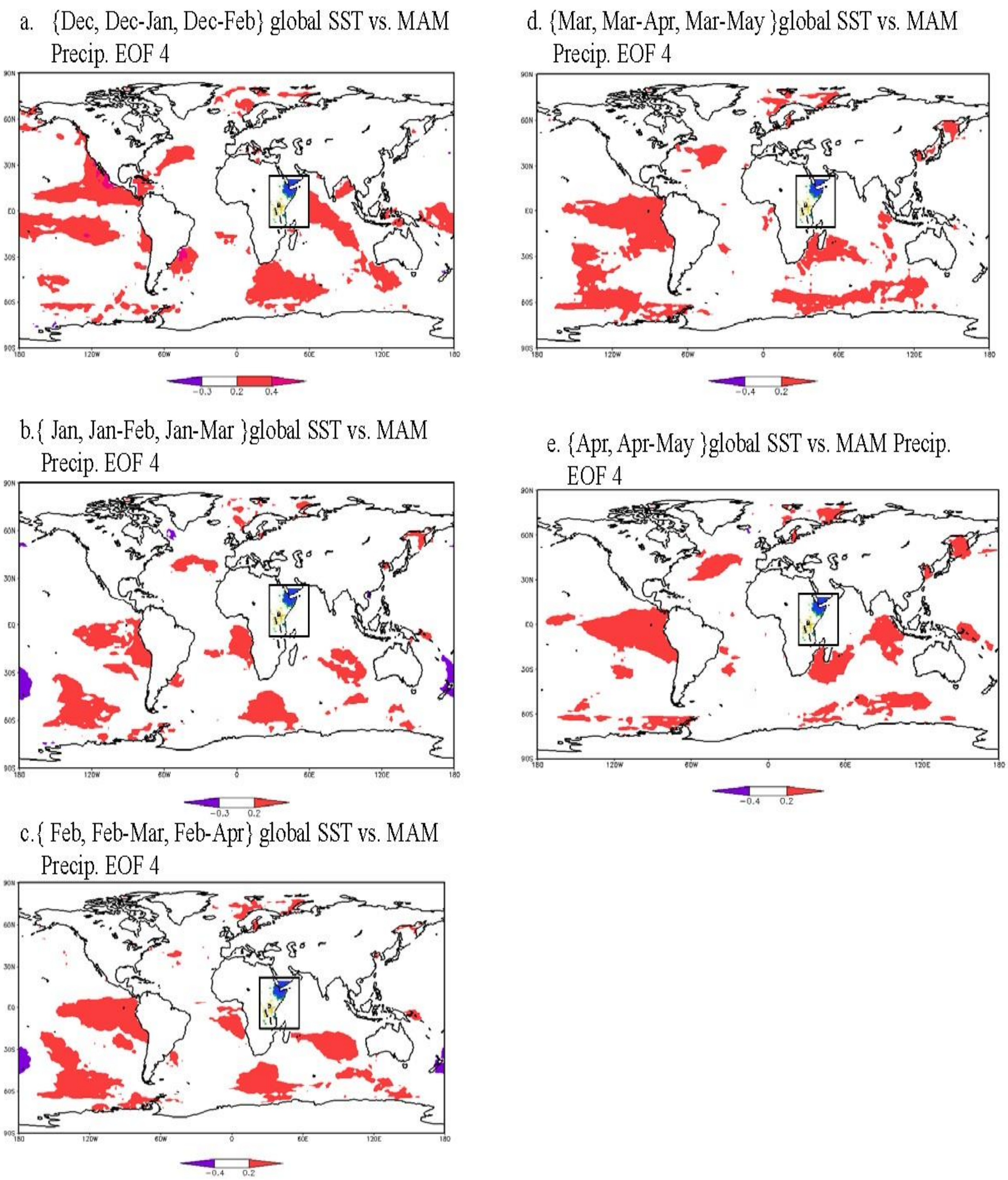

Figure 4.26- Relationship between standardized combined global SST anomalies and MAM East African precipitation EOF 4 time series at different lags. Legend is for the range of correlation coefficient. Significant areas at 95% confidence level, using ttest, are shaded. The precipitation spatial patterns over the region are enclosed in boxes.

Based on the evolving nature of climatic conditions (e.g. on monthly, bimonthly and seasonal timescales), the influence of global SST features were investigated on a combined timescale. First of all, the grid-point correlations between the rainfall modes and the standardized global SST anomalies (combined) are presented at various time lags (Figures 4.24-4.26). Just as shown on the three key timescales, the combined timescale showed the three captured modes (i.e. EOF 1, EOF 3 and EOF 4) responding differently to the Pacific ENSO, Atlantic and Indian Oceans. Generally, the EOF 1 and 4 had a direct relationship with the Pacific whilst the EOF 3 showed indirect relationship with the Pacific. With respect to the EOF 1, the influence of global SST distributions on the precipitation mode was strongest on the first combined scale December (Dec), December-January (Dec-Jan), December-February (Dec-Feb) (D, DJ and DJF) (Figure 1a) and it was seen to be weakened in April, April and May (A, AM) (Figure 1e).

Despite the contribution of the Pacific, Atlantic and Indian Oceans to the EOF mode 1, the competition was clearly shown between the Pacific and the Indian Oceans. The Pacific SST enhances rainfall conditions over the area. The contribution of the Indian Ocean (Saji *et al.*, 1999) was also exhibited during {Dec, Dec-Jan, Dec.-Feb} through to {Mar, Mar-Apr, Mar.-May} with the exception of {April and April-May} (Figure 4.24e) where the signal in the Indian Ocean was weak. It can be noticed that the EOF 3 precipitation mode was shown to be indirectly related to the SST distributions in the Pacific (Figure 4.25). Meanwhile, the contribution of the warm SSTs in the North Atlantic which is suggestive of an Atlantic Multidecadal Oscillation (AMO) was seen to have direct relationship with rainfall mode. This signal was persistent through all the timesteps. The fourth and final mode, EOF 4 captured on the combined timescale, is seen to be dominated by Nino 1+2 (0^o-10^oS, 90^o-80^oW) Niño3 (5^oN-5^oS, 150^oW90^oW), Niño3.4 (5^oN-5^oS, 170^o-120^oW) during Feb, Feb.-Mar, Feb.-Apr through to May. However, the Niño 4 (5^oN-5^oS, 160^oE-150^oW) region was seen to be strongest during Dec, Dec.-Jan, Dec.-Feb.

4.2.4.3 Composites of standardized global-scale divergent circulation anomalies and East African MAM precipitation modes

Figures 4.27-4.29 show the standardized global-scale velocity potential and divergent circulation anomalies at the upper atmosphere (200 hPa) in relationship to the MAM rainfall modes. In Dec, Dec-Jan, Dec-Feb (D, DJ and DJF) and with respect to EOF 1, upper level divergence was weak over the Pacific but becomes stronger during {Jan, Jan-Feb, Jan-Mar} and {Feb, Feb-Mar, Feb-Apr}. This was indicative of rainfall enhancement over the Pacific. Correspondingly, upper level divergence was located over the Indian Ocean during {Feb, Feb-Mar, Feb-Apr} through to {Apr, Apr-May} (Figures 4.27 c, d and e). This upper level divergence weakens during May (Figure 4.27f) is suggestive of enhanced rainfall over the Indian Ocean. Significantly, an upper level divergence which is suggestive of the Tropical Easterly Jet (TEJ) was located over northern Africa. No upper level divergence was located over the East African region, which indicates deficit of rainfall.

With respect to MAM precipitation EOF 3, upper level convergence was located over the Indian Ocean. This convergence was shown on all the time steps and it's indicative of rainfall conditions over the Indian Ocean which may draw moisture from the east African region causing rainfall deficit. Over the east African region, upper level divergence was observed. This suggests enhancement of rainfall conditions recorded over the region. Again, with respect to the EOF 3 mode, upper level convergence was located over the south tropical Pacific from {Mar, Mar-Apr, MarMay} through to May. Generally, the upper level divergence over the Pacific associated with this mode was showed to be very weak. In {Dec, Dec-Jan, Dec-Feb} and with respect to MAM EOF 4, upper level divergence was located over the Indian Ocean whilst weak divergence was observed over the Pacific. Meanwhile, over the northern part of Africa, strong upper level convergence was located. During {Jan, JanFeb, Jan-Mar} strong upper level divergence associated with rainfall mode was located over the northern African and the Pacific. Interestingly, similar patterns were observed during Feb, Feb-Mar, Feb-Apr. However, convergence was shifted to the southern part of Asia in Apr, April-May.

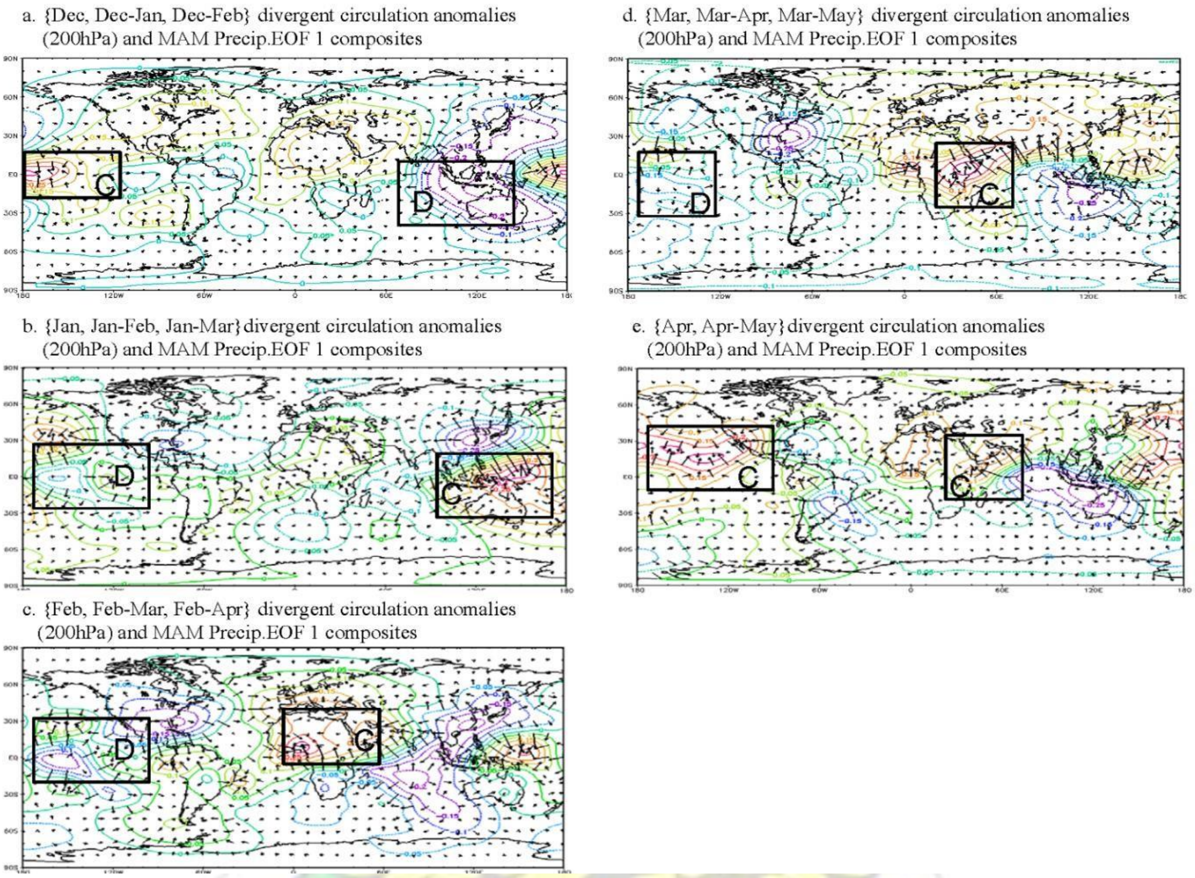

Figure 4.27-Standardized combined global divergent circulation anomalies and MAM precipitation EOF 1 mode composites at different lags. The boxes indicate centres of action: D= Divergence (which implies rainfall enhancement) and C= Convergence (which implies rainfall suppression)

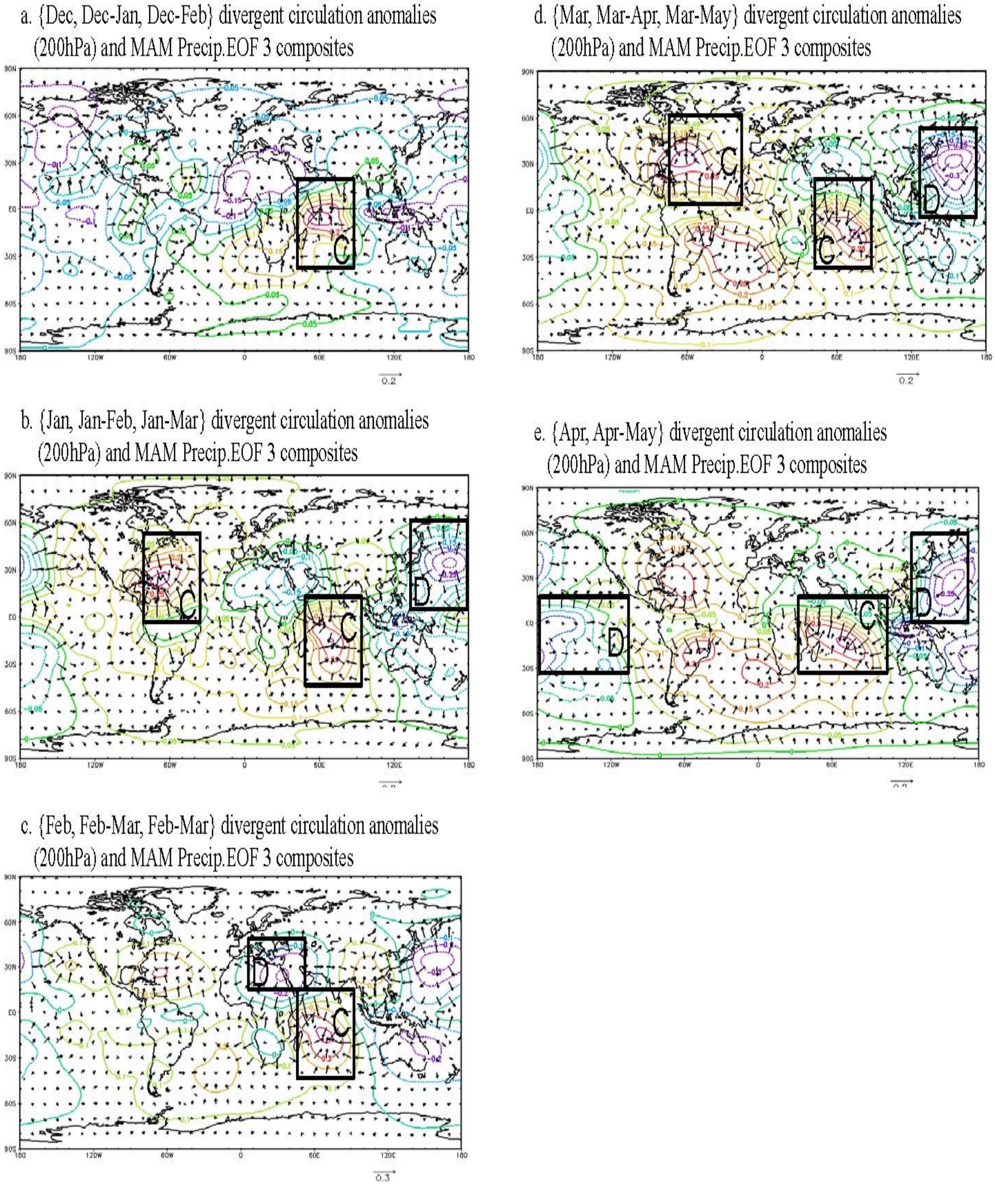

Figure 4.28- Standardized combined global divergent circulation anomalies and MAM precipitation EOF 3 mode composites at different lags. The boxes indicate centres of action: D= Divergence (which implies rainfall enhancement) and C= Convergence (which implies rainfall suppression)

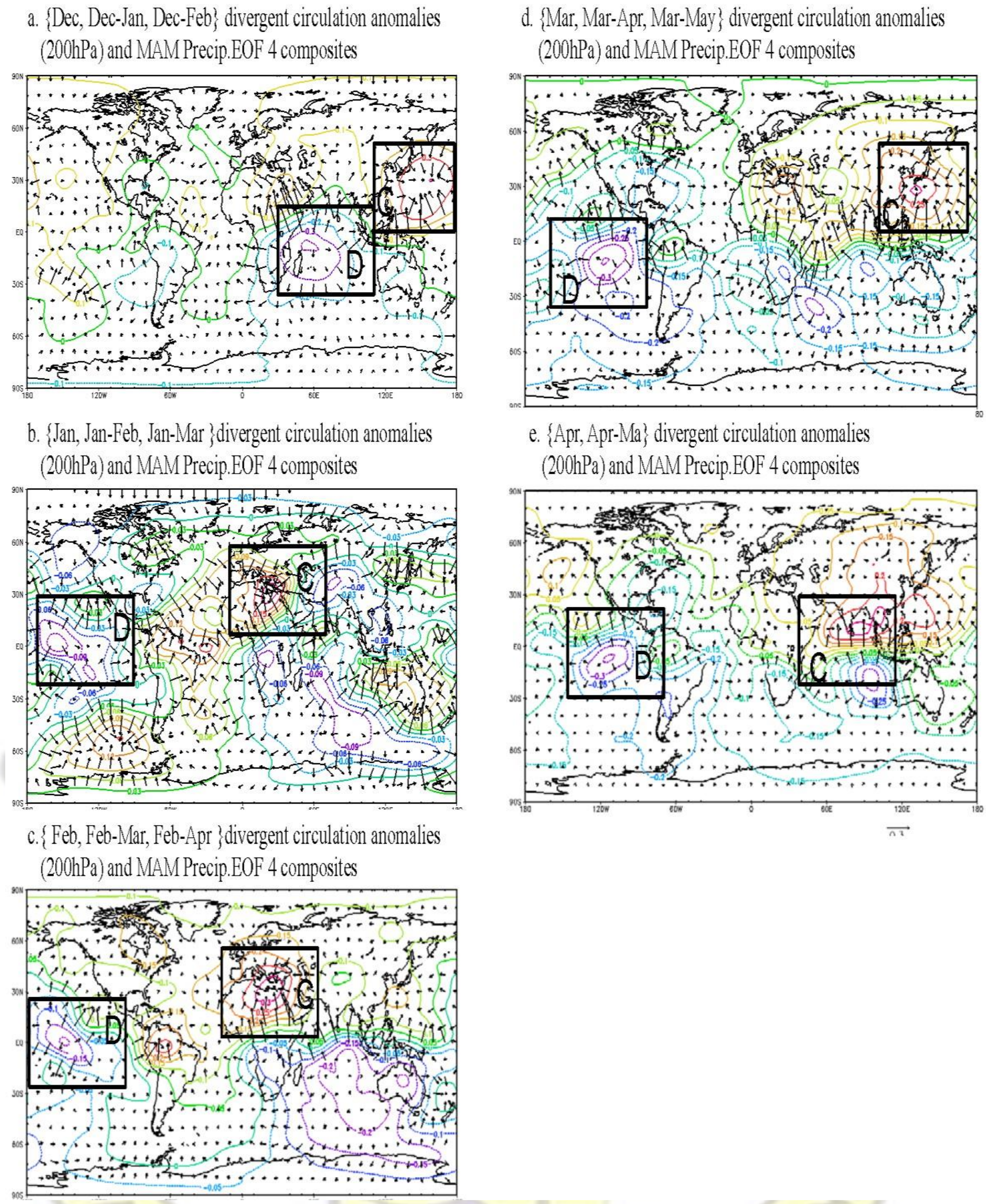

Figure 4.29- Standardized combined global divergent circulation anomalies and MAM precipitation EOF 4 mode composites at different lags. The boxes indicate centres of action: D= Divergence (which implies rainfall enhancement) and C= Convergence (which implies rainfall suppression)

4.3 Multiple Linear Regression between the Rainfall Modes and the Climate Indices

Table 5-7 presents the R^2 values of the regression between rainfall modes 1, 3 and 4 and the climate indices. The R^2 values are indicative of the variation of the dependent variable (rainfall modes) accounted for by the independent variables (climate indices). **Table 5** : R^2 values of the linear regression between rainfall EOF 1 mode and climate indices over different timescales.

MONTHLY	BIMONTHLY	SEASONAL	COMBINED
D--0.118	DJ -- 0.14	DJF-- 0.166	{D,DJ,DJF}-- 0.163
J --**0.26**	JF -- 0.11	JFM-- 0.167	{J,JF,JFM}-- 0.203
F --0.20	FM -- **0.23**	FMA-- **0.223**	{F,FM,FMA}-- **0.236**
M --0.193	MA-- 0.19	MAM-- 0.154	{M,MA,MAM}-- 0.216
A -- 0.09	AM-- 0.136		{A,AM}-- 0.164
M-- 0.0007			

Table 6: R^2 values of the linear regression between rainfall EOF 3 mode and climate indices over different timescales.

MONTHLY	BIMONTHLY	SEASONAL	COMBINED
D-- **0.301**	DJ-- **0.249**	DJF-- **0.244**	{D,DJ,DJF}--**0.273**
J-- 0.191	JF-- 0.114	JFM-- 0.214	{J,JF,JFM}-- 0.213
F-- 0.114	FM-- 0.184	FMA-- 0.193	{F,FM,FMA}-- 0.211
M-- 0.191	MA-- 0.192	MAM-- 0.218	{M,MA,MAM}-- 0.215
A-- 0.121	AM-- 0.217		{A,AM}-- 0.211
M-- 0.199			

Table 7: R^2 values of the linear regression between rainfall EOF 4 mode and climate indices over different timescales.

MONTHLY	BIMONTHLY	SEASONAL	COMBINED
D-- 0.000029	DJ-- 0.0224	DJF-- 0.0482	{D,DJ,DJF}-- 0.0337
J-- 0.055	JF-- 0.123	JFM-- 0.16	{J,JF,JFM}-- 0.127
F-- 0.2	FM-- 0.183	FMA-- 0.194	{F,FM,FMA}-- 0.218
M-- 0.151	MA-- 0.172	MAM-- **0.198**	{M,MA,MAM}-- 0.178
A-- 0.174	AM-- **0.218**		{A,AM}-- **0.209**
M-- **0.247**			

CHAPTER FIVE

5.0 Conclusions

The study primarily focused on analysis of global-scale climate features and their relationship to the dominant MAM rainfall modes over the GHA during the climatologically prominent phase of ENSO. EOF analysis isolated four dominant modes, which together contributed to 34.2% of the total explained variance. Showing distinct spatio-temporal patterns, their time series were all characterized by interannual variability. Each of the modes responded differently to the Pacific, Atlantic and Indian Oceans on the monthly, bimonthly, seasonal and combined timescales. The Pacific Niño regions were the prime factors, though the Atlantic and the Indian Oceans had their share. The associated divergent circulation displayed varied patterns in terms of their action centers, spatial extents and intensities, and these were specific to precipitation EOFs 1, 3, and 4 modes. These gave further guidance in understanding convective development or otherwise over the region. Traditionally, statistical models rely on seasonal climate features for predicting seasonal rainfall patterns. On the basis of this study, it would be useful if the specific monthly and bimonthly predictors were incorporated into the prediction scheme, to enhance climate change adaptations specific to a climatic setting. Rainfall EOF 2 practically did not relate well with the global SST on the three timescales (i.e. monthly, bimonthly and seasonal timescales), a situation which required further research. Furthermore, this observation was in consonance with an earlier study. It became clear from this study that the EOF 2 mode was perhaps governed by complex system involving land-ocean-atmosphere feedbacks, which warrants modeling studies. These observations raise questions about the dependence of seasonal climate features in predicting seasonal rainfall patterns by statistical models. In general, the modes responded differently to the Pacific, Atlantic, and Indian Oceans. They also differed with respect to specific oceanic sectors that corresponded to them. In particular, specific Niño regions were identified for each of the three precipitation modes as global ocean climate evolved with time. This underscored the importance of the Pacific, Atlantic, and Indian Ocean SST delineation for every timescale.

On which particular timescale then does global climate features best modulate the MAM rainfall? This study provided further investigation into this with a multiple regression model. The association between SST features (predictors), specifically; the Pacific ENSO; Niño3 (5^oN-5^oS, 150^oW-90^oW), Niño3.4 (5^oN-5^oS, 170^o-120^oW) and Niño 4 (5^oN-5^oS, 160^oE-150^oW) regions, the Atlantic and Indian Oceans and the rainfall EOF 1, EOF 3 and EOF 4 modes were significant on a monthly timescale (Table 6-8). This showed R^2 values of 0.26, 0.301 and 0.247 in January (Appendix A.1.2), December (Appendix B.1.1) and May (Appendix C.1.5) respectively.

5.1 Recommendations

On the basis of these conclusions, the following recommendations can be considered. The outcome of this study is very important to end users, especially policy makers to enhance climate change adaptations specific to a climatic setting. The rainfall EOF 2 which practically did not relate well with the global SST on all the three timescales merits further research. This mode may be governed by complex system involving land-ocean-atmosphere feedbacks, which warrants modeling studies. Again, further work can be done to explore the EOF 2 issue with different data sets.

Finally, numerical modeling to further establish the teleconnection between East African and the Gulf of Guinea.

REFERENCES

Akponikpe`, P.B.I., B. Ge´rard,, K. Michels and C.L. Bielders. (2010). Use of the APSIM model in long term simulation to support decision making regarding nitrogen management for pearl millet in the Sahel, *European Journal Agronomy* 32: 144-154.

Barnston, A.G. and C.F. Ropelewski, (1992). Prediction of ENSO episodes using canonical correlation analysis. *Journal of Climate* 17:1316-1345.

Berhane, F. and B. Zaitchik (2013). Modulation of daily precipitation over East Africa by Madden-Julian Oscillation. *Bulletin of American Meteorological Society*.DOI: http://dx.doi.org/10.1175/JCLI-D-13-00693.1

Black E.(2004). The relationship between Indian Ocean sea-surface temperature and East African rainfall. *Philosophical Transactions of the Royal Society*363: 43–47.

Bowden, J. H. and F. H. M. Semazzi, (2007). Empirical Analysis of Intraseasonal Climate Variability over the greater Horn of Africa. *Journal of Climate* 20:57155731.

Camberlin P. (1995). June–September rainfall in North-Eastern Africa and atmospheric signals over the tropics: A zonal perspective. International Journal of Climatology 15: 773–783.

Camberlin P, Philippon N. (2001). The East African March–May season: associated atmospheric dynamics and predictability over the 1967–68 period. *Journal of Climate* 15: 1002–1019.

Chiew FHS, Piechota TC, Dracup JA, McMahon TA. 1998. El Nin˜o/Southern Oscillation and Australian rainfall, streamflow and drought: links and potential for forecasting. *Journal of Hydrology* 204: 138–149.

Ford, J.D., L. Berrang-Ford, A. Bunce, C. McKay, M. Irwin, and T. Pearce. (2015). The status of climate change adaptation in Africa and Asia. *Regional Environmental Change* 15:801–814. DOI 10.1007/s10113-014-0648-2.

Funk C, Peterson P, Landsfeld M, Pedreros D, Verdin J, RowlandJ, Romero B, Husak G, Michaelsen J, Verdin, A. (2014).*A Quasi-global Precipitation Time Series for Drought Monitoring,* USGS, EROS Data Center, Sioux Falls, SD.

Funk, C. (2012). Exceptional warming in the Western Pacific-Indian Ocean Warm Pool has contributed to more frequent droughts in Eastern Africa, *Bulletin of American Meteorological Society* 7:1049–1051.

Hannachi A, I.T Jolliffe, and D.B Stephenson (2007). Empirical orthogonal functions and related techniques in atmospheric science: A review. *International Journal Climatology* 27: 1119–1152, doi: 10.1002/joc.1499.

Harris, I., P.D. Jones, T.J. Osborna and D.H. Lister(2014). Updated high-resolution grids of monthly climatic observations – the CRU TS3.10 Dataset. *International Journal of Climatology*34: 623–642. doi: 10.1002/joc.3711.

Hastenrath S, NicklisA.,Greischar L.(1993). Atmospheric-hydrospheric mechanisms of climate anomalies in the western equatorial Indian Ocean. *Journal of Geophysics Research*98 (C11): 20 219–20 235

Hoell, A., Funk, C., and Barlow, M. (2013). The regional forcing of Northern hemisphere drought during recent warm tropical west Pacific Ocean La Niña events, *Climate Dynamics.*, 42, 3289–3311, doi:10.1007/s00382-013-1799-4

Indeje, M., F. H. M. Semazzi and L. J. Ogallo. (2000).ENSO signals in East African rainfall seasons. *International Journal of Climatology* 20:19–46.

Indeje M, Semazzi FHM. (2000). Relationships between QBO in the lower stratospheric zonal winds and east African seasonal rainfall. *Meteorology and Atmospheric Physics*73: 227–244.

Intergovernmental Panel on Climate Change (IPCC). (2001). Climate Change 2001. Synthesis report. Cambridge University Press. Cambridge.

Janowiak JE. (1988). An investigation of interannual rainfall variability in Africa. *Journal of Climate*1: 240–255.

Kalnay E., M. Kanamitsu, R. Kistler, W. Collins, D. Deaven, L. Gandin, M. Iredell, S. Saha, G. White, J. Woollen, Y. Zhu, A. Leetmaa, R. Reynolds, M. Chelliah, W. Ebisuzaki, W. Higgins, J. Janowiak, K.C. Mo, C. Ropelewski, J. Wang, R. Jenne and D. Joseph.
(1996). The NCEP/NCAR 40-year reanalysis project. *Bulletin of American Meteorological Society* 77(3): 437–471.

Krishnamurti, T.N. (1971). Tropical east-west circulations during the northern summer. *Journal of Atmospheric Sciences* 28: 1342-1347.

Latif, M., D. Dommenget, M. Dima and Grotzner, A. (1999). The role of Indian Ocean sea surface temperature in forcing East African rainfall anomalies during December–January 1997/98. *Journal of Climate* 12: 3497–3504.

Lyon, B. and DeWitt, D. G.: A recent and abrupt decline in the East African long rains, *Geophysical Research Letters* 39, L02702, doi:10.1029/2011gl050337,2012.

Marchant, R. C. Mumbi, S. Behera and T.Yamagata. (2006). The Indian Ocean dipole – the unsung driver of climatic variability in East Africa. *African Journal of Ecology* 45: 4–16.

McHugh MJ. (2004). Near surface zonal flow and East African precipitation receipt during Austral summer. *Journal of Climate*20: 4070–4079.

McHugh MJ. (2006).Impact of south pacific circulation variability on east African rainfall.*International Journal of Climatology*26: 505-521.

Mistry VV, Conway DC. (2003). Remote forcing of East African rainfall and relationships with fluctuations in levels of Lake Victoria. *International Journal of Climatology***23**: 67–89.

Nicholson, S.E. (1996). The Limnology, Climatology and Paleoclimatology of the East African Lakes. Gordon and Breach, New York, 57 pp.

—, and J. Kim, (1997). The relationship of the El Niño-Southern Oscillation to African Rainfall. *International Journal of Climatology* 17:117–135.

North, G.R., T. L. Bell, R.F. Cahalan and F.J. Moeng (1982). Sampling Errors in the Estimation of Empirical Orthogonal Functions. *Monthly Weather Review* 110:699706.

Ogallo, L.J. (1980). Rainfall variability in Africa. *Monthly Weather Review* 107**:**1133–1139.

— (1983). Quasi-periodic patterns in East African rainfall records. *Kenya Journal of Science and Technology* A3: 43–54.

— (1988).Relationships between seasonal rainfall in East Africa and the Southern Oscillation. *International Journal of Climatology* 8**:**31–43.
(1989). The spatial and temporal patterns of the East African seasonal rainfall derived from principal component analysis. *International Journal Climatol*ogy 9: 145–167.

Ropelewski, C.F. and M.S. Halpert(1987). Global and regional scale precipitation patterns associated with the El Niño Southern Oscillation. *Monthly Weather Review* 115: 1606–1626.
Rowell DP, Ininda JM, Ward MN. (1994). The impact of global sea surface temperature patterns on seasonal rainfall in East Africa. *Proceedings of International Conference on Monsoon Variability and Prediction, Trieste, Italy, WMO* 666–672.

Saji, N.H., B.N. Goswami, P.N. Vinayachandran and T. Yamagata. (1999). A dipole mode in the tropical Indian Ocean. *Nature* 401: 360–363.

Schreck, C. J. and F. H. M. Semazzi(2004). Variability of the recent climate of eastern Africa. *International Journal of Climatology* 24:681–701.

Smith T.M, and R.W. Reynolds (2004). Improved extended reconstruction of SST (1854–1997). *Journal of Climate* 17: 2466-2477.

Smith, K.A. and F. H. M. Semazzi (2014). The Role of the Dominant Modes of Precipitation Variability over Eastern Africa in Modulating the Hydrology of Lake Victoria.
Advances in MeteorologyArticle ID 516762, 11 pp. http://dx.doi.org/10.1155/2014/516762.

Tetteh, IK. (2012). West African Seasonal Climate Variability and Predictability.*PhD Dissertation, NCSU, USA*.153pp.

Trenberth, K. E., D.P. Stepaniak, and J. M. Carbon (2000). The Global Monsoon as Seen through the Divergent Atmospheric Circulation. *Journal of Climate* 13: 39693993.

Washington, R., M. Harrison, D. Conway, E. Black, A. Challinor, D. Grimes, R. Jones, A. Morse, G. Kay, and M. Todd (2006). AFRICAN CLIMATE CHANGE Taking the Shorter Route. *Bulletin of American Meteorological Society* 1355-1366.

Wilks, D.S. (2006). Statistical Methods in the Atmospheric Sciences, 3rd Edition. Academic
Press: New York, USA.

Williams, P., Funk, C. (2011). A westward extension of the warm pool leads to a westward extension of the Walker circulation, drying eastern Africa. *Climate Dynamics***37**: 2417–2435.

APPENDICES

Appendix A

Linear Regression Output between Rainfall Mode 1 (EOF 1) and Climate Indices on All Timescales

A.1 MONTHLY TIMESCALE

A.1.1 EOF 1 and December Indices

y= EOF 1, x1=Niño 4, x2=Niño 3.4, x3=Niño 3, x4=Niño1+2, x5= PNA

Linear regression model:
y - 1 + x1 + x2 + x3 + x4 + x5 Estimated
Coefficients:

	Estimate	SE	tStat	pValue
(Intercept)	0.00050333	0.12909	0.003899	0.9969
x1	-0.031141	0.42261	-0.073687	0.94154
x2	0.47086	0.9847	0.47818	0.63453
x3	-0.69625	0.89817	-0.77518	0.44174
x4	0.58237	0.35569	1.6373	0.1076
x5	-0.19814	0.13856	-1.43	0.15869

Number of observations: 58, Error degrees of freedom: 52
Root Mean Squared Error: 0.983
R-squared: 0.118, Adjusted R-Squared 0.0334
F-statistic vs. constant model: 1. 39, p-value 0.242

A.1.2 EOF 1 and January Indices

y= EOF 1, x1=Niño 3, x2= Niño 3.4, x3Niño 4, x4= TSA, x5= PNA, x6=SOI

Linear regression model:
y - 1 + x1 + x2 + x3 + x4 + x5 + x6 Estimated
Coefficients:

	Estimate	SE	tStat	pValue	
(Intercept)	0.0002293	0.11941	0.0019203	0.99848	
x1	-0.43222	0.5813	- 0.74354	0.46057 x2	
0.38917	0.80378	0.48417	0.63034 x3		-
0.21201	0.37131	-0.57099	0.57051 x4		
0.29244	0.13121	2.2288	0.030258 x5		
-0.21581	0.12726	-1.6958	0.096016 x6		
-0.57892	0.20162	-2.8713	0.0059392		

Number of observations: 58, Error degrees of freedom: 51
Root Mean Squared Error: 0.909
R-squared: 0.26, Adjusted R-Squared 0.173
F-statistic vs. constant model: 2.99, p-value 0.0141

A.1.3 EOF 1 and February Indices

y= EOF1, x1=Niño 3, x2=Niño 3.4, x3=Niño 4, x4= TSA, x5=TNA, x6=SOI

Linear regression model:
y - 1 + x1 + x2 + x3 + x4 + x5 + x6 Estimated
Coefficients:

	Estimate	SE	tStat	pValue
(Intercept)	-0.00038742	0.12411	-0.0031215	0.99752 x1
-0.082932	0.49147	-1.6874	0.09763 x2	
1.8313	0.73922	2.4773	0.016593 x3	-
0.68443	0.38443	-1.7804	0.080971 x4	
0.22697	0.013372	1.6974	0.095712 x5	-
0.047818	0.14025	-0.34094	0.73455 x6	
0.25092	0.18609	1. 3483	0.18351	

Number of observations: 58, Error degrees of freedom: 51
Root Mean Squared Error: 0.945
R-squared: 0.201, Adjusted R-Squared 0.107
F-statistic vs. constant model: 2.13, p-value 0.0653

A.1.4 EOF 1 and March Indices

y= EOF 1, x1=Niño 3, x2=Nino 3.4, x3Niño4, x4=PNA, x5=TNA, x6=SOI

Linear regression model:
y - 1 + x1 + x2 + x3 + x4 + x5 + x6 Estimated
Coefficients:

	Estimate	SE	tStat	pValue
(Intercept)	-0.0006156	0.1247	-0.0049366	0.99608
x1	-0.3092	0.36256	-0.85282	0.39775
x2	1.0849	0.56273	1. 9278	0.059454
x3	-0.53174	0. 34311	-1.5498	0.12738
x4	0.28297	0.14957	1. 8919	0.064189
x5	-0.13993	0.14494	-0.96546	0.33887
x6	0.28637	0.18133	1.5793	0.12044

Number of observations: 58, Error degrees of freedom: 51
Root Mean Squared Error: 0.95
R-squared: 0.193, Adjusted R-Squared 0.0981
F-statistic vs. constant model: 2.03, p-value 0.0781

A.1.5 EOF 1and April Indices

y= EOF 1, x1=TSA, x2=Niño 4, x3=TNA, x4=Niño 3.4

Linear regression model:
y - 1 + x1 + x2 + x3 + x4
Estimated Coefficients:

	Estimate	SE	tStat	pValue
(Intercept)	-1. 55e-05	0.12934	-0.00011984	0.9999
x1	0.18475	0 .13183	1.4015	0.1669
x2	-0.32489	0.24366	-1.3333	0.18812
x3	-0.027155	0.1483	-0.1831	0.85541
x4	0.42945	0.24199	1.7747	0.081696

Number of observations: 58, Error degrees of freedom: 53
Root Mean Squared Error: 0.985

R-squared: 0.0978, Adjusted R-Squared 0.0297
F-statistic vs. constant model: 1.44, p-value

A.1.6 EOF 1 and May Indices

y= EOF 1, x1= TNA

Linear regression model:
y - 1 + x1
Estimated Coefficients:
Estimate SE tStat pValue
(Intercept) 1.1582e-05 0.13242 8.7464e-05 0.99993 x1
0.02707 3 0.13346 0.20286 0.83998

Number of observations: 58, Error degrees of freedom: 56
Root Mean Squared Error: 1.01
R-squared: 0.000734, Adjusted R-Squared -0.0171
F-statistic vs. constant model: 0.0412, p-value = 0.84

A.2 BIMONTHLY TIMESCALE

A.2.1 EOF 1 and December-January Indices

y= EOF 1, x1= Niño 4, x2=Niño3.4, x3=Niño 3, x4=Niño 1+2, x5= PNA, x6=SOI

Linear regression model:
y - 1 + x1 + x2 + x3 + x4 + x5 + x6 Estimated
Coefficients:
Estimate SE tStat pValue
(Intercept) -4.1508e-06 0.12874 -3.2242e-05 0.99997
x1 -0.15004 0.42607 -0.35216 0.72617
x2 0.85839 1.0349 0.82947 0.4107 x3
-0.82773 0.95798 -0.86404 0.39161 x4 0.52148
0.35292 1.4776 0.14566 x5 -0.26604
0.1427 -1.8643 0.068041
x6 0.035033 0.16505 0.21226 0.83275
Number of observations: 58, Error degrees of freedom: 51
Root Mean Squared Error: 0.98
R-squared: 0.14, Adjusted R-Squared 0.0387
F-statistic vs. constant model: 1.38, p-value 0.24

A.2.2 EOF 1 and January-February Indices

y=EOF 1, x1=PNA, x2=Niño 3, x3=Niño 3.4, x4=Niño 4, x5=SOI

Linear regression model: y - 1
+ x1 + x2 + x3 + x4 + x5
Estimated Coefficients:
Estimate SE tStat pValue
(Intercept) 2.0124e-06 0.12934 1.5559e-05 0.99999
x1 -0.16208 0.14326 -1.1314 0.26309 x2
-0.36517 0.57945 -0.6302 0.53132 x3

0.9775	0.85897	1.138	0.26034 x4 -
0.43282	0.40463	-1.0697	0.28971 x5 -
0.1095	0.26765	-0.40913	0.68413

Number of observations: 58, Error degrees of freedom: 52
Root Mean Squared Error: 0.985
R-squared: 0.115, Adjusted R-Squared 0.0297
F-statistic vs. constant model: 1.35, p-value 0.259

A.2.3 EOF 1 and February-March Indices

y= EOF 1, x1=PNA, x2=Niño 3, x3=Niño 3.4, x4Niño4, x5=TNA, x6=TSA, x7=SOI

Linear regression model:
y - 1 + x1 + x2 + x3 + x4 + x5 + x6 + x7 Estimated
Coefficients:

	Estimate	SE	tStat	pValue
(Intercept)	-1. 0876e-05	0.12306	-8.8375e-05	0.99993 x1
0.11111	0.15798	0.70328	0.48514 x2	-
0.61708	0.44376	-1.3906	0.17052 x3	
1.7341	0.67837	2.5562	0.013666 x4	-
0.6954	0.37389	-1.8599	0.068786 x5	-
0.095215	0.14409	-0.66083	0.51176 x6	
0.19064	0.1378	1. 3835	0.17267 x7	
0.38965	0.23102	1. 6867	0.097898	

Number of observations: 58, Error degrees of freedom: 50
Root Mean Squared Error: 0.937
R-squared: 0.229, Adjusted R-Squared 0.122
F-statistic vs. constant model: 2.13, p-value 0.0575

A.2.4 EOF 1 and March-April Indices

y= EOF 1, x1=TSA, x2=TNA, x3=PNA, x4=Niño 3, x5=Niño 3.4, x6=Niño 4, x7=SOI'

Linear regression model:
y - 1 + x1 + x2 + x3 + x4 + x5 + x6 + x7 Estimated
Coefficients:

	Estimate	SE	tStat	pValue
(Intercept)	4.5123e-06	0.12553	3.5945e-05	0.99997
x1	0.157	0.13794	1.1382	0.26044
x2	-0.12043	0.14948	-0.80563	0.42427
x3	0.24006	0.16335	1.4697	0.14791
x4	-0.43537	0.34427	-1.2646	0.21186
x5	1.0884	0.5533	1. 967	0.054741
x6	-0.56267	0.35751	-1.5739	0.12183
x7	0.12919	0.21314	0.60612	0.54718

Number of observations: 58, Error degrees of freedom: 50
Root Mean Squared Error: 0.956
R-squared: 0.198, Adjusted R-Squared 0.086
F-statistic vs. constant model: 1. 77' p-value 0.115

A.2.5 EOF 1 and April-May Indices

y= EOF1, x1=Niño 3.4, x2=Nino 4, x3=Niño 3, x4=PNA, x5=TSA

Linear regression model: y - l
+ xl + x2 + x3 + x4 + x5
Estimated Coefficients:
Estimate SE tStat pValue
(Intercept) 1.1529e-05 0.12781 9.021e-05 0.99993
x1 0.94201 0.55331 1.7025 0.094635
x2 -0.49166 0.33307 -1.4762 0.14593 x3
-0.5223 0.34936 -1.495 0.14095 x4
0.22078 0 .13695 1.6121 0.11299 x5
0.17748 0 .13084 1. 3564 0.18083 Number of
observations: 58, Error degrees of freedom: 52
Root Mean Squared Error: 0. 973
R-squared: 0.136, Adjusted R-Squared 0.0526
F-statistic vs. constant model: 1. 63, p-value 0.168

A.3 SEASONAL TIMESCALE

A.3.1 EOF 1 and December-February Indices

y= EOF 1, x1=PNA, x2=Niño3, x3=Niño 3.4, x4=Niño 4, x5=TSA, x6=SOI

Linear regression model:
y - 1 + x1 + x2 + x3 + x4 + x5 + x6 Estimated
Coefficients:
Estimate SE tStat pValue
(Intercept) 6.1259e-06 0.12676 4.8327e-05 0.99996
x1 -0.27494 0.1474 -1.8653 0.067898
x2 -0.42449 0.65444 -0.64864 0.51948
x3 1.1913 0.92445 1.2886 0.20335
x4 -0.44552 0.42562 -1.0468 0.30014 x5
0.25046 0.1465 1. 7096 0.093417
x6 0.11239 0.23005 0.48856 0. 62725
Number of observations: 58, Error degrees of freedom: 51
Root Mean Squared Error: 0.965
R-squared: 0.166, Adjusted R-Squared 0.0681
F-statistic vs. constant model: 1.69, p-value 0.142

A.3.2 EOF 1 and January-March Indices

y=EOF 1, x1=Niño 4, x2=TSA, x3=PNA, x4Niño3, x5=Niño3.4, x6=SOI

Linear regression model:
y - 1 + x1 + x2 + x3 + x4 + x5 + x6 Estimated
Coefficients:
Estimate SE tStat pValue
(Intercept) -4.915e-06 0.12671 -3.8788e-05 0.99997
x1 -0.66182 0.39537 -1.6739 0.10027
x2 0.28348 0.14291 1.9836 0.052699
x3 -0.14569 0.15974 -0. 9121 0.36601 x4
-0.60337 0.54105 -1.1152 0.27 x5 1.3635
0.80097 1. 7023 0.094789 x6 -0.095179
0.29869 -0.31865 0.75129

Number of observations: 58, Error degrees of freedom: 51
Root Mean Squared Error: 0.965
R-squared: 0.167' Adjusted R-Squared 0.0687
F-statistic vs. constant model: 1. 7' p-value 0.14

A.3.3 EOF 1 and February-April Indices

y= EOF 1, x1=PNA, x2=Niño 3, x3=Niño 3.4, x4=Niño 4, x5=TSA, x6=SOI

Linear regression model:
y - 1 + x1 + x2 + x3 + x4 + x5 + x6 Estimated
Coefficients:

	Estimate	SE	tStat	pValue
(Intercept)	3.5388e-06	0.12235	2.8924e-05	0.99998
x1	0.13662	0.15661	0. 87238	0.38709
x2	-0.56481	0.38604	-1.4631	0.14958
x3	1.6752	0.62871	2.6646	0.010294
x4	-0.76759	0.36506	-2.1026	0.040454
x5	0.17557	0.13356	1.3145	0.19455
x6	0. 38136	0.24939	1.5291	0.13241

Number of observations: 58, Error degrees of freedom: 51
Root Mean Squared Error: 0.932
R-squared: 0.223, Adjusted R-Squared 0.132
F-statistic vs. constant model: 2.44, p-value 0.0376

A.3.4 EOF 1 and March-May Indices

y= EOF 1, x1=Niño 4, x2=PNA, x3=Niño3, x4=Niño3.4, x5=TNA'

Linear regression model:
y - 1 + x1 + x2 + x3 + x4 + x5
Estimated Coefficients:

	Estimate	SE	tStat	pValue
(Intercept)	1. 786e-06	0.12642	1. 4127e-05	0.99999
x1	-0.57383	0. 35772	-1.6041	0.11474
x2	0.28065	0.14549	1.9291	0.059185
x3	-0.54245	0.34409	-1.5765	0.12098
x4	1.0648	0.57238	1. 8604	0.06849
x5	-0.106	0.14677	-0.72218	0.47342

Number of observations: 58, Error degrees of freedom: 52
Root Mean Squared Error: 0.963
R-squared: 0.154, Adjusted R-Squared 0.073
F-statistic vs. constant model: 1.9, p-value 0.111

A.4COMBINED TIMESCALE

A.4.1 EOF 1 and D_DJ_DJF Indices

y=EOF 1, x1=Niño 4, x2=Niño 3.4, x3=Niño 3, x4Niño1+2, x5=PNA, x6=SOI, x7=TSA

Linear regression model:
y - 1 + x1 + x2 + x3 + x4 + x5 + x6 + x7 Estimated
Coefficients:
Estimate SE tStat pValue
(Intercept) 0.00036389 0.12824 0.0028375 0.99775
x1 -0.27724 0.44277 - 0.62614 0.53407 x2
1.0252 1. 042 0.98396 0.32987 x3 -
0.84788 0.99074 -0.8558 0.39619 x4
0.40095 0.43066 0.93101 0.35632 x5 -
0.28643 0.15211 - 1.883 0.065525 x6
0.0424 0.20736 0.20448 0.83881
x7 0.1831 0.16877 1.0849 0.28318
Number of observations: 58, Error degrees of freedom: 50
Root Mean Squared Error: 0.977
R-squared: 0.163, Adjusted R-Squared 0.0461
F-statistic vs. constant model: 1.39, p-value 0.229

A.4.2 EOF 1 and J_JF_JFM Indices

y= EOF 1, x1= Niño3, x2= Niño3.4, x3=Niño4, x4= SOI, x5=PNA, x6=TSA

Linear regression model:
y - 1 + xl + x2 + x3 + x4 + x5 + x6 Estimated
Coefficients:
Estimate SE tStat pValue
(Intercept) 3.9137e-05 0.l2392 0.00031583 0.99975 x l
-0.59177 0.57927 -1.0216 0.3118 x2
0.89611 0.83313 1.0756 0.28717 x3 -
0.48415 0.39365 -1.2299 0.22438 x4 -
0.4592 0.28253 -1.6253 0.11026 x5 -
0.23296 0.l4868 -l.5668 0.l2333
x6 0.3136 0.13866 2.2617 0.02801
Number of observations: 58, Error degrees of freedom: 51
Root Mean Squared Error: 0.944
R-squared: 0.203, Adjusted R-Squared 0.l09
F-statistic vs. constant model: 2.17 p-value 0.0615

A.4.3 EOF 1 and F_FM_FMA Indices

y= EOF 1, x1=Niño 3, x2=Niño3.4, x3=Niño4, x4=TSA, x5=SOI, x6=TNA, x7=PNA

Linear regression model:
y - 1 + xl + x2 + x3 + x4 + x5 + x6 + x7 Estimated
Coefficients:
Estimate SE tStat pValue
(Intercept) -0.00015879 0.12258 -0.0012955 0.99897
x1 -0.70328 0.45123 -1.5586 0.1254 x2
1. 8646 0.69749 2.6733 0.010117 x3 -
0.74589 0.38441 -1.9404 0.057986 x4
0.19123 0.13727 1. 3931 0.16974 x5 0.4264
0.23882 1.7855 0.08025 x6 -0.08071 0.14319
-0.56366 0.5755
x7 0.13765 0.16098 0.85505 0.3966
Number of observations: 58, Error degrees of freedom: 50
Root Mean Squared Error: 0.934

R-squared: 0.236, Adjusted R-Squared 0.129
F-statistic vs. constant model: 2.2, p-value 0.0498

A.4.4 EOF 1 and M_MA_MAM Indices

y= EOF 1, x1=PNA, x2=Niño 3, x3=Niño3.4, x4=Niño 4, x5=TNA, x6=SOI, x7=TSA

Linear regression model:
y - 1 + x1 + x2 + x3 + x4 + x5 + x6 + x7 Estimated
Coefficients:

	Estimate	SE	tStat	pValue
(Intercept)	-0.0002032	0.1241	-0.0016374	0.9987 x1
0.27545	0.16502	1. 6692	0.10133 x2	-
0.50276	0.35652	-1.4102	0.16468 x3	1.
2235	0.5774	2.1189	0.039087 x4	-
0.61145	0.35834	-1.7063	0.094152 x5	-
0.11878	0.14656	-0.81046	0.42152 x6	0.17171
0.20378	0.84263	0.40345 x7	0.16889	0
.13518	1.2494	0.21735 Number of observations: 58,		

Error degrees of freedom: 50
Root Mean Squared Error: 0. 945
R-squared: 0.216, Adjusted R-Squared 0.107
F-statistic vs. constant model: 1. 97' p-value 0.0776

A.4.5 EOF 1 and A_AM Indices

y=EOF 1, x1=TSA, x2=Niño 4, x3=Niño 3.4, x4=TNA, x5=Nino 3, x6=PNA

Linear regression model:
y - 1 + x1 + x2 + x3 + x4 + x5 + x6 Estimated
Coefficients:

	Estimate	SE	tStat	pValue
(Intercept)	-4.0282e-05	0.12695	-0.00031731	0.99975
x1	0.17006	0.13014	1.3067	0.19718
x2	-0.49464	0.30687	-1.6119	0.11316
x3	0.96655	0.48261	2.0028	0.050534
x4	-0.082051	0.1468	-0.55892	0.57866
x5	-0.51029	0.30268	-1.6859	0.097927
x6	0.22385	0.13841	1. 6173	0.11198

Number of observations: 58, Error degrees of freedom: 51
Root Mean Squared Error: 0.967
R-squared: 0.164, Adjusted R-Squared 0.0652
F-statistic vs. constant model: 1.66, p-value 0.149

Appendix B

Linear Regression Output between Rainfall Mode 3 (EOF 3) and Climate Indices on All Timescales

B.1 MONTHLY TIMESCALE

B.1.1 EOF 3 and December Indices

y= EOF 3, x1=Niño4, x2=Niño3.4, x3=Niño 3, x4=Niño 1+2, x5=PNA, x6=AMO

Linear regression model:
y - 1 + x1 + x2 + x3 + x4 + x5 + x6 Estimated
Coefficients:
Estimate SE tStat pValue
(Intercept) 0.00080663 0.11606 0.0069499 0.99448
xl -0.011873 0.3954 -0.030027 0.97616 x2
-0.31287 0.90591 -0.34536 0.73124 x3 -
0.0085468 0.81293 -0.010514 0.99165 x4 0.13405
0.31999 0.41893 0.67703 x5 -0.32287 0.12686
-2.5452 0. 013991 x6 0.39921 0.12498
3.1943 0.0024042

Number of observations: 58, Error degrees of freedom: 51
Root Mean Squared Error: 0.884
R-squared: 0.301, Adjusted R-Squared 0.219
F-statistic vs. constant model: 3. 66, p-value 0.00426

B.1.2 EOF 3 and January Indices

y= EOF 3, x1=Niño 3, x2=Nino 3.4, x3=Niño4, x4=AMO

Linear regression model:
y - 1 + x1 + x2 + x3 + x4
Estimated Coefficients:

	Estimate	SE	tStat	pValue
(Intercept)	-2.9472e-05	0.12248	-0.00024063	0.99981
x1	-0.18686	0.5789	-0.32279	0.74813
x2	0.11912	0.82749	0.14395	0.88609
x3	-0.224	0.38934	-0.57533	0.5675
x4	0.34567	0.12694	2.7231	0.0087371

Number of observations: 58, Error degrees of freedom: 53
Root Mean Squared Error: 0.933
R-squared: 0.191, Adjusted R-Squared 0.13
F-statistic vs. constant model: 3.13, p-value 0.022

B.1.3 EOF 3 and February Indices

y= EOF 3, x1=AMO

Linear regression model:
y - 1 + x1
Estimated Coefficients:

	Estimate	SE	tStat	pValue
(Intercept)	-9.7401e-06	0.1247	-7.8111e-05	0.99994
x1	0.33762	0.12578	2.6841	0.0095469

Number of observations: 58, Error degrees of freedom: 56
Root Mean Squared Error: 0.95
R-squared: 0.114, Adjusted R-Squared 0.0982
F-statistic vs. constant model: 7.2, p-value 0.00955

B.1.4 EOF 3 and March Indices

y= EOF 3, x1=Niño4, x2=PNA, x3=AMO

Linear regression model: y
- 1 + x1 + x2 + x3
Estimated Coefficients:

	Estimate	SE	tStat	pValue
(Intercept)	0.0003264	0.12131	0.0026907	0.99786
x1	-0.21308	0.13065	-1.6309	0.10874
x2	-0.12015	0.13104	-0.91689	0.36328
x3	0.32436	0.12275	2.6425	0.010746

Number of observations: 58, Error degrees of freedom: 54
Root Mean Squared Error: 0.924
R-squared: 0.191, Adjusted R-Squared 0.147
F-statistic vs. constant model: 4.26, p-value 0.00897

B.1.5 EOF 3 and April Indices

y=EOF 3, x1=PNA, x2=AMO

Linear regression model:
y - 1 + x1 + x2 Estimated
Coefficients:
Estimate SE tStat pValue
(Intercept) 0.00019998 0.12536 0.0015953 0.99873 x1
0.08958 0.12649 0.70818 0.48182
x2 0.33774 0.12649 2.67 0.0099526
Number of observations: 58, Error degrees of freedom:
Root Mean Squared Error: 0.955
R-squared: 0.121, Adjusted R-Squared 0.0886
F-statistic vs. constant model: 3.77, p-value 0.0292

B.1.6 EOF 3 and May Indices

y=EOF 3, x1=Niño4, x2=Niño3, x3=Niño3.4, x4=AMO, x5=SOI

Linear regression model:
y - 1 + x1 + x2 + x3 + x4 + x5 Estimated
Coefficients:
Estimate SE tStat pValue
(Intercept) -3.8448e-07 0.12305 -3.1247e-06 1 x1
-0.33078 0.32727 -1.0108 0.31682 x2
0.19621 0.35894 0.54662 0.58698 x3 -
0.066519 0.54535 -0.12197 0.90339 x4 0.37092
0.1266 2.9299 0.0050263 x5 0.013822
0.165 0.083772 0.93356
Number of observations: 58, Error degrees of freedom: 52
Root Mean Squared Error: 0.937
R-squared: 0.199, Adjusted R-Squared 0.122
F-statistic vs. constant model: 2. 58, p-value 0.0368

B.2 BIMONTHLY TIMESCALE

B.2.1 EOF 3 and December-January Indices

y=EOF 3, x1=Niño 4, x2=Niño 3.4, x3=Niño 3, x4=PNA, x5=AMO

Linear regression model:
y - 1 + x1 + x2 + x3 + x4 + x5 Estimated
Coefficients:
Estimate SE tStat pValue
(Intercept) -3.1942e-06 0.1191 -2.6819e-05 0.99998 x1
-0.18617 0.40978 -0.45432 0.65149 x2 -
0.02414 0.89648 -0.026928 0.97862 x3 -
0.012643 0.62846 -0.020118 0.98403 x4 -
0.23794 0.13126 -1.8127 0.075654 x5
0.37604 0.12626 2.9784 0.0043943

Number of observations: 58, Error degrees of freedom: 52
R-squared: 0.249, Adjusted R-Squared 0.177
F-statistic vs. constant model: 3.46, p-value

B.2.2 EOF 3 and January-February Indices

y= EOF 3, x1=AMO

Linear regression model:
y - 1 + x1
Estimated Coefficients:
Estimate SE tStat pValue
(Intercept) -2.4391e-06 0.12468 -1.9562e-05 0.99998 x1
0.33784 0.12577 2.686 0.0094976
Number of observations: 58, Error degrees of freedom: 56
Root Mean Squared Error: 0.95
R-squared: 0.114, Adjusted R-Squared 0.0983
F-statistic vs. constant model: 7.21, p-value 0.0095

B.2.3 EOF 3 and February-March Indices

y=EOF 3, x1=PNA, x2=AMO

Linear regression model:
y - 1 + x1 + x2 Estimated
Coefficients:
Estimate SE tStat pValue
(Intercept) 5.8483e-06 0.12076 4.8429e-05 0.99996 x1
-0.26458 0.12187 -2.1709 0.034268 x2 0.32939
0.12187 2.7027 0.0091295 Number of observations: 58,
Error degrees of freedom: 55
Root Mean Squared Error: 0.92
R-squared: 0.184, Adjusted R-Squared 0.154
F-statistic vs. constant model: 6.2, p-value 0.00375

B.2.4 EOF 3 and March-April Indices

y= EOF 3, x1=PNA, x2=Niño 3, x3=Niño3.4, x4=Niño4, x5=AMO

Linear regression model: y - l
+ x1 + x2 + x3 + x4 + x5
Estimated Coefficients:

	Estimate	SE	tStat	pValue
(Intercept)	-2.615e-06	0.1236	-2 .1158e-05	0.99998
x1	0.0025879	0.15221	0.017002	0.9865
x2	-0.079167	0.33609	-0.23556	0. 8147
x3	0.24873	0.54488	0.45649	0.64994
x4	-0.44118	0.33836	-1.3039	0.19802
x5	0.34897	0.12691	2. 7497	0.0081854

Number of observations: 58, Error degrees of freedom: 52
Root Mean Squared Error: 0. 941
R-squared: 0.192, Adjusted R-Squared 0.114
F-statistic vs. constant model: 2.47, p-value 0.0444

B.2.5 EOF 3 and April-May Indices

y=EOF 3, x1=Niño 3.4, x2=Niño 4, x3=Niño3, x4=PNA, x5=AMO, x6=SOI

Linear regression model:
y - 1 + x1 + x2 + x3 + x4 + x5 + x6 Estimated
Coefficients:

	Estimate	SE	tStat	pValue
(Intercept)	-9.0478e-06	0.12281	-7.3671e-05	0.99994
x1	-0.096824	0.53376	-0.18114	0.85677 x2
-0.19871	0.36452	-0.54513	0.58804 x3	0.14977
0.34262	0. 43713	0.66386 x4	0.13706	0.13391
1.0235	0.3109 x5	0.37719	0.1256	3.003
0.0041339 x6		0.13246	0.22365	0.59227
0.55629				

Number of observations: 58, Error degrees of freedom: 51
Root Mean Squared Error: 0.935
R-squared: 0.217, Adjusted R-Squared 0.125
F-statistic vs. constant model: 2. 36, p-value 0.0436

B.3 SEASONAL TIMESCALE

B.3.1 EOF 3 and December-February Indices

y= EOF 3, x1=PNA, x2=Niño 3, x3=Niño 3.4, x4Niño4, x5=AMO

Linear regression model: y - 1
+ x1 + x2 + x3 + x4 + x5
Estimated Coefficients:

	Estimate	SE	tStat	pValue
(Intercept)	1. 3186e-05	0.11954	0. 0001103	0.99991
x1	-0.24787	0.13552	-1.829	0.07313 x2
-0.10518	0.60094	-0.17503	0.86174 x3	
0.14388	0.86385	0.16656	0.86836 x4	-
0.23094	0.40335	-0.57255	0.56941	
x5	0.36912	0.12409	2.9747	0.0044397

Number of observations: 58, Error degrees of freedom: 52
Root Mean Squared Error: 0.91
R-squared: 0.244, Adjusted R-Squared 0.171
F-statistic vs. constant model: 3.35, p-value 0.0106

B.3.2 EOF 3 and January-March Indices

y= EOF 3, x1=PNA, x2=Niño3, x3=Niño3.4, x4Niño4, x5=AMO

Linear regression model: y - 1
+ x1 + x2 + x3 + x4 + x5
Estimated Coefficients:

	Estimate	SE	tStat	pValue
(Intercept)	-1. 2469e-05	0.12185	-0.00010233	0.99992 x1

-0.19642 0.14292 -1.3743 0.17524 x2 -
0.16842 0.5128 -0.32842 0.74391 x3 0.35248
0.75373 0.46764 0.642 x4 -0.36959 0.38054
-0.97123 0.33593 x5 0.34345 0.12486
2.7507 0.0081628

Number of observations: 58, Error degrees of freedom: 52
Root Mean Squared Error: 0.928
R-squared: 0.214, Adjusted R-Squared 0.139
F-statistic vs. constant model: 2.84, p-value 0.0243

B.3.3 EOF 3 and February-April Indices

y= EOF 3, x1=PNA, x2=Niño 3, x3=Niño3.4, x4=Niño 4, x5=AMO

Linear regression model: y - 1
+ x1 + x2 + x3 + x4 + x5
Estimated Coefficients:

	Estimate	SE	tStat	pValue
(Intercept)	-2.9363e-06	0.1235	-2.3776e-05	0.99998
x1	-0.10864	0.14641	-0.74203	0.46141
x2	-0.068545	0.3906	-0.17549	0.86138
x3	0.27251	0.62529	0.43582	0.66477
x4	-0.42082	0.36632	-1.1488	0.2559
x5	0.33666	0.12655	2.6604	0.010354

Number of observations: 58, Error degrees of freedom: 52
Root Mean Squared Error: 0.941
R-squared: 0.193, Adjusted R-Squared 0.115
F-statistic vs. constant model: 2. 49, p-value 0.0429

B.3.4 EOF 3 and March-May Indices

y=EOF 3, x1=Niño3, x2=Niño3.4, x3=AMO, x4=SOI
Linear regression model:
y - 1 + x1 + x2 + x3 + x4 + x5 + x6 Estimated
Coefficients:
Estimate SE tStat pValue
(Intercept) 7.848e-06 0.12276 6.3932e-05 0.99995 x1
-0.29576 0.35653 -0.82957 0.41065 x2 0.027496
0.14002 0.19636 0. 84511 x3 0.075678
0.34099 0.22193 0.82525 x4 0.20479
0.55865 0.36658 0.71545 x5 0.35165
0.12566 2.7984 0.0072304 x6 0.2762
0.22596 1. 2223 0. 22721
Number of observations: 58, Error degrees of freedom: 51
Root Mean Squared Error: 0.935
R-squared: 0.218, Adjusted R-Squared 0.126
F-statistic vs. constant model: 2.37, p-value 0.0428

B.4 COMBINED TIMESCALE

B.4.1 EOF 3 and D_DJ_DJF Indices

y=EOF 3, x1=Niño 3, x2=Niño3.4, x3=Niño4, x4PNA, x5=AMO, x6=Niño 1+2

Linear regression model:
y - 1 + xl + x2 + x3 + x4 + x5 + x6 Estimated
Coefficients:

	Estimate	SE	tStat	pValue
(Intercept)	0.00026923	0 .11834	0.0022751	0.99819
xl	-0.06327	0.89859	-0.07041	0.94414
x2	-0.041577	0.96055	-0.043284	0.96564
x3	-0.14844	0. 4118	-0.36048	0.71998
x4	-0.31967	0.1437	-2.2245	0.030567
x5	0.38889	0.12574	3. 0928	
0.0032128				
x6	0.069837	0.35371	0.19744	0.84427

Number of observations: 58, Error degrees of freedom: 51
Root Mean Squared Error: 0.901
R-squared: 0.273, Adjusted R-Squared 0.188
F-statistic vs. constant model: 3.2, p-value 0.00969

B.4.2 EOF 3 and J_JF_JFM Indices

y=EOF 3, x1=AMO, x2=Niño 3, x3=Niño 3.4, x4=Niño 4, x5=PNA

Linear regression model: y - 1
+ x1 + x2 + x3 + x4 + x5
Estimated Coefficients:

Estimate	SE	tStat	pValue	
(Intercept)	-4.5161e-05	0.12194	-0.00037037	0. 99971
x1	0.34802	0.12539	2.7756	0.00764
x2	-0.16773	0.56045	-0.29928	0.76592 x3
0.29075	0.80941	0.35921	0. 72089	

Number of observations: 58, Error degrees of freedom: 52
Root Mean Squared Error: 0. 929
R-squared: 0.213, Adjusted R-Squared 0.138
F-statistic vs. constant model: 2.82, p-value 0.0251

B.4.3 EOF 3 and F_FM_FMA Indices

y= EOF 3, x1=AMO, x2=PNA, x3=Niño 3, x3=Niño3.4, x4=Niño 4

Linear regression model:
y - 1 + x1 + x2 + x3 + x4 + x5 Estimated
Coefficients:

	Estimate	SE	tStat	pValue
(Intercept)	-4.3699e-07	0.12215	-3.5775e-06	1 x1
0.333	0.12506	2.6628	0.010289 x2	-
0.19114	0.14656	-1.3042	0.19792 x3	-
0.051285	0.38387	-0.1336	0.89424 x4	0.31417
0.6197	0.50697	0.61432 x5		-0.44423
0.36297	-1.2239	0.22652		

Number of observations: 58, Error degrees of freedom: 52
Root Mean Squared Error: 0.93
R-squared: 0.211, Adjusted R-Squared 0.135
F-statistic vs. constant model: 2.77, p-value 0.027

B.4.4 EOF 3 and M_MA_MAM Indices

y= EOF 3, x1=PNA, x2=Niño4, x3=AMO, x4=Niño3.4, x5=Niño 3, x6=SOI

Linear regression model:
y - 1 + x1 + x2 + x3 + x4 + x5 + x6 Estimated
Coefficients:

	Estimate	SE	tStat	pValue
(Intercept)	5.2836e-05	0.12296	0.0004297	0.99966
x1	-0.055858	0.15694	-0.35591	0. 72337
x2	-0.31296	0.36795	-0.85054	0.399 x3
0.33423	0.12588	2.6552	0.010548 x4	
0.24938	0.57465	0.43397	0.66614 x5	
0.076856	0.35447	0.21682	0.82921 x6	0.2729
0.2213	1. 2331	0.22317		

Number of observations: 58, Error degrees of freedom: 51
Root Mean Squared Error: 0.936
R-squared: 0.215, Adjusted R-Squared 0.123
F-statistic vs. constant model: 2.33, p-value 0.0456

B.4.5 EOF 3 and A_AM Indices

y= EOF 3, x1=PNA, x2=AMO, x3=Niño 3.4, x4=Niño4, x5=Niño3, x6=SOI

Linear regression model:
y - 1 + x1 + x2 + x3 + x4 + x5 + x6 Estimated
Coefficients:

	Estimate	SE	tStat	pValue
(Intercept)	0.00017527	0.12252	0.0014306	0.99886 x1
0.16058	0.14193	1.1314	0.26318 x2	0.37532
0.12503	3.0019	0. 0041465 x3		-0.092772
0.53135	-0.1746	0.86209 x4	-0.20267	0.36207
-0.55974	0.5781 x5	0.14239	0.34189	0.41648
0.6788 x6	0.13538	0.22305	0.60696	0.54657

Number of observations: 58, Error degrees of freedom: 51
Root Mean Squared Error: 0.933
R-squared: 0.221, Adjusted R-Squared 0.129
F-statistic vs. constant model: 2.41, p-value 0.0396

Appendix C

Linear Regression Output between Rainfall Mode 4 (EOF 4) and Climate Indices on All Timescales

C.1 MONTHLY TIMESCALE

C.1.1EOF 4 and December Indices

y=EOF 4, x1=TSA

Linear regression model:
y - 1 + x1
Estimated Coefficients:

Estimate	SE	tStat	pValue (Intercept)
-1.3437e-05	0.13245	-0.00010144	0.99992

x1 -0.017145 0.13361 -0.12832 0.89835
Number of observations: 58, Error degrees of freedom: 56
Root Mean Squared Error: 1.01
R-squared: 0.000294, Adjusted R-Squared -0.0176
F-statistic vs. constant model: 0.0165, p-value 0.898

C.1.2 EOF 4 and January Indices

y= EOF 4, x1= Niño 1+2

Linear regression model:
y - 1 + x1
Estimated Coefficients:
Estimate SE tStat pValue
(Intercept) -1.2308e-06 0.12875 -9.5595e-06 0.99999 x1
0.23541 0.12988 1.8126 0.075253

Number of observations: 58, Error degrees of freedom: 56
Root Mean Squared Error: 0.981
R-squared: 0.0554, Adjusted R-Squared 0.0386
F-statistic vs. constant model: 3.29, p-value

C.1.3 EOF 4 and February Indices

y= EOF 4, x1=Niño3, x2=Niño3.4, x3=SOI, x4= TSA, x5=Niño1+2

Linear regression model:
y - 1 + x1 + x2 + x3 + x4 + x5 Estimated
Coefficients:

	Estimate	SE	tStat	pValue
(Intercept)	0.00020531	0.12293	0.0016701	0.99867
x1	0. 65394	0.50496	1.295	0.20103
x2	-0.5151	0.44143	-1.1669	0.24857
x3	0.22067	0.18353	1.2024	0.23467
x4	0.093181	0 .13153	0.70842	0.48185
x5	0.25096	0.21285	1.179	0.24375

Number of observations: 58, Error degrees of freedom: 52
Root Mean Squared Error: 0.936
R-squared: 0.2, Adjusted R-Squared 0.124
F-statistic vs. constant model: 2.61, p-value

C.1.4 EOF 4 and March Indices

y=EOF 4, x1=Niño3, x2=Niño 3.4, x3Niño1+2, x4=SOI

Linear regression model:
y - 1 + x1 + x2 + x3 + x4
Estimated Coefficients:
Estimate SE tStat pValue (Intercept)
-5.9456e-07 0.12547 -4.7386e-06 1 x1 0.40388

0.42652	0.94691	0.34798 x2	-0.33894
0.32638	-1. 0385	0.30376 x3	0.24096
0.23574	1. 0222	0. 31135 x4	-0.0074353
0.17929	-0.041472	0. 96708	

Number of observations: 58, Error degrees of freedom: 53
Root Mean Squared Error: 0.956
R-squared: 0.151, Adjusted R-Squared 0.0869
F-statistic vs. constant model: 2. 36, p-value 0.0654

C.1.4 EOF 4 and April Indices

y= EOF 4, x1=AMO, x2=Niño1+2, x3=Niño 3, x3=Niño 3.4

Linear regression model:
y - 1 + x1 + x2 + x3 + x4
Estimated Coefficients:

Estimate		SE	tStat	pValue	
(Intercept)	-5.4555e-09		0.12375	- 4.4086e-08	1 x1
0. 06572		0.12694	0.51773	0.6068 x2	0.36747
0.26364	1.3938	0.16918 x3		0.16032	0.38704
0.41421	0.68039 x4		-0.15906	0.25306	-
0.62853	0.53236				

Number of observations: 58, Error degrees of freedom: 53
Root Mean Squared Error: 0. 942
R-squared: 0.174, Adjusted R-Squared 0.112
F-statistic vs. constant model: 2. 79, p-value 0.0353

C.1.5 EOF 4 and May Indices

y= EOF 4, x1= Niño3, x2=Niño3.4, x3=AMO, x4=SOI, x5Niño1+2

Linear regression model:
y - 1 + x1 + x2 + x3 + x4 + x5 Estimated
Coefficients:

	Estimate	SE	tStat	pValue
(Intercept)	4.2432e-06	0.11927	3.5576e-05	0.99997
x1	0.99381	0.46841	2.1216	0.038652
x2	-0.49084	0.31636	-1.5515	0.12684
x3	0.020153	0.12498	0.16124	0. 87253
x4	-0.15281	0.15399	-0.99232	0.32564
x5	-0.18861	0.31732	-0.59437	0.55484

Number of observations: 58, Error degrees of freedom: 52
Root Mean Squared Error: 0.908
R-squared: 0.247, Adjusted R-Squared 0.175
F-statistic vs. constant model: 3.42, p-value

C.2 BIMONTHLY TIMESCALE

C.2.1 EOF 4 and December-January Indices

y= EOF 4, x1=Niño1+2

Linear regression model:
y - 1 + x1
Estimated Coefficients:

Estimate	SE	tStat	pValue	
(Intercept)	-5.1997e-07	0.13098	-3.9698e-06	1 x1
0.14966	0.13213	1.1327	0.26218	

Number of observations: 58, Error degrees of freedom: 56
Root Mean Squared Error: 0.998
R-squared: 0.0224, Adjusted R-Squared 0.00494
F-statistic vs. constant model: 1.28, p-value = 0.262

C.2.2 EOF 4 and January-February Indices

y= EOF 4, x1=Niño 1+2, x2Niño3, x3=Niño3.4

Linear regression model: y
- 1 + x1 + x2 + x3
Estimated Coefficients:

Estimate	SE	tStat	pValue	
(Intercept)	-2.5059e-06	0.12609	-1. 9874e-05	0.99998
x1	0.43652	0.26282	1. 6609	0.10253
x2	0.13968	0.67858	0.20584	0.83769
x3	-0.35529	0.54547	-0.65135	0.51758

Number of observations: 58, Error degrees of freedom: 54
Root Mean Squared Error: 0.96
R-squared: 0.126, Adjusted R-Squared 0.0779
F-statistic vs. constant model: 2.61, p-value

C.2.3 EOF 4 and February-March Indices

y= EOF 4, x1= Niño3, x2=Niño 3.4, x3=TSA , x4=Niño1+2

Linear regression model:
y - 1 + x1 + x2 + x3 + x4
Estimated Coefficients:

	Estimate	SE	tStat	pValue
(Intercept)	3.1333e-06	0.12307	2.546e-05	0.99998
xl	0.53867	0.476	1.1317	0.26287
x2	-0.54915	0.37884	-1.4496	0.15307
x3	0.049603	0.12826	0.38673	0.70051
x4	0.2895	0.22494	1.287	0.20368

Number of observations: 58, Error degrees of freedom: 53
Root Mean Squared Error: 0.937
R-squared: 0.183, Adjusted R-Squared 0.122
F-statistic vs. constant model: 2. 97' p-value 0.0275

C.2.4 EOF 4 and March-April Indices

y= EOF 4, x1=Niño 1+2, x2Niño3, x3=Niño3.4, x4=AMO

Linear regression model:
y - 1 + x1 + x2 + x3 + x4
Estimated Coefficients:

	Estimate	SE	tStat	pValue
(Intercept)	-2.4237e-06	0.12389	-1.9564e-05	0.99998
x1	0.31894	0.28074	1.1361	0.26104
x2	0.27319	0.44583	0.61277	0.54265
x3	-0.24702	0.29129	-0.84803	0.40023
x4	0.02406	0.1264	0.19035	0.84976

Number of observations: 58, Error degrees of freedom: 53
Root Mean Squared Error: 0. 943
R-squared: 0.172, Adjusted R-Squared 0.11
F-statistic vs. constant model: 2. 76, p-value 0.0371

C.2.5 EOF 4 and April-May Indices

y= EOF 4, x1= Niño 1+2, x2=Niño3, x3=Niño 3.4, x4=SOI, x5=AMO

Linear regression model:
y - 1 + x1 + x2 + x3 + x4 + x5 Estimated
Coefficients:

	Estimate	SE	tStat	pValue
(Intercept)	-6.3846e-06	0.12157	-5.2518e-05	0.99996
x1	0.059182	0.3162	0.18716	0.85226
x2	0.66561	0.45853	1.4516	0.15261
x3	-0.50194	0.3382	-1.4842	0.1438
x4	-0.21044	0.19798	-1.0629	0.29274
x5	0.040447	0.12571	0.32175	0.74893

Number of observations: 58, Error degrees of freedom: 52
Root Mean Squared Error: 0.926
R-squared: 0.218, Adjusted R-Squared 0.143
F-statistic vs. constant model: 2.9, p-value 0.0221

C.3 SEASONAL TIMESCALE

C.3.1 EOF 4 and December-February Indices

y= EOF 4, x1=Niño 1+2

Linear regression model:
y - 1 + x1
Estimated Coefficients:

	Estimate	SE	tStat	pValue
(Intercept)	-6.3013e-07	0.12924	-4.8755e-06	1
x1	2.556	1.5185	1.6833	0.09788

Number of observations: 58, Error degrees of freedom: 56
Root Mean Squared Error: 0.984
R-squared: 0.0482, Adjusted R-Squared 0.0312
F-statistic vs. constant model: 2.83, p-value

C.3.2 EOF 4 and January-March Indices

y= EOF 4, x1=Niño 1+2, x2Niño3, x3=Niño 3.4

Linear regression model:
y - 1 + x1 + x2 + x3 Estimated
Coefficients:

Estimate	SE	tStat	pValue	
(Intercept)	5.5276e-07	0.12366	4.4699e-06	1 x1
0.46671	0.25625	1.8213	0.074102 x2	
0.18947	0.60781	0.31172	0.75645 x3	
-0.39483	0.47938	-0.82362	0.41378	

Number of observations: 58, Error degrees of freedom: 54
Root Mean Squared Error: 0.942
R-squared: 0.16, Adjusted R-Squared 0.113
F-statistic vs. constant model: 3.42, p-value 0.0235

C.3.3 EOF 4 and February-April Indices

y== EOF 4, x1=Niño 1+2, x2=Niño 3, x3=Niño3.4, x4= AMO

Linear regression model:
y - 1 + x1 + x2 + x3 + x4
Estimated Coefficients:

Estimate	SE	tStat	pValue	
(Intercept)	1. 0465e-06	0.12227	8.5592e-06	0.99999
x1	0.34452	0.26459	1.3021	0.19851
x2	0.39213	0.48197	0.8136	0.41951
x3	-0.41275	0.34252	-1.205	0.23354
x4	0.00079888	0.12441	0. 0064213	0.9949

Number of observations: 58, Error degrees of freedom: 53
Root Mean Squared Error: 0.931
R-squared: 0.194, Adjusted R-Squared 0.133
F-statistic vs. constant model: 3 .18, p-value 0.0204

C.3.4 EOF 4 and March-May Indices

y= EOF 4, x1=Niño1+2, x2=Niño 3', x3=Niño 3.4, x4=AMO

Linear regression model:
y - 1 + x1 + x2 + x3 + x4
Estimated Coefficients:

	Estimate	SE	tStat	pValue
(Intercept)	-3.3944e-06	0.12196	-2 0 7832e-05	0.99998
x1	0.11425	0.3254	0.3511	0.72691 x2
0.59774	0.48648	1. 2287	0.22461 x3	-
0.34958	0.28845	-1.2119	0.23091	x4
0.030047	0.12471	0.24094	0.81053	

Number of observations: 58, Error degrees of freedom: 53
Root Mean Squared Error: 0.929
R-squared: 0.198, Adjusted R-Squared 0.137
F-statistic vs. constant model: 3.27, p-value 0.0181

C.4 COMBINED TIMESCALE

C.4.1 EOF 4 and D_DJ_DJF Indices

y= EOF 4, x1=TSA, x2=Niño1+2

Linear regression model:
y - 1 + x1 + x2 Estimated
Coefficients:
Estimate SE tStat pValue
(Intercept) -8.6312e-05 0.1314 -0.00065685 0.99948 x1
-0.10924 0.14844 -0.7359 0.46492 x2
0.37729 0.27379 1.3781 0.17377

Number of observations: 58, Error degrees of freedom: 55
Root Mean Squared Error: 1
R-squared: 0.0337, Adjusted R-Squared -0.00148
F-statistic vs. constant model: 0.958, p-value = 0.39

C.4.2 EOF 4 and J_JF_JFM Indices

y= EOF 4, x1=Niño 1+2, x2=Niño3, x3Niño3.4

Linear regression model:
y - 1 + x1 + x2 + x3 Estimated
Coefficients:

	Estimate	SE	tStat	pValue
(Intercept)	-1.6438e-06	0.12607	-1.3039e-05	0.99999
x1	0.39748	0.29093	1.3662	0.17753
x2	0. 2944	0.686	0.42916	0.66951
x3	-0.46553	0.53092	-0.87682	0.38447

Number of observations: 58, Error degrees of freedom: 54
Root Mean Squared Error: 0.96
R-squared: 0.127, Adjusted R-Squared 0.0782
F-statistic vs. constant model: 2.61, p-value

C.4.3 EOF 4 and F_FM_FMA Indices

y=EOF4, x1=Niño 1+2, x2=Niño 3, x3=Niño 3.4, x4=TSA, x5=SOI, x6=AMO

Linear regression model:
y - 1 + x1 + x2 + x3 + x4 + x5 + x6 Estimated
Coefficients:
Estimate SE tStat pValue
(Intercept) 7.1596e-05 0.12279 0.00058309 0.99954 x1
0.29573 0.24509 1. 2066 0.23314 x2
0.55568 0.49996 1.1114 0.27159 x3 -
0.41922 0.41018 -1.0221 0. 31158 x4
0.086806 0 .13068 0.66424 0.50953 x5

0.20915 0.18481 1.1317 0.26304 x6 -
0.034999 0.12646 -0.27677 0.78308
Number of observations: 58, Error degrees of freedom: 51
Root Mean Squared Error: 0.935
R-squared: 0.218, Adjusted R-Squared 0.126
F-statistic vs. constant model: 2.36, p-value 0.0432

C.4.4 EOF 4 and M_MA_MAM Indices

y= EOF 4, x1=Niño 1+2, x2=Niño 3, x3=Niño3.4, x4=AMO, x5=SOI

Linear regression model:
y - 1 + x1 + x2 + x3 + x4 + x5 Estimated
Coefficients:
Estimate SE tStat pValue
(Intercept) 2.5255e-07 0.12468 2.0257e-06 1 x1
0.22722 0.29667 0.76591 0.44719 x2 0.46033
0.48636 0.94649 0.34828 x3 -0.3182
0.32056 -0.99266 0.32547 x4 0.0098175
0.12752 0.076991 0.93893 x5 0.02897 0.18031
0.16067 0.87297

Number of observations: 58, Error degrees of freedom: 52
Root Mean Squared Error: 0.949
R-squared: 0.178, Adjusted R-Squared 0.0985
F-statistic vs. constant model: 2.24, p-value 0.0635

C.4.5 EOF 4 and A_AM Indices

y= EOF 4, x1=AMO, x2=Niño1+2, x3Niño, x4=Niño 3.4, x5=SOI

Linear regression model: y - l
+ x1 + x2 + x3 + x4 + x5
Estimated Coefficients:

	Estimate	SE	tStat	pValue
(Intercept)	-2.8876e-06	0.12228	-2.3614e-05	0.99998
x1	0.043527	0.12646	0.34419	0.73209
x2	0.19331	0.29681	0.6513	0.51772
x3	0.45835	0.43348	1.0574	0.29522
x4	-0.45865	0.32711	-1.4021	0.16682
x5	-0.24047	0.19506	-1.2328	0.22321

Number of observations: 58, Error degrees of freedom: 52
Root Mean Squared Error: 0.931
R-squared: 0.209, Adjusted R-Squared 0.133
F-statistic vs. constant model: 2.75, p-value